Probing the molecular basis of melanopsin induced light sensitivity

Dr Athanasios N. Vachtsevanos

Nuffield Laboratory of Ophthalmology,
Department of Clinical Neurosciences
& Green Templeton College,
University of Oxford

Submitted for the Degree of MSc (Research)

Medical Sciences Division

1 September 2012

Abstract

Probing the molecular basis of melanopsin induced light sensitivity

A. Vachtsevanos

Nuffield Laboratory of Ophthalmology, Department of Clinical Neurosciences and Green Templeton College, University of Oxford

It has been demonstrated that retinal photoreception among mammals extends beyond rods and cones to include a small number of intrinsically photosensitive retinal ganglion cells (pRGCs), which are capable of responding to light due to expression of the melanopsin (*OPN4)* photopigment. *OPN4* may have therapeutic potential if ectopically expressed in the degenerate retina in cases where photoreceptors are lost, but the other molecules involved in this light induced transduction cascade are less well characterized. Therefore I sought to probe further the mechanism of *OPN4* mediated light sensitivity by siRNA mediated knock down of specific molecules in two mice models in which complete loss of rods and cones renders them almost exclusively dependent on the *OPN4* pathway for light sensitivity.

I generated siRNA probes against the long transcript variant of murine Opn4 mRNA and first tested these probes on the murine Neuro2A (N2a) cell line, before assessing effects in *C3H/HeN rd* and rodless/coneless *rd/rd cl* mice. siRNA was injected intravitreally into one eye and pupillometry was assessed, combined with molecular analyses at various timepoints. Reverse transcription polymerase chain reaction (RT-PCR) analysis in N2a cells confirmed Opn4 knockdown and immunolabelling techniques identified >85% silencing with siRNA. Pupil responses in the *rd* and *rd/rd cl* mice were inhibited by the siRNA injections *in vivo* which confirmed the functional effect of *Opn4* silencing detected by molecular analysis.

I therefore present a novel reproducible *in vivo* model in which siRNA induced silencing of the melanopsin pathway can be assessed by pupillometry and compared to levels of mRNA and protein at specific timepoints. Probes against other putative candidate genes, such as *TRPC3*, may unravel the molecular interactions of this pathway. This may help in future to induce light sensitivity in other retinal neurons in patients who are completely blind from photoreceptor loss.

Acknowledgments

I would like to express my gratitude to my supervisor, Prof Robert E MacLaren, whose expertise, understanding, and patience, added considerably to my graduate experience. It was though his persistence, kindness and understanding that made all this possible. A very special thanks goes out to Dr. Stuart Peirson, without whose motivation and encouragement I would not have made it. He provided me with direction, support and advice when it was most needed. I must also acknowledge Dr Aarti Jagganath for her suggestions and guidance which was always valuable. Appreciation also goes out to Dr Steven Hughes and Dr Carina Pothecary for their skills and advice throughout my graduate program at all the instances. I would like to thank my friends and colleagues Dr Peter Charbel Issa and Dr Mandeep Singh for our philosophical debates, exchanges of knowledge, skills, and venting of frustration during my graduate program, which helped enrich the experience. Special thanks goes to everyone at the Nuffield Laboratory of Ophthalmology. They have contributed in various capacities and helped this project come to a successful conclusion. I would also like to thank my family, my parents and my brother, for the support they provided me through my entire life. I must also acknowledge my friend, Georgia, whose encouragement and support; helped me finish this thesis.

Contents

Chapter 2: Methodology and Materials

Chapter 3: Results

Glossary of Acronyms

AH	Anterior hypothalamic nucleus
ARP	Acidic Ribosomal Associated Protein
BST	Bed nucleus of the stria terminalis
cDNA	complementary Deoxyribonucleic Acid
cGMP	cyclic Guanosine Monophosphate
DAG	diacyl glycerol
DNA	Deoxyribonucleic Acid
dsRNA	double stranded Ribonucleic Acid
GAPDH	Glyceraldehyde-3-phosphate dehydrogenase
IGL	Intergeniculate leaflet
INL	Inner nuclear layer
INL	Inner limiting membrane
IP3	inositol 1,4,5-trisphosphate
IPL	Inner plexiform layer
LH	Lateral hypothalamus
LHb	lateral habenula
LGd	Dorsal lateral geniculate nucleus
LGv	Ventral lateral geniculate nucleus
MA	Medial amygdaloid nucleus
mRNA	messenger Ribonucleic Acid
N2a	Neuro2a Cell line
NIF	Non-image forming
ONL	Outer nuclear layer
ONL	Outer limiting membrane
OPL	Outer plexiform layer
OPN	Olivary Pretectal Nucleus
Opn4	Melanopsin
PAG	Periaqueductal gray
pSON	Peri-supraoptic nucleus
PLR	Pupillary Light Reflex
PO	Preoptic area
pRGCs	photosensitive Retinal Ganglion Cells

qPCR	quantitative Polymerase Chain Reaction
rd	retinal degeneration mouse
rd/rd cl	rodless/coneless mouse
RNA	Ribonucleic Acid
RNAi	Ribonucleic Acid interference
RPE	Retinal pigment epithelium
RT-qPCR	Real Time quantitativepolymerase chain reaction
SC	Superior colliculus
SCN	Suprachiasmatic Nucleus
SPZ	Subparaventricular zone
siRNA	short interfering Ribonucleic Acid
cSLO	confocal Scanning Laser Ophthalmoscope
TRPC3	transient receptor potential cation channel 3
VLPO	Ventrolateral Preoptic area

List of Figures

List of Tables

ARVO Paper Presentation

Association for Research into Vision and Ophthalmology (ARVO) May 1-5, 2011

Tuesday, May 3, 2011 9:30 - 9:45 AM

2564 - Application Of RNAi To Unravel The Melanopsin Phototransduction Pathway

Athanasios Vachtsevanos, Stuart Peirson, Aarti Jagannath, Steve Hughes, Georgia Perganta, Robert E. MacLaren.

Purpose: It has been demonstrated that retinal photoreception among mammals extends beyond rods and cones to include a small number of intrinsically photosensitive retinal ganglion cells (pRGCs), which are capable of responding to light due to expression of the melanopsin (*OPN4*) photopigment. OPN4 may have therapeutic potential if ectopically expressed in the degenerate retina in cases where photoreceptors are lost, but the molecules involved in this *OPN4* light induced transduction cascade are less well characterized. We therefore sought to probe further the mechanism of *OPN4* mediated light sensitivity by siRNA medicated knock down of specific molecules in the aged *rd* mouse, which is almost exclusively dependent on the *OPN4* pathway for light sensitivity.

Methods: We generated siRNA probes against the long transcript variant of murine *Opn4* mRNA (UCG CAC UGA UUG UCA UUC UUC) and tested these probes on the murine Neuro2A (N2a) cell line. Mice on the *C3H/HeN* background harboring the *rd* mutation were aged to 80 days. At this point virtually all surviving cone cells are lost - similar to end-stage retinitis pigmentosa in humans. siRNA was given by intravitreal injection into one eye and pupillometry was assessed combined with molecular analyses at 1, 3 and 5 days.

Results: Reverse transcription polymerase chain reaction (RT-PCR) analysis in N2a cells confirmed Opn4 knockdown and immunolabelling techniques identified >85% silencing with siRNA *OPN4*. Pupillometry in the mouse was also affected by the siRNA injections *in vivo* and this was correlated to silencing of the murine *Opn4* at all time points. We also used immunolabelling to identify the distribution of the cation channel *TRPC3,* which interacts with melanopsin *in vivo*.

Conclusions: We present a reproducible *in vivo* model in which siRNA induced silencing of the melanopsin pathway can be assessed by pupillometry and compared to levels of mRNA and protein at specific timepoints. Probes against other putative second messengers, such as *TRPC3*, may unravel the molecular interactions of this pathway. This may help in future to induce light sensitivity in other retinal neurons, which may benefit patients who are completely blind from photoreceptor loss.

Chapter 1: Introduction

1 Anatomy of the eye

The eye (Fig 1.1) is the principal mediator of light input to the central nervous system. It is a complex optical system which collects light from the surrounding environment, regulates its intensity, focuses it through an adjustable lens to form an image, converts this image into a set of electrical signals, and transmits these signals to the brain through complex neural pathways that connect the eye via the optic nerve to the visual cortex and other areas of the brain.

The eye structure (Fig 1.1):

- **Vitreous gel** is the transparent gelatinous mass occupying the posterior compartment (the space between the crystalline lens and the retina of the eye), which is enclosed by a delicate hyaloid membrane; composed of water (99%), collagen fibrils, highly hydrated hyaluronic acid, hyalocytes, inorganic salts, sugar, and ascorbic acid.
- **Optic Nerve** is the sensory nerve which carries electrical impulses from visual stimuli in the retina out of the eye, across the optic chiasm, and to the ventral part of the diencephalon, on their way to the visual cortex in the occipital cortex of the brain for interpretation.
- **Macula** is an oval-shaped highly pigmented yellow spot near the center of the retina of the human eye. It has a diameter of around 1.5 mm and is often histologically

defined as having two or more layers of ganglion cells. Constitutes the region of maximum visual acuity and is made up almost wholly of retinal cones, which secrete luteal pigment to filter short wavelength light and thereby maximize sensitivity for medium to long wavelength (green and red) foveal cones.

- **Fovea** is a small shallow depression or pit at the center of the macula, caused by an almost complete absence of inner retinal layers, containing only cones (and no rods) and which affords the most acute vision
- **Retina** is the layer of nervous tissue, covering the posterior two-thirds of the eyeball, in which stimulation by light initiates an electrochemical reaction in which electrical impulses are transmitted to the brain, producing the sensation of vision; actually an extension of the brain, formed embryonically from brain tissue and connected to the brain proper by the optic nerve
- **Iris** is opaque muscular contractile diaphragm that is suspended in the aqueous humor in front of the lens of the eye; perforated by the pupil and continuous peripherally with the ciliary body; possesses a deeply pigmented posterior surface, which excludes the passage of light except through the pupil, and a colored anterior surface which determines the color of the eye.
- **Cornea** is the transparent, anterior, dome-shaped portion of the eyeball that covers the iris and pupil, which acts as the principal refracting surface of the eye.
- **Lens** is transparent lens-shaped or nearly spherical body in the eye, situated immediately behind the pupil, which focuses light rays entering the eye typically onto the retina.
- **Pupil** is the contractile, usually round aperture in the iris of the eye which allows light to pass into the crystalline lens

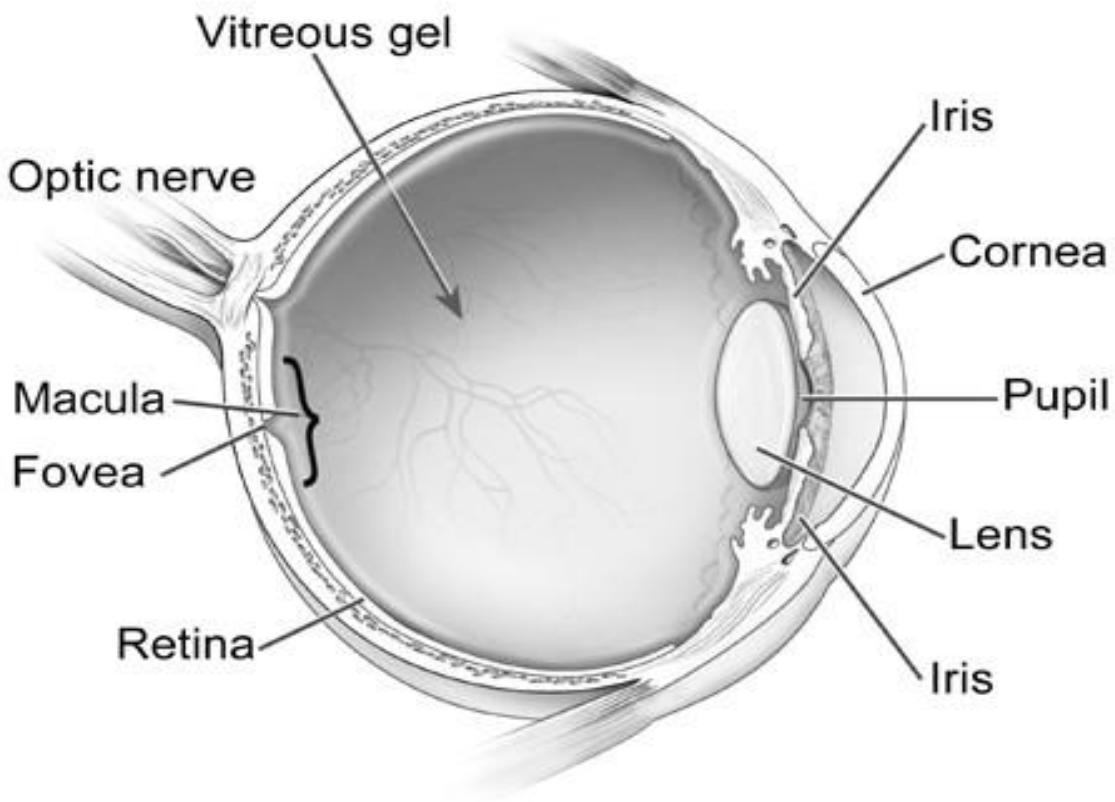

Fig 1.1 Schematic diagram of the human eye showing the macula and the fovea and the rest parts of the eye. Reproduced from National Eye Institute. (http://www.nei.nih.gov/health/eyediagram/eyeimages3.asp)

1.1 Structure of the Retina

The vertebrate retina is a light-sensitive tissue lining the inner surface of the eye. When light strikes light sensitive cells within the retina it initiates a cascade of chemical and electrical events that ultimately trigger nerve impulses. The retina has a layered structure with several layers of neurons interconnected by synapses. The only neurons that are directly sensitive to light are the photoreceptor cells. These are mainly of two types: the rods and cones. Rods function mainly in dim light and provide black-and-white vision, while cones support high resolution daytime vision and the perception of color through the parvocellular pathway. A third, type of photoreceptor, the photosensitive ganglion cell (pRGCs), are maximally sensitive to the blue spectrum (480 nm), are important for reflexive responses to bright daylight such as circadian rhythm, pupillometry and higher cortical responses that are only just beginning to be understood (Hankins et al., 2008).

Layers of the retina: Moving radially along the path of incident light, the individual layers of the retina are as follows (Fig 1.2):

1. Inner limiting membrane (ILM) – glial cell fibers separating the retina from the vitreous body comprised of Müller cell footplates.
2. Layer of optic nerve fibers –axons of the ganglion cell nuclei coursing towards the optic nerve.
3. Layer of ganglion cells - contains nuclei of ganglion cells, the axons of which form the optic nerve which projects predominantly in the lateral geniculate nucleus (LGN) and the pRGCs which also project to other brainstem and hypothalamic nuclei. Interspersed are also some displaced amacrine cells.

4. Inner plexiform layer (IPL) –the connecting axons linking cells in the INL with the ganglion cell layer and also vertical fibres of Müller cells.
5. Inner nuclear layer (INL) –contains the nuclei and surrounding cell bodies of the bipolar cells, horizontal cells, and amacrine cells.
6. Outer plexiform layer (OPL) –projections of rods and cones ending in the rod spherule and cone pedicle, respectively. These form tri-lobed ribbon synapses with bipolar cells and horizontal cells. Photoreceptor synapses also inter-connect directly to mediate lateral inhibition.
7. Outer nuclear layer (ONL) –comprising cell bodies of rods and cones.
8. Outer limiting membrane (OLM) – processes of Müller glial cells through which rods and cone inner segments project.
9. Layer of rods and cones – The photoreceptor layer, predominantly inner and outer segment processes.
10. Retinal pigment epithelium (RPE) – a single cubic layer of heavily pigmented epithelial cells.
11. Bruch's membrane – basal membrane of retinal pigment epithelial cells which also provides an anatomical barrier to prevent ingress of blood vessels into the transparent retina from the choriocapillaris.

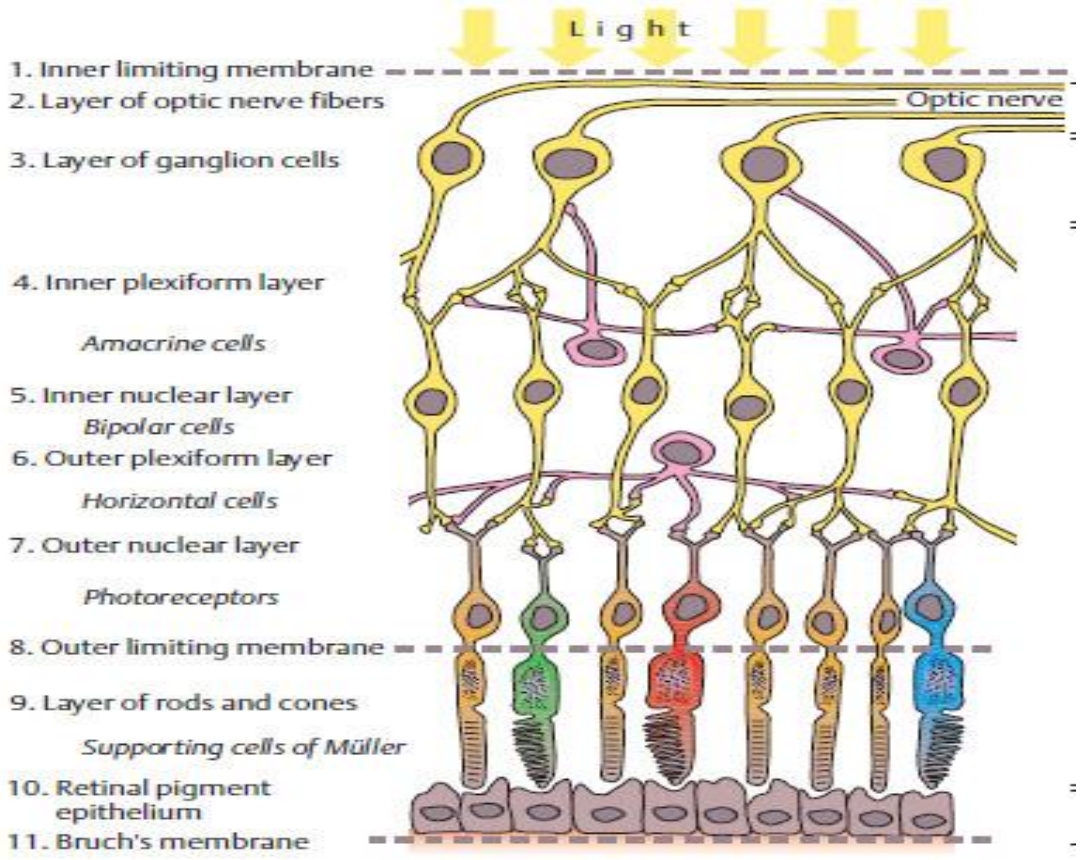

Fig 1.2. The layers of the retina. Diagram showing how retina is constituted by several layers of different cell types. All layers are described in the text. (Reproduced from Lang K, Atlas of Ophthalmology)

1.2 The Dual Function of the Eye

The eye is the principal mediator of light input to the central nervous system (CNS). In addition to vision and image forming, the vertebrate eye mediates several non image forming responses to light (Fig 1.3). Image-forming vision, with its high spatial and temporal resolution, enables the animal to detect and track objects in the visual world. Non-image-forming vision, however, provides a measure of the ambient luminance for the purposes of synchronizing the animal's biological clock with the surrounding light–dark cycle (circadian photoentrainment), controlling the pupil size, and other functions such as acute suppression of locomotor behaviour (negative masking) in rodents (Foster et al., 2002).

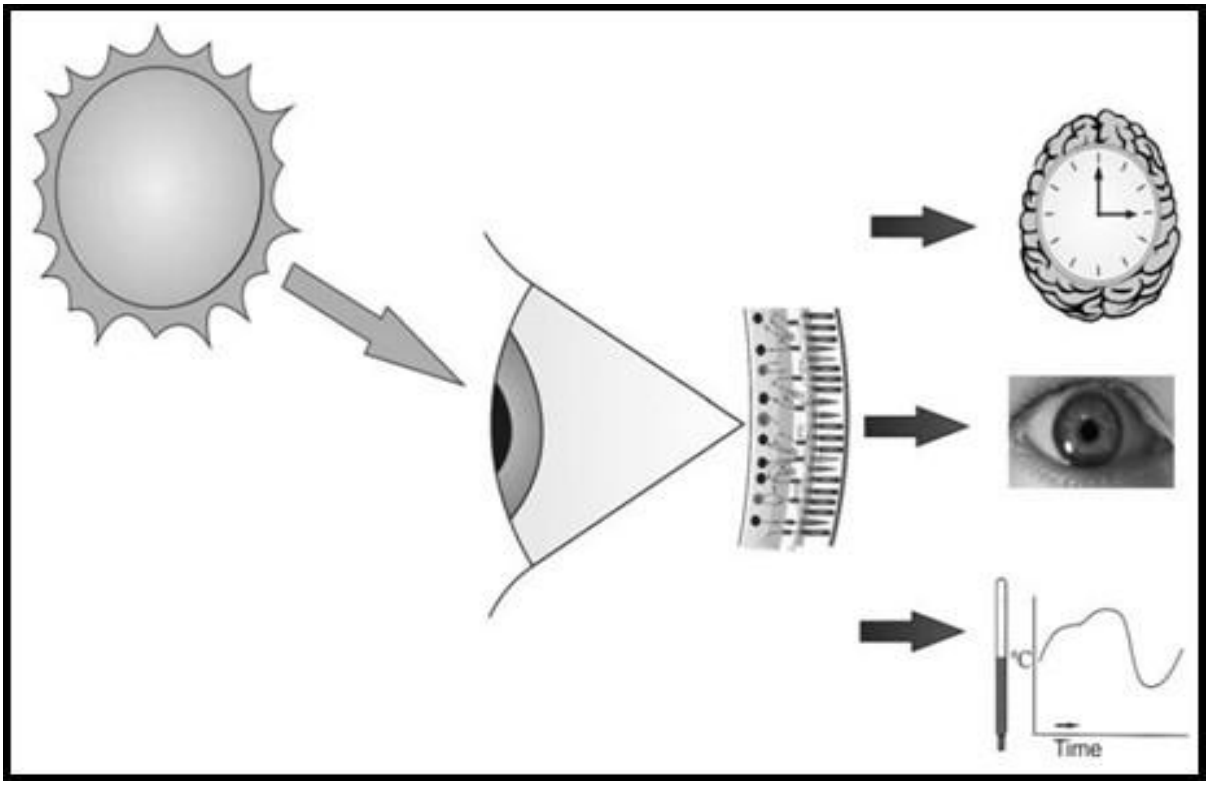

Fig 1.3 - A schematic figure of the non-image-forming (NIF) visual system in mammals involving pRGCs. Light falling on the retina is detected by rod and cone photoreceptors and by the melanopsinphototransduction cascade in pRGCs. The resultant signals are combined by pRGCs to send an integral signal of irradiance to thebrain. In turn, light information is passed to the brain down the opticnerve, triggering a diverse range of non image-forming responses in addition to normal form vision. NIF responses comprise the entrainment of circadian rhythms including sleep propensity (shown here by an image of a clock superimposed on a brain), the pupil light reflex, regulation of pineal melatonin levels and, in humans, regulation of body temperature and mood. (Reproduced from Bailes and Lucas, 2010).

Acute light stimuli directly modulate activity by a mechanism independent of the pacemaker. It has two forms: a suppression of activity usually caused by a bright light in the dark period (negative masking) and an enhancement of activity caused by either a dark pulse in the light period or dim light during the dark period (positive masking) (Mrosovsky 1999). Positive masking is completely lost in retinally degenerative mice (Mrosovsky et al., 1999) thus is mediated by the classical photoreceptor system and doesn't rely on pRGC function. Mice lacking rods and cones retain negative masking (Mrosovsky et al., 2001). Mice lacking the melanopsin gene display normal negative masking to dim light pulses but demonstrate impaired suppression of activity to bright light pulses (Mrosovsky & Hattar, 2003). This would suggest that rods, cones and pRGCs all contribute to the negative masking response. Indeed, mice lacking all three photoreceptors do not display negative masking (Hattar et al., 2003). Interestingly, mice in which the melanopsin cells are ablated demonstrate a complete absence of negative masking (Hatori et al., 2008; Goz et al., 2008). This would imply that rod and cone contributions to negative masking are relayed via the melanopsin expressing RGCs.

Circadian photoentrainment affects a whole host of functions such as melatonin release, body-temperature regulation and regulation of sleep. One of non-vision mediators of light is the photopigment melanopsin (Opn4).

1.3 General overview of Melanopsin (Opn4) and photosensitive retinal ganglion cells (pRGCs)

The isolation of both human and mouse melanopsin was originally described in 1998 (Provencio et al, 1998; 2000; 2002) and was first isolated from the photosensitive melanophores of Xenopus. In 1999, the Foster group showed that entrainment of mice to a light-dark cycle was maintained in the absence of rods and cones (Lucas et al., 1999). Such an observation led him to the conclusion that neither rods nor cones, located in the outer retina, are necessary for circadian entrainment and that a third class of photoreceptor exists in the mammalian eye (Freedman et al, 1999; Lucas et al., 1999). Subsequent experiments in melanopsin knockout mice confirmed that the pupil response was partly driven by melanopsin acting as the light sensitive pigment (Lucas et al., 2003).

Melanopsin is expressed in a subset of photosensitive retinal ganglion cells (pRGCs). These cells are capable of autonomous photo-transduction and are thus true photoreceptors (Berson et al., 2002; Warren et al., 2003; Viney et al., 2007; Graham et al., 2008; Schmidt et al., 2008; Do et al., 2009; Schmidt and Kofuji, 2009). Melanopsin is involved in non-image forming responses to light measuring environmental irradiance or the brightness of the light. The pRGCs constitute 2 – 4 % of all RGCs of the total RGC population (Moore et al., 1995; Gooley et al., 2001; Morin et al., 2003; Sollars et al., 2003, Berson et al., 2010).

1.3.1 Projection of the pRGCs

Axons of pRGCs project to specific brain nuclei involved in non-image forming responses (Fig 1.4):

i. The Olivary Pretectal Nucleus (OPN) which is responsible for controlling pupillary constriction.

ii. The Suprachiasmatic Nucleus (SCN) of the hypothalamus which is the master pacemaker and regulates circadian rhythms.

iii. The ventrolateral preoptic area (VLPO) which regulates sleep.

iv. Other less well characterised CNS projections include the periaqueductal grey matter (PAG), the superior colliculus (SC), the peri-supraoptic nucleus (pSON), the subparaventricular zone (SPZ), the lateral habenula (LHb), the intergeniculate leaflet (IGL), the lateral geniculate nucleus, ventral division (LGv), the lateral geniculate nucleus, dorsal division (LGd), the bed nucleus of the stria terminalis (BST), the medial amygdaloid nucleus (MA), the lateral hypothalamus (LH), the anterior hypothalamic nucleus (AH).

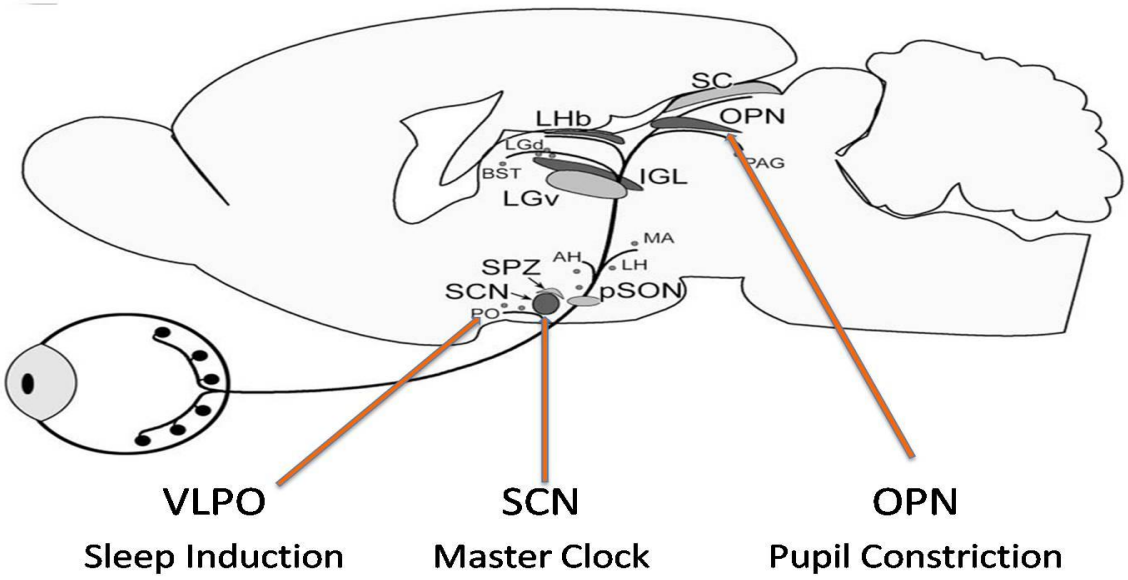

Fig 1.4 Projections of pRGCs to the brain. A schematic of the mouse brain in sagittal view showing a sampling of regions innervated by pRGCs (Hattar et al, 2006). PO, preoptic area; SCN, suprachiasmatic nucleus; SPZ, subparaventricular zone; pSON, peri-supraoptic nucleus; AH, anterior hypothalamic nucleus; LH, lateral hypothalamus; MA, medial amygdaloid nucleus; LGv, ventral lateral geniculate nucleus; IGL, intergeniculate leaflet; BST, bed nucleus of the stria terminalis; LGd, dorsal lateral geniculate nucleus; LHb, lateral habenula; SC, superior colliculus; OPN, olivary pretectal nucleus; PAG, periaqueductal gray.

1.3.2 Retinal connections relevant to pRGCs

The pRGCs are distinguished from conventional RGCs by their melanopsin expression or intrinsic photosensitivity, which is present on both the soma and the dendrites at comparable densities (Hattar et al., 2002; Provencio et al., 2002; Belenky et al., 2003; Berson et al., 2002; Do et al.,2009). Melanopsin-expressing pRGCs were previously considered to be a homogenous cell population, with sparsely branched dendritic arbors stratifying in the outermost sublamina of the inner plexiform layer (IPL) (Berson et al., 2002; Hattar et al., 2002; Provencio et al., 2002). Subsequent work revealed morphological and functional diversity among ganglion cells expressing melanopsin or exhibiting intrinsic photosensitivity (Baver et al., 2008; Dacey et al., 2005; Sekaran et al., 2003; Tu et al., 2005; Viney et al., 2007). Since the original descriptions however at least three anatomically distinct subtypes have been reported, termed M1–3. Over recent years, there has been a rapid increase in our understanding of the anatomical variety of pRGC subtypes. To date, the classification of pRGCs has extended to include five classes of pRGC, which are distinguished based on levels of melanopsin expression and the stratification of their dendrtites within specific sublaminae of their IPL (Do et al., 2010; Schmidt et al., 2011) (Fig 1.5). The dendrites of pRGCs receive synapses from bipolar and amacrine cells (Belenky et al., 2003; Ostergaard et al., 2007; Viney et al., 2008; Dumitrescu et al., 2009; Hoshi et al., 2009). Ganglion cells in the vertebrate retina receive synaptic input in the inner plexiform layer (IPL), which can be subdivided into anatomically distinct sublaminae. The major distinction is between sublamina a, closest to the rods and cones, in which pRGCs make connections with so-called OFF bipolar cells that are excited by decrements in light intensity, and sublamina b, proximal to the major concentration of ganglion cell bodies, characterized by synaptic input from ON bipolars excited by light

increments. Dendrites from the M1 cells stratify in sublamina a, those of M2 in sublamina b, while M3 ganglion cells are bistratified with dendrites in both a and b sublaminae (Hattar et al., 2006; Viney et al., 2007; Baver et al., 2008; Schmidt et al., 2008). M4 type and M5 type pRGCs who most recently have been identified are both similar in morphology to M2 type pRGCs with dentrites located in the ON layers of the IPL, yet are distinguished based on the size and complexity of their dentritic fields (Ecker et al., 2010). The levels of melanopsin expression in M4 and M% pRGCs are seemingly very low (Berson et al., 2010; Ecker et al., 2010). Most recently it has come clear that M1 subclass of pRGCs is further subdivided (Chen et al., 2011).

The axons of the pRGCs also express melanopsin, but only up to the optic disc and not beyond (Hattar et al., 2002). Among the pRGC subclasses, the M1 cells have noticeably higher melanopsin immunoreactivity (Hattar et al., 2006; Baver et al., 2008; Hattar et al., 2009; Schmidt et al., 2009). M1 cells have somata of ~15 μm diameter, most of which are located in the ganglion cell layer (GCL), although some are displaced to the inner nuclear layer (INL). Even though the M1 cells constitute just 1% (~700–900 overall) of the total mouse RGC population, their ~300μm diameter dendritic fields overlap to cover the entire retina in what has been termed a so called photoreceptive net (Hattar et al., 2002; Provencio et al, 2002; Berson et al., 2010). Compared with M1 cells, rodent M2 cells have larger (~20 μm) somata and more regular-branching dendrites that cover a larger area (~400 μm) (Baver et al., 2000; Hattar et al., 2006; Viney et al., 2008; Schmidt et al, 2009; Berson et al., 2010;). M2 cells are as numerous as M1 cells (Hattar et al., 2006; Viney et al., 2008; Baver et al., 2008; Berson et al., 2010) and cover the entire retina (Berson et al., 2010). M3 cells, stratify their dendrites in both the ON and OFF - sublaminae of the IPL (Schmidt et al, 2008; Viney et al., 200; Berson et al., 2010). M3 cells comprise approximately 10% of the pRGCs (Schmidt

et al., 2008; Viney et al., 2008; Berson et a.l, 2010) and they do not cover the entire retina. It is possible that may not constitute a true cell type (Berson et al., 2010). M4 cells are characterized by a large soma size and dendritic field. The M5 classification has small, bushy dendritic arbors (Berson et al 2010; Ecker et al., 2010). Many of their properties, including their sensitivity to light and synaptic inputs, have not yet been determined. Preliminary evidence suggests the existence of additional pRGC subtypes (Hattar et al., 2009; Berson et al., 2010).

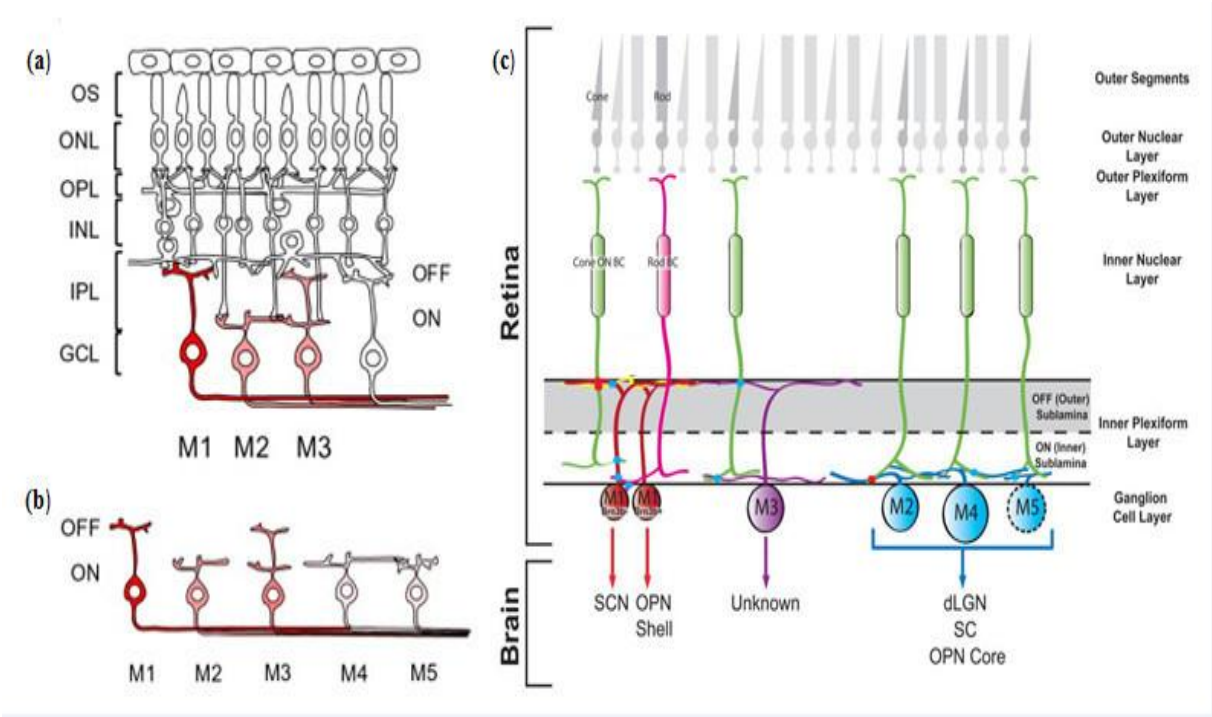

Fig. 1.5. A schematic diagram of retinal connections relevant to pRGCs in the rodent retina.

(a) Schematic showing the layers and cell types of the mammalian retina, including the melanopsin-expressing photosensitive ganglion cells (pRGCs). (b) Schematic showing the different levels of melanopsin expressed in pRGC subtypes (denoted by intensity of red coloring) and differing patterns of stratification within the inner plexiform layer (adapted from Hughes et al., 2012a). (c) Schematic diagram illustrating the connectivity and location of the five distinct morphological subtypes (M1–M5) of pRGCs and projections to their predominant targets in the brain. M1 pRGCs stratify in the OFF sublamina (red); M2, M4, M5, stratify in the ON sublamina (blue); and M3, stratify in the ON and OFF sublamina (purple) of the IPL of the retina. M4 pRGCs have the largest cell body size, and M1 cells have smaller body size than M2–M4 cells (Schmidt et al., 2009; Ecker et al., 2010; Schmidt et al.,2011). The cell body size of M5 is not known (dotted line). The proportion of ON and OFF stratification in M3 ipRGCs varies considerably between cells (Schmidt et al., 2011). Recent findings suggest that the M1 subtype consists of two distinct subpopulations that are molecularly defined by the expression of the Brn3b transcription factor (Brown et al., 2010). Red dots indicate synaptic connections for which both functional and anatomical evidence exists (Belenky et al., 2003; Viney et al., 2007; Dumitrescu et al., 2009; Hoshi et al., 2009; Schmidt et al., 2010). Blue dots indicate synaptic connections for which either functional or anatomical evidence exists (Ostergaard et al., 2007; Zhang et al., 2008; Ecker et al., 2010;

Schmidt et al., 2011). pRGC subtypes project to distinct non-image and image-forming nuclei in the brain (Hattar et al., 2006; Ecker et al., 2010). M1cells predominantly project to non-image forming centers such as the suprachiasmatic nucleus (SCN) to control circadian photoentrainment and the shell of the olivary pretectal nucleus (OPN) to control the PLR. M1 pRGCs predominantly projecting to the SCN (Chen et al., 2011). M3 brain targets are completely unknown at this time. M2, M4 and M5 are included together since no specific genetic marker exists for a single subtype. Collectively, they project to image forming areas in the brain such as the lateral geniculate nucleus (LGN) and the superior colliculus (SC), but also to the core of the OPN of which no specific function is assigned to this brain region (Ecker et al., 2010; Brown et al., 2010). Retrograde analysis confirms that M2 cells project minimally to the SCN and strongly to the OPN (Baver et al.,2008).(Adapted from Schmidt et al., 2011).

1.3.3 The Opn4 Isoforms

There are two identified distinct isoforms of melanopsin in the mouse retina, a long isoform (*Opn4Long*) and a short isoform (*Opn4Short*), the latter of which more closely resembles the sequences of rat and human melanopsin (Pires et al., 2009). Both isoforms are expressed in the ganglion cell layer of the retina and are capable of forming functional pigments in vitro. *Opn4Long* and *Opn4Short*) are generated by alternative splicing of the murine *Opn4* gene (Pires et al., 2009). These two isoforms of melanopsin differ only in their C-terminal regions and are differentially expressed in pRGCs in the adult mouse retina. The *Opn4Short*) is the most abundant isoform in the mouse retina, although *Opn4Long* is actually expressed in all pRGCs (M1-M3), with expression *of Opn4Short*) restricted to M1 and bistratified at M3 cells (Pires et al., 2009, Hughes et al., 2012b). *Opn4Long* and *Opn4Short*)are differentially expressed during postnatal development. There are two distinct phases of increased melanopsin expression during postnatal development, an initial increase between P0 and P3 driven primarily by an increase in *Opn4Short*) expression, and a second increase that occurs between P10 and P14 driven by changes in *Opn4Long* expression. The two phases of increased melanopsin expression would seem to correlate with the functional maturation of M1 and M2 type pRGCs. This suggesting that the specific functions associated with M1 and M2 type pRGCs will mature at different times during postnatal development (Hughes et al., 2012b)..

1.3.4 The phototransduction cascade

Phototransduction is a process by which light is converted into electrical signals in the rod cells, cone cells and photosensitive ganglion cells (pRGCs) of the retina of the eye. The visual cycle is the biological conversion of photon into an electrical signal in the retina. This process occurs via G-protein coupled receptors called opsins which contain the chromophore 11-cis retinal. 11-cis retinal is covalently linked to the opsin receptor via Schiff base forming retinylidene protein. When struck by photon, 11-cis retinal undergoes photoisomerization to all-trans retinal which changes the conformation of the opsin GPCR leading to signal transduction cascades which causes closure of cyclic GMP-gated cation channel, and hyperpolarization of the photoreceptor cell. Following isomerization and release from the opsin protein, all-trans retinal is reduced to all-trans retinol and travels back to the retinal pigment epithelium to be "recharged. Finally, it is oxidized to 11-cis retinal before traveling back to the rod outer segment where it is again conjugated to an opsin to form new, functional visual pigment (rhodopsin) (Arendt, 2003; Fu and Yau, 2007), (Fig. 1.6).

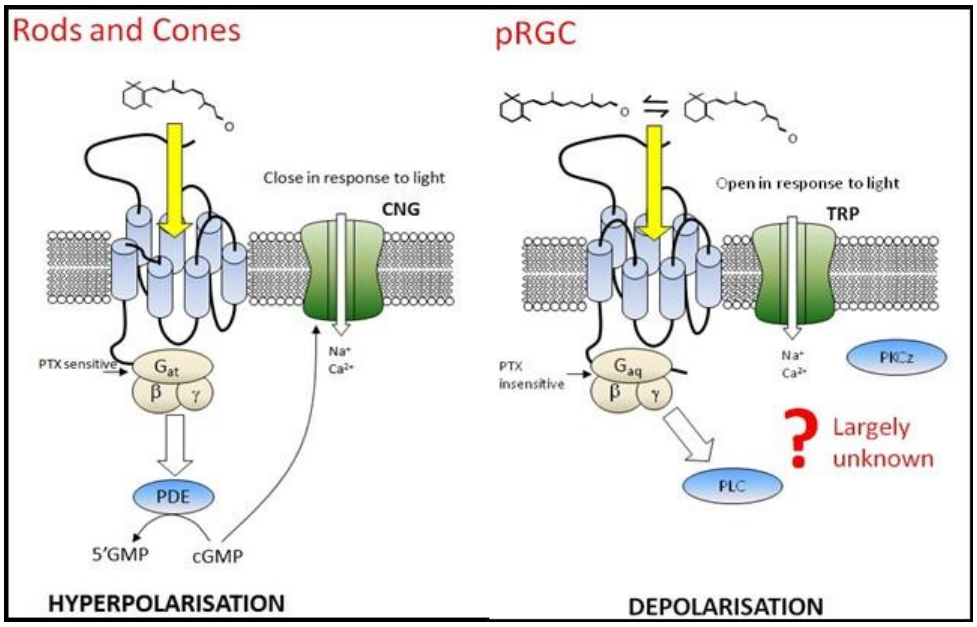

Fig. 1.6. Phototransduction cascade of rods, cones and pRGCs. Comparison of phototransduction cascades associated with opsin-dependent light detection in a vertebrate (rod/cone), and in mammalian pRGCs. Detailed discussion of these cascades is provided in the text. In rods and cones, cells are depolarized in darkness and the effect of light is to close a channel in the plasma membrane resulting in hyperpolarisation. By contrast, in pRGCs, light is coupled to the opening of a nonspecific cation channel that leads to cellular depolarisation. In each case, opsin photopigments are G-protein-coupled receptors. A photon of light (hV) is absorbed by the chromophore, leading to a confirmation change in the opsin. This leads to the activation of a multimeric G protein composed of an a, b and g subunit. The a subunit in the rod/cones is transducin (Gat) and in the pRGCs it is believed to be Gaq/11.

1.3.5 Melanopsin Signalling – pRGC phototransduction

Phototransduction in pRGCs begins with light absorption by the photopigment melanopsin (Provencio et al., 2000; Hattar et al., 2002; Berson et al., 2003; Lucas et al., 2003; Melyan et al., 2005; Panda et al., 2005; Qiu et al., 2005). Melanopsin is a member of the opsin sub group of G-protein-coupled receptors. Across the animal kingdom, there are examples of opsins coupling to G-proteins from Gt, Gq-, Go- and Gs classes (Terakita et al., 2005; Koyanagi et al., 2008). Vertebrate rod and cone opsins couple to a Gt-protein (transducin) and trigger a phosphodiesterase-dependent cascade resulting in cyclic nucleotide gated channel closure. How melanopsin leads to membrane depolarization is still unclear (Fig 1.6). However, most available evidence supports the hypothesis that its cognate G-protein is of the Gq/11 family, activation of phospholipase C (PLC) and subsequent opening of transient receptor potential channels (TRPCs) resulting in the depolarisation of the cell membrane, similar to many invertebrate phototransduction cascades (Arshavsky et al., 2002; Qiu et al., 2005; Panda et al., 2005; Koyanagi et al., 2005; Fu et al., 2005; Isoldi et al., 2005; Warren et al., 2006; Contin et al., 2006; Berson et al., 2007; Sekaran et al., 2007; Contin et al., 2009;). Light triggers an increase in intracellular calcium in pRGC somata and calcium responses are highly correlated with action potential firing (Sekaran et al., 2003; Newman et al., 2003; Melyan et al., 2005; Hartwick et al., 2007). *In vivo* data implicate canonical TRP (Warren et al., 2006; Sekaran et al., 2007) and/or voltage gated calcium channels (Hartwick et al., 2007) as the origin of this calcium increase. Direct evidence for melanopsin interactions with Gq/11 G-proteins is currently limited to heterologous cell expression studies (Panda et al., 2005). Melanopsin can also bind other G-proteins under these conditions (Newman et al., 2003, Melyan et al., 2005), but there is always the possibility of non-specific G-protein interactions outside of a native cellular environment (Hermans et al., 2003). Nonetheless, pRGCs express

Gq and G11 G-proteins as well as several phospholipase C isozymes (Graham et al., 2008) and TRP cation channel channels C6 and C7; (Warren et al., 2006; Sekaran et a.l, 2007). Moreover, the pRGC intrinsic photo-response has been inhibited using pharmacological blockers of phospholipase C (Graham et al, 2008) and transient receptor potential (TRP) channels, specifically TRPC6 and TRPC7 channels (Warren et al., 2006; Sekaran et al., 2007).

In a mouse with genetically ablated rods and cones (*rd/rd cl*), approximately 30% of the ocular transcriptome is transiently regulated in response to nocturnal light exposure (3112 genes). A total of 163 of these genes were associated with the ‘‘intracellular signaling’’ gene ontology term. On the basis of their similarity to invertebrate phototransduction genes, 14 were selected for further study. Laser capture microdissection demonstrated that eight of these genes (Gnas, Gnb2l1, Gnaq, Prkcz, Pik3r1, Inadl, Slc9a3r1, and Drd1a) colocalized with melanopsin (Peirson et al., 2007). The impact of genetic ablation of one of these genes, protein kinase C zeta (Prkcz), was assessed. Prkcz2/2 animals show attenuated phase-shifting responses to light, reduced period lengthening under constant light, and attenuated pupillary responses at high irradiances, as well as impaired light-induced gene expression in the suprachiasmatic nuclei (SCN). These attenuated responses are indistinguishable from the deficits observed in melanopsin knockout mice (Peirson et al., 2007). The further study of the genes candidates might provide an improved understanding of the molecular processes underlying nonvisual photoreception in the mammalian retina and the melanopsin signaling pathway (Peirson et al., 2007).

Until now, it has been a dogma that the PLR in mammals generally requires neuronal circuitry connecting the eye and the brain. It has been reported by Xue et al at 2011 that melanopsin signaling exists in both iris and retina, involving a *PLCβ4*- mediated pathway that nonetheless diverges in the two locations. While intrinsic component of the PLR requires

melanopsin, it also requires *PLCβ4*, the vertebrate homolog of the Drosophila NorpA phospholipase C mediating rhabdomeric phototransduction. The *Plcβ4*−/− genotype, besides removing the intrinsic PLR, also essentially eliminates the intrinsic light response of the M1-subtype of melanopsin-expressing, intrinsically-photosensitive retinal ganglion cells (M1-pRGCs), by far the most photosensitive pRGCs and with the largest responses. Ablating in mouse the expression of both *TRPC6* and *TRPC7*, members of the TRP channel superfamily, likewise essentially eliminated the M1-pRGC light response, but spared the intrinsic PLR Xue et al., 2011).

1.3.6 Role of melanopsin in health

The discovery of melanopsin photosensitive retinal ganglion cells (pRGCs) has raised important questions such as how melanopsin contributes to vision or whether its function could benefit people with retinal diseases. The clinical relevance of melanopsin has just begun to be explored.

The fact that the eye has other functions besides image forming could explain the great prevalence of sleep-wake disturbances in patients with progressive degenerative ocular disease. The disruption of circadian rhythms and the disorders of the sleep-wake cycle have been linked with Alzheimer's patients (Glickman et al., 2006), intercontinental travel and jet lag, seasonal affective disorder (SAD), diabetes, cardiovascular disease, obesity, and even cancer (Sahar et al., 2008; Takahashi et al., 2008; Green et al., 2008; Laposky et al., 2008; Reid et al., 2009).

Even the signaling from the pRGCs themselves has most recently been implicated in the exacerbation of migraines by light (Nosed et al., 2010). pRGCs are also compromised in glaucoma (Li et al, 2006; Wang et al, 2008), a disease that affects circadian rhythms secondary to compromising vision (Drouyer et al., 2008). Since exposure to short-wavelength light has a huge impact on mood and vitality, disturbances in the pRGC photoreception can lead to physiological and psychological problems (Klerman et al, 2005; Buijs et al, 2006;).

Blue light exposure acutely increases core body temperature, heart rate (Cajochen et al, 2005), alertness (Cajochen et al, 2005; Lockley et al., 2006) and cognition (Vandewalle et al, 2007). With age, the crystalline lens absorbs more light (Weale et al, 1985; Pokorny et al., 1987; Turner and Mainster, 2008) and the pupil area decreases (Verriest et al., 1971; Yang et

al., 2002); thus, blue light transmission is reduced. This could result in impaired circadian photoreception (Herljevic et al., 2005) and be in part responsible for the changes observed in the sleep-wake cycle and circadian rhythmicity in the elderly (Bliwise et al., 1993; Duffy et al., 1998).

Finally, melanopsin itself has been delivered to the eyes of mice with degenerated rods and cones as one experimental strategy to restore vision. For therapy in human photodegenerations, melanopsin has many advantages like recovery of the PLR and should be a candidate in an attempt to restore vision (Lin et al, 2008). Thus not only may the study of the melanopsin system offer us insights into health and disease, but it may also directly provide tools for therapeutic intervention to restore vision in patients who are completely blind from photoreceptor loss.

1.4 Generation of *C3H/HeN* and *rd/rd cl* mouse models

The *rd* mouse model combines the natural *rd* mutation with gene encoding a diphtheria toxin expressed in cone photoreceptors to induce their degeneration (*cl*- coneless). The *rd* mutation occurs naturally in the beta6 subunit of cGMP phosphodiesterase (Bowes et al, 1990) and is functionally null (Pitter and Baehr, 1991). cGMP phosphodiesterase is essential to the normal functioning of the rod phototransduction pathway and without this enzyme there is a buildup of intracellular cGMP causing apoptotic cell death, possibly through unregulated calcium cation influx (Chang et al, 1993; Lolley et al, 1977). The result of this mutation is severe rod degeneration within the first 4 weeks of life and a rapid secondary cone loss (Carter–Dawson et al, 1978).

The *rd* mutation primarily affects the rod photoreceptors, but it also causes a slow degeneration of cone photoreceptors through secondary mechanisms that remain poorly defined. Although mice with a mutation in the *rd* allele possess no rod photoreceptors after 36 days, 5% of cone photoreceptor nuclei may persist in the retinal periphery until 18 months, although they are morphologically abnormal with no outer segments (Carter–Dawson et al, 1978). No visual responses can be detected in *rd* mice well before 18 months, however as cones persist at this time (even though dysmorphic) it is not possible to be absolutely sure that some responses may occur, albeit well below the detection limit (Provencio et al, 1994; Garcia–Fernandez et al, 1995). Despite the loss of visual function, these mice do indeed maintain circadian light responses, but the lack of any circadian changes throughout the period of cone degeneration has been proposed as a strong argument that cones play a minimal role in this response (Foster et al, 1991; Provencio et al, 1994). It is nevertheless still possible that non-image forming responses, such as the pupil light response (PLR), might be attributed at least in part to the small surviving population of cone photoreceptors.

In order to probe the residual cone issue conclusively (thereby indicating that a novel inner-retinal photoreceptor system was responsible for these light responses), a model was needed in which no cones existed. This was achieved by generating a transgenic mouse that expressed a diphtheria toxin specific to cones which resulted directly in cone loss and back crossing this mouse on to mice homozygous for the *rd* mutation to generate rodless/coneless (*rd/rd cl*) mice (Freedman et al, 1999; Lucas et al, 1999). The *cl* transgene consists of an attenuated form of the diphtheria toxin gene driven by a region of the human red opsin promoter that causes selective lesion of the mouse cones (Wang et al, 1992; McCall et al, 1992; Soucy 1998; Lucas and Foster, 1999). The combined effect of the *rd* mutation and the *cl* transgene also causes the degeneration of both cone classes as murine S-cones also express long wavelength opsin (Banin et al, 1999). Hence in *rd* mice there exist neither rods nor cones (Lucas et al, 1999).

In the *rd* retina there is a complete ablation of rod and outer-segment containing cone photoreceptors by 80 days of age (Lucas and Foster, 1999). However despite this, non-image forming visual responses still remain, including circadian photo-entrainment (Lucas and Foster, 1999) and phase-shifting (Hattar et al, 2003).

An entraining stimulus such as light pulse applied to an animal in constant darkness will shift the onset of the activity rhythm (Pittendrigh and Daan, 19746). However, the amplitude of the shift produced depends on both the signal strength and the circadian time at which it is applied. Light administered early in the subjective night causes a phase delay, and light administered late in the night causes a phase advance, whereas light administered during the subjective day has little effect ,producing a ‘dead zone’ of response. A phase response

curve represents the amplitude of the phase shift response plotted against the time the light pulse was administered across the circadian cycle. Phase shift behavior can be used as a tool to probe circadian function.

Similarly these mice maintain light-evoked suppressions of pineal melatonin (Lucas and Foster, 1999) and pupil constriction (Lucas et al, 2001). The degeneration of the *rd* retina actually continues after 80 days and affects the inner retina, as well as rods and cones (possibly related to the diphtheria transgene). Nevertheless aging studies have shown that circadian responses can still be demonstrated up to 700 days of age in the *rd* mice, at which time there is significant inner retinal degeneration in addition to photoreceptor loss (Semo et al, 2003). These studies suggested that visual responses could be elicited in the absence of photoreceptors and that pRGCs were a major cellular component of non-image forming visual responses.

1.5 RNA interference (RNAi)

1.5.1 The evolution of RNAi (Fig 1.7).

RNA interference (RNAi) is a naturally occurring cellular mechanism whereby gene expression may be regulated at the level of RNA. Although a physiological response, the small size, high specificity and rapid onset of action of RNA interference has also made it a valuable tool for investigations into gene expression in research studies in a variety of mammalian systems. The inner retina, arguably the most accessible part of the CNS, is an ideal model system in which to investigate the effects of RNAi. The pupil response mediated by pRGC activity provides an ideal functional assessment of the melanopsin pathway in mice with no photoreceptors and developing this experimentally is the focus of the work submitted within this MSc thesis.

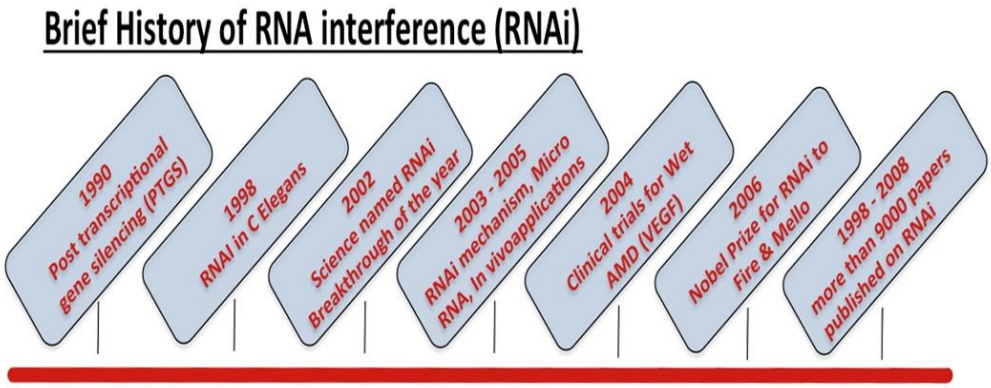

Fig 1.7. Evolution of RNAi. A brief history of RNA interference (RNAi). In the early 1990s, a number of scientists observed independently that RNA inhibited protein expression in plants and fungi. This phenomenon, identified but not understood, was then known as "posttranscriptional gene silencing". In 1998 Fire and Mello observed in Caenorthabditis elegans that double-stranded RNA (dsRNA) was the source of sequence-specific inhibition of protein expression, which they called "RNA interference". In 2002 RNAi was named "breakthrough of the year" by the magazine Science. In 2004 RNAi reached its first clinical study on Age-Related Macular Degeneration (AMD) only six years after ist discovery. From 2003 until 2005 RNAi mechanism and micri-RNAs were described and passed in many *in vivo* applications. Fire and Mello won the 2006 Nobel Prize in Physiology or Medicine for their discovery of RNA interference. From 1998 until 2008 more than 900 papers have been published on RNAi studies.

In the early 1990s, a number of scientists observed independently that RNA inhibited protein expression in plants and fungi. This phenomenon, identified but not understood, was then known as "post transcriptional gene silencing" and "quelling". In 1998 Fire and Mellow observed in Caenorthabditis (C.) elegans that double-stranded RNA (dsRNA) was the source of sequence-specific inhibition of protein expression, which they called "RNA interference" (Fire et al., 1998). While the studies in C. elegans were encouraging at that time, the use of RNAi as a tool was limited to lower organisms because delivering long dsRNA for RNAi was nonspecifically inhibitory in mammalian cells. Fire and Mellow were subsequently awarded the 2006 Nobel Prize in Physiology or Medicine for their discovery of RNA interference. Further studies in plants and invertebrates demonstrated that the actual molecules mediating RNAi were short dsRNA oligonucleotides, 21 nucleotides in length, processed internally by the enzyme "Dicer" (Billy et al., 2001; Hutvagner et al., 2001). The Dicer cleavage products were referred to as "short interfering RNA" now popularly known as "siRNA". Subsequently in 2001, it was demonstrated that siRNA could directly trigger RNAi in mammalian cells without evoking nonspecific effects, thereby producing a highly effective and precise gene silencing (Bernstein et al., 2001).

Since the discovery that siRNAs can enter the RNAi pathway and mediate gene knockdown, researchers have invested considerable effort in optimizing the technology for functional genomics studies. As is the case with most new technologies, the transition of RNAi into a research tool has had its obstacles. Initial problems associated with inconsistent siRNA functionality were addressed by detailed studies that identified functional attributes associated with duplex performance. (Khvorova et al., 2003; Reynolds et al., 2004). More recently, widespread, nonspecific effects that complicate the interpretation of data generated

from siRNA-mediated knockdown studies have been observed. Non-specific effects resulting from the introduction of siRNA appear to have three separate origins, the lipid-mediated response (Fedorov et al., 2005), the interferon response (Sledz et al., 2003) , and the RISC-dependent off-target effects (Jackson et al., 2003; Semizarov et al., 2004; Scacheri et al., 2004; Snove et al., 2004; Jackson et al., 2004). Considerable research on off-target effects found that a combination siRNA pooling strategies, chemical modifications, and novel rational design filters can significantly reduce off-targets without jeopardizing on-target gene knockdown. siRNA design and chemical modification can potentially reduce off-target effects, the differences in transcript regulation between species will necessitate a paradigm change in the clinical development of therapeutic siRNAs (Jackson et al., 2010 review).

Today we have a greater understanding of the components that are part of the RNAi pathway, the efficiency with which these components function, the specificity of sequence recognition and cleavage of cellular mRNA and many of the key requirements for designing and generating extremely effective RNAi sequences. All these offer optimism for RNAi becoming a therapeutic reality to treat human disease in the coming decades.

1.5.2 RNAi and Medicine

In only 8 years from its discovery, RNAi reached clinical trials. Although it is difficult to introduce long dsRNA strands into mammalian cells due to the interferon response (an immunological mechanism evolved to combat retroviruses which use dsRNA) the use of short interfering RNA (siRNA) has been more successful (Paddison et al., 2002). Among the first applications to reach clinical trials were to develop a treatment for macular degeneration. (Kaiser et al., 2010). At the first a single intravitreal dose of Sirna-027 was well tolerated in patients with CNV resulting from neovascular AMD that had been refractory to other therapies. Stabilization or improvement in visual acuity and foveal thickness was observed while no dose-response or dose-limiting effects were noted (Kaiser et al., 2010). The former highlighting the therapeutic benefits of targeting the eye as intravitreal injections are well tolerated and can present high local concentrations of RNA to the retina.

RNAi has also been shown to be effective in the reversal of induced liver failure in mouse models (Zender et al., 2003). There are many ongoing clinical trials of RNAi-based therapeutics, including HIV virus, Hepatitis A and B, neurodegenerative diseases such as Huntington's disease. RNA interference is also often seen as a promising way to treat cancer by silencing genes differentially upregulated in tumor cells or genes involved in cell division (Izquierdo et al., 2005). The future of antiviral RNAi therapeutics is very promising.

1.5.3 RNAi pathway

RNAi is a cellular pathway of gene silencing in a sequence-specific manner at the mRNA (messenger RNA) level (Fig. 1.8). The basic mechanism behind RNAi is the breaking of a dsRNA (double-stranded RNA) template matching a specific gene sequence into short pieces of RNAs called siRNA (small interfering RNA). siRNAs are 21–23 nt (nucleotides) dsRNA duplexes with symmetric 2–3 nt 3' overhangs and 5'-phosphate and 3'-hydroxyl groups, which trigger the degradation of complimentary mRNA matching its sequence (Cioca et al, 2003). Interference of gene expression by siRNA is now recognized as a naturally occurring biological strategy for silencing alleles during development in plants, invertebrates, and vertebrates (Dykxhoorn et al., 2003).

RNA silencing occurs in a broad range of eukaryotic organisms including fungi - where is known as quelling (Fulci and Macino, 2003), animals (RNAi), and plants (PTGS, Post-Transcriptional Gene Silencing). In all these organisms, the process is triggered by dsRNA and requires a conserved set of gene products. The mechanism for RNA silencing (Fig 1.8) involves the chopping of dsRNA into smaller pieces of a defined length corresponding to both sense and antisense strands of the target gene by the RNAse-III (Ribonuclease-III) family member, Dicer in an ATP-dependent reaction. Dicer chops dsRNA into two classes of smaller RNAs—miRNAs (microRNAs) and siRNAs—that are around 21–23 nt in length. Dicer delivers the siRNAs to a group of proteins called the RISC (RNA-Inducing Silencing Complex), which uses the antisense strand of the siRNA to bind to and degrade the corresponding mRNA, resulting in gene silencing (Yu et al, 2002). There is a

strict requirement for the siRNA to be 5' phosphorylated to enter into RISC, and siRNAs that lack a 5' phosphate are rapidly phosphorylated by an endogenous kinase. Although the uptake of siRNAs by RISC is independent of ATP, the unwinding of the siRNA duplex requires ATP. Once unwound, the single-stranded antisense strand guides RISC to mRNA that has a complementary sequence, which results in the endonucleolytic cleavage of the target mRNA. The target mRNA is cleaved at a single site in the centre of the duplex region between the guide siRNA and the target mRNA, 10 nt from the 5' end of the siRNA for degradation (Dykxhoorn et al, 2003).

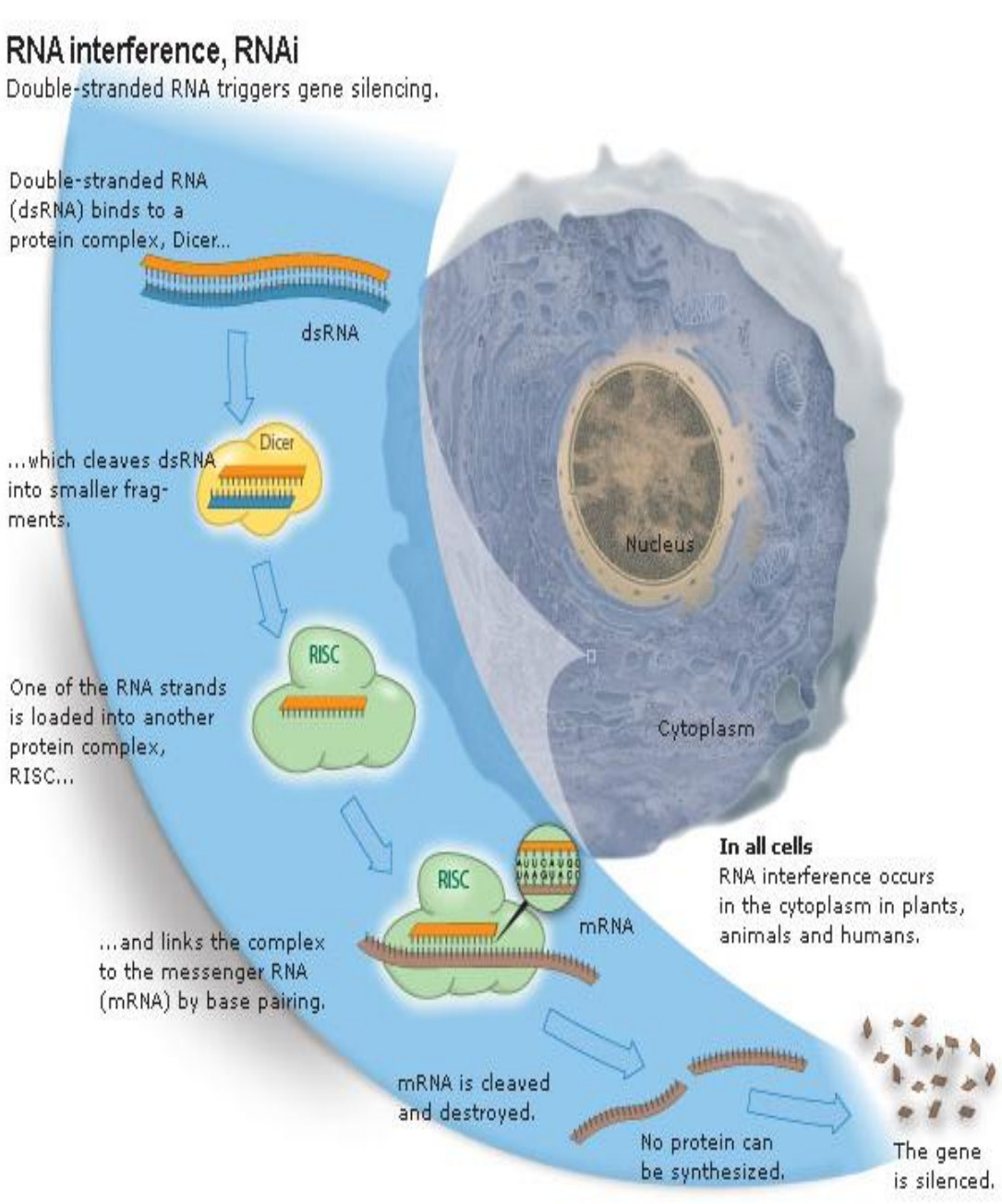

Fig 1.8 RNA interference mechanism: ds RNA binds to Dicer which cleaves it into smaller fragments. The protein complex RISC then loads one of the strands as a template which is used to identify and extinguish mRNA of the matching complimentary sequence, thus achieving gene-specific silencing (Adapted from Fire & Mello, 2006 Nobel Lecture).

1.6 General aims

The general aims of the work in this thesis are to:

- develop an RNAi based method for identifying the genes that express proteins in the intracellular cascade that are critical to melanopsin (Opn4) induced light sensitivity.
- explain the functional diversity observed between different subsets of pRGCs and the specific contributions of *Opn4L* and *Opn4S* isoforms to the different functional responses observed from individual pRGCs.
- investigate siRNA techniques applied to mice lacking rods and cones, similar to end stage retinitis pigmentosa through intravitreal delivery to the eye
- investigate the pharmacokinetics of the siRNA elicited effect, specifically how long it would take to become maximal and for how long the silencing effect might be seen *in vivo*.
- compare the consensual pupillary reflex between the transgenic strains *C3H/HeN rd* and *rd/rd cl*

Analytically, developing an RNAi based method for identifying the genes that express proteins in the intracellular cascade that are critical to melanopsin (Opn4) induced light sensitivity is one of the main targets of this thesis. The non-image forming visual responses, mediated by pRGCs in the retina devoid of photoreceptors, provide the ideal system in which to probe this response with RNAi. The rapid onset but short half life of RNAi makes the PLR a more practical response than assessment of circadian function with which to probe the Opn4 pathway, which remains poorly defined.

Since Opn4 can impart light sensitivity to any neuronal cell under certain circumstances, the molecule may also have therapeutic potential if ectopically expressed in the degenerate retina in cases where photoreceptors are lost (Melyan et al., 2005). The demonstration that subretinal electronic retinal implants can restore sight in patients who are blind from retinitis pigmentosa is a clear demonstration that bipolar cells can be reactivated and relay light impulses back to the visual cortex long after photoreceptor degeneration (Zrenner et al., 2011). From the therapeutic perspective, it is therefore of potential clinical interest to identify the other molecules involved in the *Opn4* light induced transduction cascade. The complexity of the melanopsin signaling pathway also offers a potential mechanism to explain the functional diversity observed between different subsets of pRGCs and the specific contributions of *Opn4L* and *Opn4S* isoforms to the different functional responses observed from individual pRGCs. It would therefore be of great interest to evaluate the contribution of each isoform to more complex behavioral responses such as pupillary light responses. Indeed previous work by Liao and Yau (2007) has shown that polyethylenimine targeting of shRNA against melanopsin can abolish pupillary responses to bright light in wildtype mice. Although that work was suboptimal as there was only small effect size, due to the large rod/cone contribution to the PLR (Liao and Yau, 2007). To provide a more robust system within which to assess pupil changes, we therefore decided to investigate siRNA techniques applied to mice lacking rods and cones, similar to end stage retinitis pigmentosa. With this system we would have a much stronger *in vivo* silencing effect. Indeed optimal siRNA silencing might be expected to inhibit pupil constriction in these mice completely. We also wanted to investigate the pharmacokinetics of the siRNA elicited effect, specifically how long it would take to become maximal and for how long the silencing effect might be seen *in vivo*.

Pupillometry was also used to compare the consensual pupillary reflex between the transgenic strains *C3H/HeN rd* and *rd/rd cl*. The consensual reflex is much more reliable in these tests as it is not directly illuminated and direct heat effects can therefore largely be excluded. Furthermore the eye imaged is not the same eye that receives the intravitreal siRNA injection which removes any effects of low grade inflammation (uveitis) on pupil movements. By comparing the *rd* mice to the rodless and coneless *rd/rd cl* mice, we were able to determine if the residual cone cell bodies of the *C3H/HeN* might be contributing to the pupillary light reflex. The transgenic strains were also compared anatomically using SLO imaging to evaluate the phenotype and confirm visible retinal degeneration in all mice suitable for our experiments.

We generated siRNA probes against the long, short and pan-Opn4 transcript variant of murine Opn4 mRNA and first tested these probes on the murine Neuro2A (N2a) cell line. Mice on the *C3H/HeN* background harboring the *rd* mutation were aged to 80 days. At this time point virtually all surviving cone cells are lost – similar to end-stage retinitis pigmentosa in humans and the mouse is almost exclusively dependent on the Opn4 pathway for light sensitivity. After *in vitro* characterization siRNA was given by intravitreal injection into one eye and was assessed *in vivo* with molecular analyses and immunolabelling at 1, 3 and 5 days to determine the siRNA effect. To confirm the level of knockdown we used molecular analysis with RT-qPCR and immunohistochemistry.

Finally we sought to probe further the mechanism of Opn4 mediated light sensitivity (including the different isoforms) by siRNA medicated knock down of the pupillary light response the aged *rd* and *rd/rd cl* mice strains.

Chapter 2: Methodology and Materials

This chapter details the specific methodologies used in this thesis. All experiments were carried out based in these protocols unless otherwise stated in the chapter. All animal care and experimental procedures were performed with the approval of the Oxford University Institutional Animal Care and Use Committee and in accordance with the UK/ British Home Office Animals (Scientific Research) Act, 1986. All efforts were made to minimise suffering.

2.1 Animal Methodology

All data in this study were obtained from two retinal degenerate mice models which were used in this thesis: a *C3H/HeN* carrying the *rd* mutation (Charles River) and a rodless/coneless *(rd/rd cl)* mouse model on a *C3H/HeN* background. All the models were aged more than 80 days to allow sufficient time for degeneration of any residual cone photoreceptor cells (Lucas et al., 2001).

All animal care and experimental procedures were performed with the approval of the Oxford University Institutional Animal Care and Use Committee and in accordance with the UK/ British Home Office Animals (Scientific Research) Act, 1986. All animals were killed by cervical dislocation according to Schedule 1 of the UK Home Office Animals (Scientific Procedures) Act 1986. Eyes were removed immediately after death, punctured at the limbus and a slit cut was made in sclera to remove the cornea, lens and vitreous, prior to fixation in 4% paraformaldehyde as required. The eyes were either processed for immunohistochemistry for the visualization of pRGCs or retina dissected and snap frozen on dry ice at -80° C for q PCR.

During the conducted experiments and were was needed mice were anesthetized by intraperitoneal injection of 1 mg/kg medetomidine (Dormitor 1 mg/mL; Pfizer, Sandwich, UK) and 60 mg/kg ketamine (Ketaset 100 mg/kg; Fort Dodge, Southampton, UK). Animals were recovered by intraperitoneal injection of atimpamezole 1 mg/kg (Antisedan, 5 mg/ml, Pfizer, Sand- wich, UK).

2.2 Molecular Biology

2.2.1 RNA Isolation

To obtain RNA from frozen retina tissue, the All Prep RNA/Protein kit from Qiagen was used. All centrifugation and mixing steps were performed at room temperature. To ensure an RNase free working environment, all surfaces and instruments were cleaned with RNaseZap (Ambion).

Retinas of *C3H/HeN* and *rd/rd cl* mice were thawed on ice and were homogenized with a pestle in 500µl of Trizol Reagent for 20-40 seconds and incubated in room temperature for 5 minutes. The sample was transferred to a new DNase Free tube and 0.2µl per 1.0ml of Trizol Reagent was added. The samples were vortexed and homogenization was continued at RT for 5 minutes. The samples were centrifuged at 12000 rpm for 10 minutes. The upper aqueous phase was transferred to a new tube and the volume was measured.

2.2.2 RNA Purification - DNase Treatment

Immediately after completing the above step, 1 ml volume of 70% ethanol was added and mixed well by pipetting. Up to 700ml of sample was then pipetted into an RNeasy spin column which was placed within a 2ml collection tube. The samples were centrifuged at 10,000 rpm for 1 minute and the flow through discarded. Following the Qiagen instructions, 350µl of wash buffer RW1 was added to each sample, centrifuged at 10000 rpm for 15 seconds and the flow through discarded.

To perform DNase digestion, 80µl of DNaseI incubation mix (made by adding 10µl of DNaseI stock solution to 70µl of buffer RDD) was added directly to the spin column membrane and incubated at room temperature for 15 minutes. 350µl of wash buffer RW1 was then added and centrifuged at 12000rpm for 15 seconds. The flow through was discarded. 500µl of buffer RPE was added to each sample and centrifuged at 12000rpm for 30 seconds. The flow through was discarded. Another 500µl buffer RPE was added to the samples and centrifuged at 12000rpm for 30 seconds (to dry the membranes). The flow through and collection tubes were discarded. The spin columns were placed in a new 2ml collection tube which were then centrifuged full speed for 1 minute to eliminate any residual ethanol. The collection tubes were discarded. To elute the RNA, the spin columns were placed in a sterile, RNase free 1.5ml microcentrifuge tube, 30µl of RNase free water was added and the samples were centrifuged at 12000rpm for 1 minute. The RNA was quantified (section 2.5.2) and sample stored at -70^{O}C

2.2.3 Quantification of RNA

Absorbance measurements were made on a nanometer /spectrophotometer of all molecules in the sample at the wavelength of interest. Since nucleotides, RNA, ssDNA, and dsDNA all absorb at 260 nm, they will contribute to the total absorbance of the sample. Therefore, to ensure accurate results, nucleic acid samples will require purification prior to measurement.

The ratio of absorbance at 260 nm and 280 nm is used to assess the purity of RNA. For each RNA sample obtained, the nucleic acid concentration and A260/280 ratios were obtained using a Nanometer (NanoDrop™ Spectrophotometer 1000, Thermo Scientific). An A260:280 ratio of 1.8– 2.1 (Fig. 2.1) was considered acceptable.

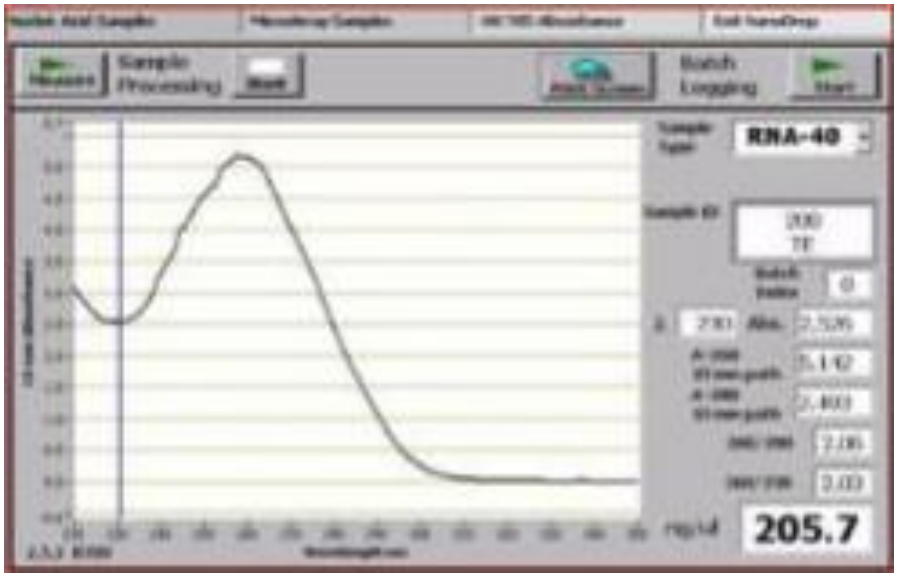

Fig.2.1.Nanodrop absorbance spectra of RNA. This figure illustrates the RNA absorbance spectra of RNA that is pure.

The OD A260/A280 is 2.0. The ratio of absorbance at 260 nm and 280 nm is used to assess the purity of DNA and RNA. A ratio of ~1.8 is generally accepted as “pure” for DNA; a ratio of ~2.0 is generally accepted as “pure” for RNA. If the ratio is appreciably lower in either case, it may indicate the presence of protein, phenol or other contaminants that absorb strongly at or near 280 nm.

2.3 Assessment of gene expression

Quantitative real-time PCR was performed on Applied Biosystems 7500 Real-Time PCR System (Fig. 2.0) using SYBR Green PCR Master Mix. Gene amplification data were analyzed using Applied Biosystems 7500 System Sequence Detection Software version 1.2.3. Results were expressed as n-fold change in expression relative to P0 retinae, using the ΔΔCT method.

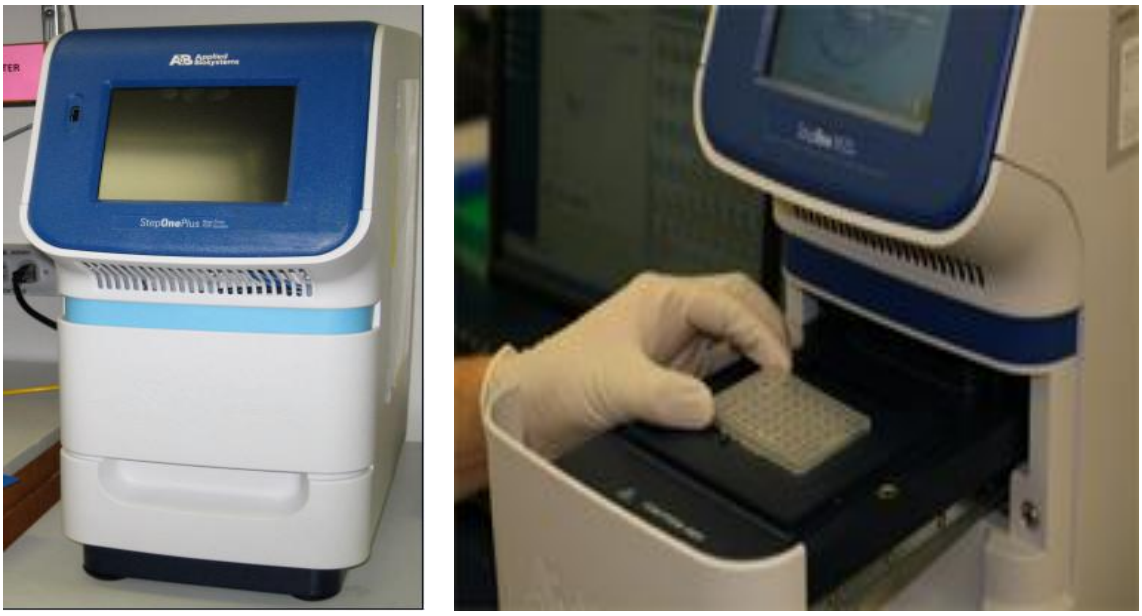

Fig 2.0 The RT-qPCR apparatus (StepOne™ Real-Time PCR Systems, Applied Biogenics) in which all qPCR experiments were contacted. The StepOne System features a 48-well block and 3-color detection.

2.3.1 First strand synthesis

Samples of RNA to be tested were thawed on ice. The following were mixed together: up to 5µl total RNA, 5µl random 6-mer/9-mer Primer and RNA -free water to a total volume of 30.5 µl. The mixture was then incubated at 85^{O}C for 15 minutes and placed on ice for 2 minutes. The cDNA synthesis master mix was prepared in a 1.5ml microcentrifuge tube by adding for each sample: 10µl of First strand buffer, 5µl of 0.1M DTT, 2.5µl of d NTP and 1µl of RNaseOUT Inhibitor. 18.5µl of synthesis mix was added to each RNA / primer mix, mixed gently and collected by brief centrifugation. The samples were incubated at RT for 2 minutes. 1µl Superscript III Reverse Transcriptase was added to each tube and incubated at 25^{O}C for 5 minutes, then at 50 ^{O}C for 1 hour. cDNA was stored at -20^{O}C.

2.3.2 PCR Set Up

The SYBR® Green QPCR Master Mix (Agilent) was used. The master mix contains *Taq*DNA polymerase, dNTPs, and the double-stranded DNA-binding dye SYBR Green I. Each reaction contained 10 µl SYBR, 0.50µl of forward and reverse primer, 8µl of free DNase water and 1 µl of template DNA in a total volume of 20 µl. At always a no template control was run for each gene to confirm the absence of contamination. Real time qPCR assays were carried out in a Real-Time PCR System (Applied Biosystems) consisted of incubation times as follows 65°C for 5 min, 4°C for 2 min, 50°C for 60 min, 70°C for 15 minutes at the recommended annealing temperature of each gene, based on GC and TA ratios.

2.3.3 Analysing results

All quantitative PCR results calculated were relative. That is, the change in the expression of a gene was calculated relative to a pool of reference genes from within the eye and then compared to a similarly normalized sample from the control eye in each experiment.

Quantitative real-time PCR (qPCR), using cDNA synthesized as described above and the primer pairs was performed using Sybr Green I on a StepOne thermal cycler (Applied Biosystems).Relative quantification of transcript levels was performed as previously described (Peirson et al, 2003). Three genes were used for normalization, acidic ribosomal phosphoprotein (ARP), Glyceraldehyde-3-phosphate dehydrogenase (GAPDH) and β-actin, primer sequences were as previously described (Peirson et al, 2004). Results were then also normalised against the geometrical mean of three control genes which are considered to be unchanged between the reference and test samples.

2.3.4 List of primers used for RT-qPCR

Primer sequences were checked against sequences available in the GenBank database, using the Basic Local Alignment Search Tool (BLAST) from the National Center for Biotechnology Information (NCBI,http://www.ncbi.nlm.nih.gov/blast/Blast.Cgi) to check for any possible non-specific binding and amplification.

	Real-Time PCR Primer list Sequences	Tm (^{O}C)
ARP	Forward: CGACCTGGAAGTCCAACTAC	76
	Reverse: ATCTGCTGCATCTGCTTG	
β-actin	Forward: ACCAACTGGGACGATATGGAGAAGA	84
	Reverse: CGCACGATTTCCCTCTCAGC	
GAPDH	Forward: TGCACCACCAACTGCTTAG	82
	Reverse: GATGCAGGGATGATGTTC	
Melanopsin All Isoforms	Forward: TCACAGGGATGCTGGGCAATC	81
	Reverse: TTCTTGTAGAGGCTGCTGGCAAAG	
MelanopsinShort Isoform	Forward: TCACAGGGATGCTGGGCAATC	83
	Reverse: AGTCTGGATCTCGGGATGTAG	
Melanopsin Long Isoform	Forward: TCACAGGGATGCTGGGCAATC	84
	Reverse: GTGACTCTCAGACATCTGTAG	

Table 2.1 Real-Time PCR Primer list Sequences. Sequence and annealing temperature of primers used in RT-PCR analysis (all primers obtained from Invitrogen, UK). All primers were checked for any possible non-specific binding and amplification using BLAST.

2.4 Immunohistochemistry

2.4.1 Fixation and sectioning

Whole eyes were removed and the lens punctured with a fine needle to allow subsequent access of fixative and 30% sucrose in PBS cryoprotectant. Whole eyes were fixed in freshly prepared 4% PFA (Thermo Scientific) diluted with PBS for 24 hours. Eyes were washed in PBS 3 times to remove PFA then placed into 30% sucrose solution for 48 hours. Eyes should sink upon successful penetration of the cryoprotectant. Eyes were washed briefly in PBS to remove excess sucrose from the outside of the eye and then placed into a mould filled with OCT (Sakura Finetek) compound. Moulds containing eyes were then placed onto dry ice, frozen and then stored at -80 C prior to use. Cryostat sections (Leica CM1850 cryostat - Leica Microsystems) were cut at 18μm and collected onto on poly-Llysine coated slides (Thermo Scientific) and stored at -20 C following drying. Slides were air dried for at least 1-2 hours prior to staining to prevent detachment of sections.

2.4.2 Fluorescent Immunolabeling

Fluorescent immunolabelling was performed using standard techniques. Slides were removed from freezer and allowed to dry at room temperature (RT) for at least 1 hour. Sections were drawn around with ‘pap’ pen barrier pen and barrier was allowed to dry completely. Sections were permeabilised by immersion in PBS with 2% Triton-X for 20 minutes. All washes were performed with PBS 0.05% Tween to facilitate uniform spreading of fluid. All slides were background blocked for 1 h at RT in PBS Triton-X containing 5% serum from the same species as the corresponding secondary antibodies. All antibodies were

diluted in PBS Triton-X with 2.5% serum. All wash steps were performed with PBS Tween (0.1%) for 5 min. Incubated with antibodies (1:100) for 1 h at RT, followed by secondary (1:100) for 1 h at RT. Slides were counterstained with 4',6'-diamidino-2-phenylindole dihydrochloride (DAPI) (Invitrogen). Melanopsin anti-mouse polyclonal UF006 antibody (Advanced Targeting Systems, San Diego, CA) PAS8331 anti-*Opn4L* and anti-*Opn4S* antibodies (Pires et al., 2009) were incubated for 1 h at RT diluted 1:100. Alexa-labeled secondary antibodies (Life Technologies) were incubated for 1 h at RT diluted 1:400. Slides were mounted with anti-fade mountant with a DAPI nuclear counter stain (Invitrogen).

2.5 Cell Culture

Neuro-2A cells (ECACC) expressing *Opn4*, *Opn4S* and *Opn4L* stored at -80 degrees were thawed prior to use and cultured in DMEM (Sigma) supplemented with 10% FBS, 1% (v/v) penicillin/streptomycin and 2mM L-glutamine (Invitrogen). All cells were incubated in a humidified chamber at 37°C with 5% CO2, fed fresh media every 2–3 days, and passaged before reaching confluence. Cells were trypsinised, diluted and cultured at 1×10^5 cells per ml in 90 mm dishes for 24 h before transfection.

2.5.1 *In vitro* siRNA Transfection

Transfection of Neuro-2a Cells (ECACC) with *Opn4*, *Opn4Short* and *Opn4Long* siRNA *Opn4* was performed using the Genejuice transfection reagent (Novagen) according to the manufacturer's guidelines.

Neuro-2A cells were seeded at a density of 220-250,000 per 24 well for 24 hours prior to transfection and cultured overnight. Following overnight incubation, cultured cells were 70-75% confluent. Media were removed from cells and replaced with 2ml RPMI-1640 (Sigma) media containing 10% FCS and 1% L-glutamine only without any antibiotics during transfection. For each dish to be transfected 200ml serum free RPMI-1640 was placed into an Eppendorf 1.5 ml tube. 6µl of Genejuice transfection reagent (Novagen) was added per 200 µl of serum free media into the Eppendorf and then briefly vortexed and left to stand at RT for 5 minutes. Plasmid DNA (2µg) was then added and mixed by gentle inversion. Left to stand at RT for 15 minutes to allow DNA reagent complexes to form, gently inverting the tube every few minutes. Transfection solution was added directly to the dishes/wells ensuring an even spread over the culture surface. Cell cultures were incubated for 6 hours. Transfection was evident by 24 hours and optimum transfection levels were observed at 48 hours before RNA isolation.

2.5.2 Cells Immunocytochemistry

Cells were fixed using 4% paraformaldehyde and permeabilized in 0.3% Triton X-100. All blocking and incubation performed in 2% bovine serum albumin, 2.5% goat serum, 0.3% Triton-X 100. Antibody concentrations were 1:5000 anti-Opn4 serum and 1:1000 Alexa 488 Alexa-labeled secondary antibodies (Life Technologies).

2.6 Antibodies

The primary polyclonal antiserum melanopsin antibody UF006 (Provencio et al, 2002) was raised in rabbit against a synthetic peptide consisting of the 15 N-terminal amino acids of mouse melanopsin (GenBank AccessionNP_038915) conjugated to keyhole limpet hemocyanin. Specificity of this antiserum has been confirmed in control studies showing a dose-dependent loss of immunoreactivity by preabsorption with the immunogen and by the lack of immunoreactivity in the retinas of melanopsin-null mice (Panda et al., 2002). The secondary antibody was either Cy3-conjugated or green donkey anti-rabbit IgG (Jackson ImmunoResearch Laboratories, West Grove, PA), for immunofluorescence. We also used a-*TRC3* (1:500, 1:700) (Alomone Labs, Jerusalem, Israel), *Opn4 Long* and *Short* antibodies (Pires et al., 2009).

2.7 Immunofluorescence Microscopy and Analysis

Immuno-fluorescent images were captured using a Carl Zeiss fluorescent microscope to image *Opn4* positive cells with at 20x objective and at excitation 405, 488, and 543 nm with emission wavelengths of 420–450, 505–530, and 550–754 nm for DAPI, green, and red fluorescence, respectively. Photo-montages were made with Image J and Photoshop 6.0 (Adobe Systems).

2.8 Confocal Microscopy

Images were obtained of *Opn4* positive RGCs in cross sections of mouse injected siRNA OPN4 retinas. Retinal sections were viewed on a confocal microscope (Zeiss LSM710). Opn4 positive RGCs were located using epifluorescence illumination before taking a series of XY optical sections. Images were taken with the 40x and 63x oil immersion objective lenses. All are single (nonstacked) confocal images from 30-mm retinal sections, with a depth of field of only 1-2 micrometers. Melanopsin fluorescent immunolabeling is in green and siRNA (red Cy3 fluorescence) labeling is in red. Excitation 405, 488, and 543 nm with emission wavelengths of 420–450, 505–530, and 550–754 nm for DAPI, green, and red fluorescence, respectively. Photomontages were made in Volocity 3D Image Analysis Software (PerkinElmer Inc., Waltham MA, USA) and Photoshop 6.0 (Adobe Systems Inc., San Jose, CA, USA).

2.9 Pupillometry

Monochromatic light stimulations were used to record the consensual pupillary light reflex (PLR). As light source a xenon arc lamp was used with stimulus irradiance, duration and generation under computer control.

A stepper-controlled variable neutral-density filter, a mechanical shutter with a fiber optic and an integrating sphere were also used. An infrared camera documented the stimuli presented to the right eye by evaluating the consensual pupil response of the non-illuminated eye, which was uninjected or injected with scrambled siRNA (non sequenced control). Use of the consensual reflex avoided any confounding influences of intravitreal surgery on the pupil response, as might occur for instance with iritis. The pupil constriction was measured at 2 different wavelengths. At 480nm, which is the maximal wavelength of Opn4 stimulation with light intensity at 14.8 log photons/cm2/s and at the 350 UV wavelength with light intensity at 11 log photons/cm2/s as an internal control (Lucas et al, 2001; MacLaren et al., 2006). Experiments were conducted during the light phase of the normal LD cycle to avoid any effects of circadian variation in the PLR (MacLarenn et al., 2006)

Following dark adaptation for >8 h, during the light phase of the mouse light-dark cycle, unanesthetized mice were held with the right eye facing an infrared camera. The left eye was subjected to a 100-ms duration white light through a light guide from a 100-W xenon arc lamp (LOTOriel) via a Ganzfeld sphere to ensure reproducible and directionally independent full field retinal illumination. The pupil of the stimulated eye was dilated by topical application of tropicamide 1% on the cornea. Stimuli were presented in ascending irradiance controlled by neutral density filters, with completion of recordings at one intensity

at a time for all animals. Animals were left unrestrained in complete darkness for >30 min between exposures in each eye. Pupil area was measured 1.9 s after stimulus offset (ai) (this latency was consistently on the downslope of the initial fast phase of the pupil constriction curve) and was normalized to prestimulus pupil area (a0) for comparisons between individuals. In each group, pupillometry curves were generated before at 24h, 3days and 5 days after siRNA Opn4 intarvitreal injection following the identical protocol.

Data, pupil area and circularity coefficient were collected at a sampling rate of 100 images/sec. Irradiance levels and spectral distribution were monitored with a with a lux meter (Macam Photometrics) or a spectrometer (Ocean Optics Inc). Data were analyzed using Excel (Microsoft, Seattle WA, USA) and Image J (NIH, Bethesda MD, USA). Artifacts in pupil measures, for example due to eye movements were eliminated using the circularity coefficient of the pupil outline to detect eccentric fixation.

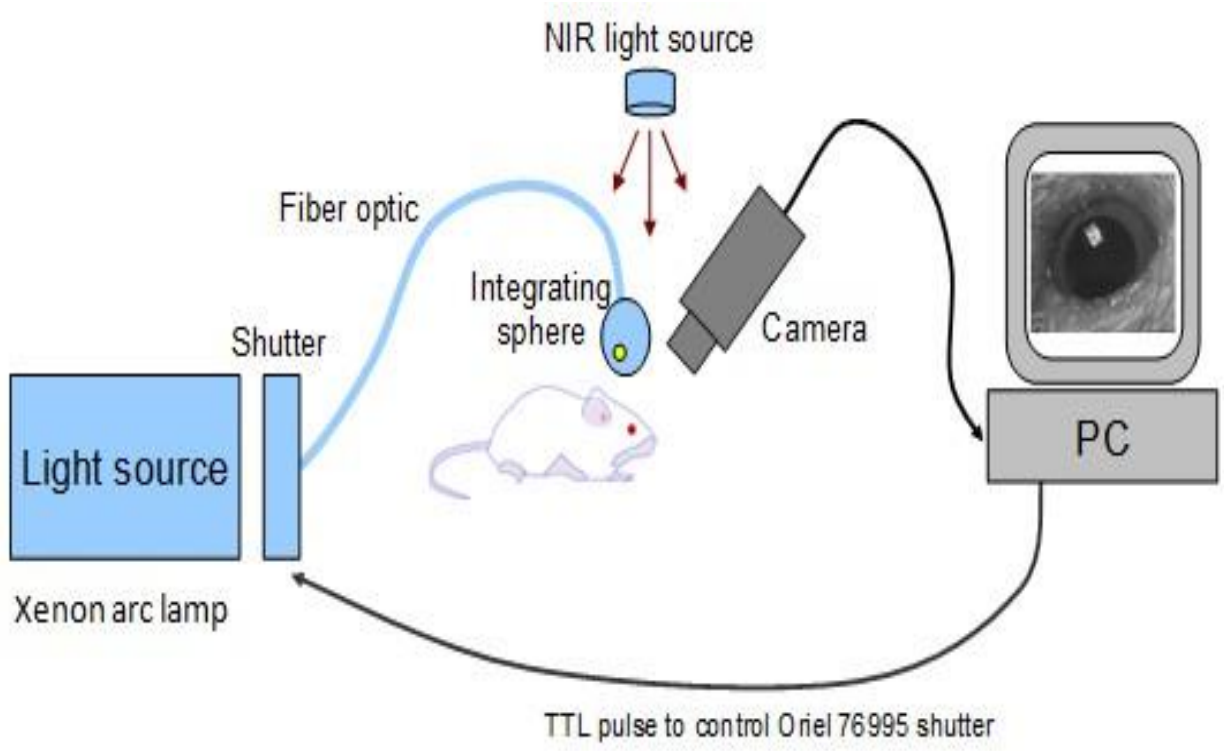

Fig 2.1 Pupillometry experimental set up. The right eyes of unanaesthetised mice were filmed under infrared illumination by a camera fitted with a zoom lens (giving a field of view of 8.7×6.9 mm), positioned in a plane parallel to the pupil. White light was delivered to the eye being filmed through a fibre optic (Leica CLS 100x). After at least 5 hours of dark adaptation, a light stimulus was delivered for 20 s. Animals were subjected to 2 different light intensities presented in ascending order of brightness with at least 2 min between stimulus presentations. note that the infra-red camera and light source are targeted at different eyes.

2.10 Scanning Laser Ophthalmoscope (cSLO)

Fundus imaging was performed under general anesthesia using a confocal scanning laser ophthalmoscope (cSLO; Spectralis HRA, Heidelberg Engineering, Heidelberg, Germany) without any use of fluorophoreand after the procedure the animal were sacrificed according to the UK/ British Home Office Animals (Scientific Research) Act, 1986. Their pupils were dilated with tropicamide (Mydriaticum 1%; Bausch & Lomb, Kingston-on-Thames, UK) and phenylephrine (phenylephrine hydrochloride 2.5%; Bausch & Lomb) eyedrops. A custom-made contact lens was used for all recordings to prevent corneal desiccation and subsequent cataract formation and to improve image quality (PMMA mouse lens, back optic zone radius of 1.7 mm, total diameter of 3.2 mm, center thickness of 0.4 mm, straight sides; Cantor and Nissel, Brackley, UK). Lubricating eyedrops (HypromelloseBPC 0.3%; Matindale Pharmaceuticals, Romford, UK) were used as viscous coupling fluid between the contact lens and the cornea. The near-infrared (NIR) reflectance mode (820 nm laser) was used for camera alignment. For recordings from the outer retina with the optic disc centered in the image, the plane of highest reflectivity was identified. After switching to the autofluorescence mode (excitation wavelength: 488 nm, emission recorded between 500 and 700 nm) and slight focus adjustments (due to the dioptric shift between the different wavelengths), images were recorded using the automated real time (ART) mode. Up to 100 consecutive frames were averaged in real time at a frame rate of 4.8 frames per second, resulting in an improved signal-to-noise ratio. All images were recorded with an intensity resolution of 8 bits/pixel in the high-resolution mode (1536x1536 pixels) using a 55 degree lens. Normalized images (i.e. automatic software enhancement of contrast by histogram stretching) were used to increased contrast.

For image acquisition, the animal was placed on a platform mounted on the chin rest of the imaging device so that its eyes were positioned approximately at the level of the marking for a “human patients” eye position. If prolonged imaging is required, a heat mat can be used to maintain body temperature.

2.11 Intravitreal Injections

Intravitreal injections were performed under general anesthesia in accordance with the UK/ British Home Office Animals (Scientific Research) Act, 1986. A Hamilton syringe with a sharp 34-gauge needle was used to inject 1µl of siRNA into the vitreous cavity through an oblique self-sealing entry site 1–2 mm behind the limbus of the mouse eye and avoiding the lens.

During the conducted experiments and were was needed mice were anesthetized by intraperitoneal injection of 1 mg/kg medetomidine (Dormitor 1 mg/mL; Pfizer, Sandwich, UK) and 60 mg/kg ketamine (Ketaset 100 mg/kg; Fort Dodge, Southampton, UK). Animals were recovered by intraperitoneal injection of atimpamezole 1 mg/kg (Antisedan, 5 mg/ml, Pfizer, Sand- wich, UK).

Were necessary animals were sacrificed according to the UK/ British Home Office Animals (Scientific Research) Act, 1986. All efforts were made to minimise suffering.

2.12 siRNA Preparation

siRNAs were obtained from Dharmacon and Invitrogen. All sequences 5'-3', sense strand only, are as follows: UACOpn4 pan-Melanopsin: UCG CAC UGA UUG UCA UUC UUC, Opn4 Long : GUA GCC UAA GGG GUG ACC, Opn4 Short : UCG CAC AAU CCC AUU AUC. All primers were checked for any possible non-specific binding and amplification using BLAST.

siRNAs probes were stored in 100-500μg pellets (Dharmacon, Invitrogen) which were then diluted as 10 μg/μl stocks. Our injections used 1.2 μg of siRNA diluted in 1 – 2 μl of total volume of injection. siRNAs were removed from the freezer and left 30 minutes at a shaker in RT. siRNA filters were soaked in DCP water for 1 hour in 37^0 C. Washed and spinned 5 times with RNase free water. Glucose was added to the siRNA tubes 10 times the volume of the siRNA probe. For every μg of siRNA, 1μl of invivofectamine reagent was used and added at the siRNA tubes. Centrifuged for 50 minutes in 14,000 rpm at 22^0C. The flow was discarded and centrifuged for 30 minutes, then centrifuged with the filters inverted for 2 more minutes. Then it was frozen until use. Cy3 red and fluorescein green were used as immunofluorescent labels.

2.13. Statistical Analysis

All data are shown ± standard error of mean and statistical analysis was performed using single factor ANOVA and two-tailed unpaired Student's t-Test. Pupillometry results were analyzed using paired two-tailed Student t tests (with Bonferroni correction where appropriate). Quantitative PCR and relative pupil constriction amplitude data were analyzed using one-way ANOVA and Games–Howell post hoc or Mann–Whitney U test as appropriate.

Chapter 3: Results

3.1 *C3H/HeN rd* vs *rd/rd cl*

To investigate retinal function we first established a baseline and examined the pupillary light reflex (PLR) in *C3H/HeN rd* and *rd/rd cl* transgenic mice. A reduced response is observed in many retinal degeneration rodents, including mice (Lucas et al, 2001; Lucas et al, 2003). We were interested to test the response *of C3H/HeN* retinal degeneration mice so we could determine if any one of the strains was more suitable in our project and see if the remaining cones in *C3H/HeN* mice were contributing to the PLR in our specific experimental set up at the 80 day age tested.

3.1.2 *C3H/HeN rd* vs *rd/rd cl c*SLO images

Comparing the strains of transgenic mice we used SLO imaging to compare the gross anatomical differences without the use of any fluorophore. We captered cSLO images comparing the strains of transgenic mice *C3H/HeN rd* vs *rd/rd cl* with the wild type controls at > 80 days. The infrared images provide anatomical information on outer retinal structures including the retinal pigment epithelium (RPE) and choroidal blood vessels. The autofluorescence detects mainly flourophores such as lipofuscin accumulating in the outer retina, which is a measure of normal photoreceptor function and therefore has a more uniform appearance. The infrared image of *rd/rd cl* shows presumed RPE changes and choroidal atrophy which matches a ring of autofluorescence. The cSLO appearance of the *rd* mouse is very similar to *rd/rd cl*, even to the experienced observer. This is in keeping with the observation that the cones degenerate anyway in the *rd* mouse and by 80 days both *rd* and *rd/rd cl* are essentially very similar pathologically. Both *rd* and *rd/rd cl* mice had no obvious gross difference between them however, were markedly different compared to the wild type controls (Fig 3.1). The use of the SLO also provided a useful screening tool to confirm prior to experiments that mice were indeed homozygous for the *rd* mutation.

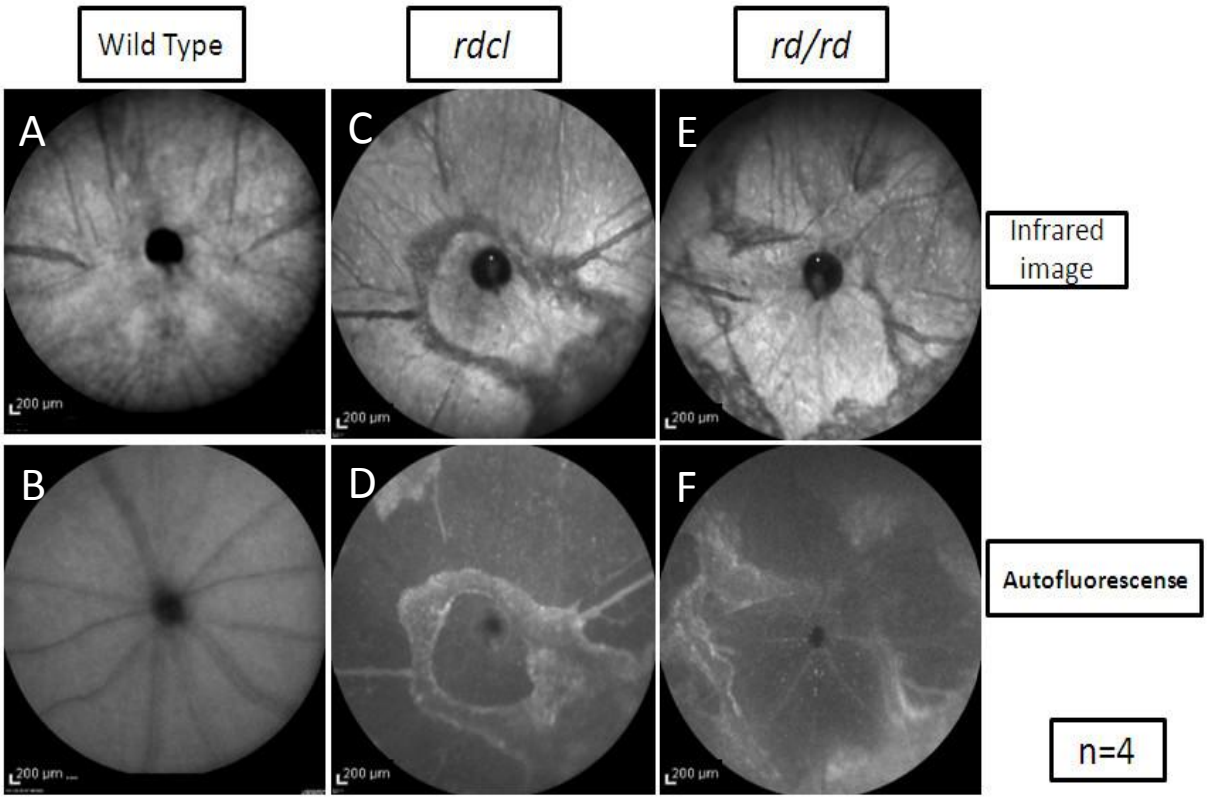

Fig 3.1. cSLO images comparing the strains of transgenic mice *C3H/HeN rd* vs *rd/rd cl* with the wild type controls at > 80 days, representative images of n=4 per genotype. (A) The infrared images providing anatomical information on outer retinal structures including the retinal pigment epithelium (RPE) and choroidal blood vessels. (B) The autofluorescence detecting mainly flourophores such as lipofuscin accumulating in the outer retina. (C) The infrared image of *rd/rd cl* shows presumed RPE changes and choroidal atrophy which matches a ring of autofluorescence. (D). The SLO appearance of the *rd* mouse (E and F) is very similar to *rd/rd cl*.

3.1.3 C3H/HeN *rd* vs *rd/rdcl* pupillometry

The pupil constriction was measured at two different wavelengths and the residual value is quoted as a percentage of baseline (i.e. 100% represents no constriction and 20% represents 80% constriction, etc.). At 480 nm which is the wavelength with light intensity at 14.8 log photons/cm2/s of maximal *OPN4* stimulation and at the 350 nm UV wavelength with light intensity at 11 log photons/cm2/s, which is shifted towards the wavelength of S cone stimulation (largely independent of Opn4). We wanted to investigate if any residual cones (S-cones) contributed to the PLR. In a series of four experiments, we found that the pupil response to 350 nm light in the adult *rd/rd* mice achieved 52% ± 5% pupil constriction, whereas the *rd/rdcl* mice achieved 54% ± 6%, which was not significantly different (t= *unpaired two-tailed t-test, p=0.5, n=4, all data represent mean ± SEM)*. As expected, a much greater pupil constriction response was seen in the *rd* (10%±4%) and *rd/rdcl* mice (20%±5%) to 480 nm light, in keeping with an Opn4 mediated response, but which was also not significantly different between the two strains (*t= unpaired two-tailed t-test, p=0.52, n=4, all data represent mean ± SEM*). Comparing the same strain to the two different wavelengths however revealed a significantly greater pupil constriction in both groups with a more marked reaction to the Opn4 wavelength (*t= unpaired two-tailed t-test, p<0.05, n=4, all data represent mean ± SEM*). Hence we can conclude that there is no difference between the pupil phenotype of *rd/rd* and *rd/rdcl* mice and that both show responses that are consistent with regard to wavelength sensitivity to an Opn4 mediated response. (Fig 3.2)

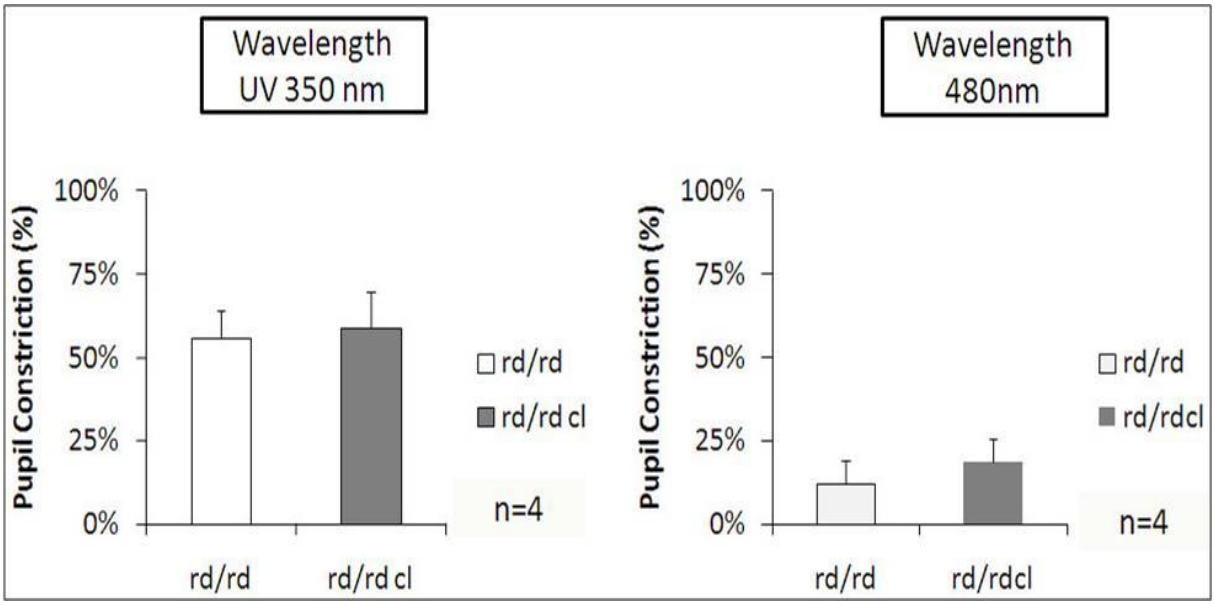

Fig 3.2 Pupillometry data comparing transgenic mice. Illustrates the relative pupil area of the *rd* mice compared with the levels of pupil constriction of the *rd/rdcl* mice. There is no difference between pupil phenotype of *rd/rd* and *rd/rdcl* mice and both show greater responses to the 480 nm (Opn4-specific) wavelength. The pupil area is defined as the area in the light relative to the area measured in the dark. Between strains, *unpaired two-tailed t-test, p=0.5. All data represent mean ± SEM.*

3.2 siRNA Melanopsin (*Opn4*) silencing

We generated siRNA probes against the transcript variant of murine Opn4 mRNA and tested them *in vitro* using cellular models to evaluate RNA knockdown and *in vivo* performing bilateral intravitreal injections into *rd* mice. At this point virtually all surviving cone cells are lost – similar to end-stage retinitis pigmentosa in humans. To confirm the level of knockdown we used molecular analysis with RT-qPCR and immunohistochemistry. We also performed pupillometry so we can assess the behavior of the pupillary light reflex (PLR).

3.2.1 siRNA Pan-Melanopsin (*Opn4*) *in vitro*

We tested the probes that we generated against the *Opn4* mRNA on the murine Neuro2A (N2a) cell line and Rt-qPCR analysis confirmed Opn4 knockdown siRNA *Opn4* (Fig.3.3). Pan-melanopsin refers to an RNA sequence that is present in both isoforms of *Opn4* and hence all splice variants should be silenced.

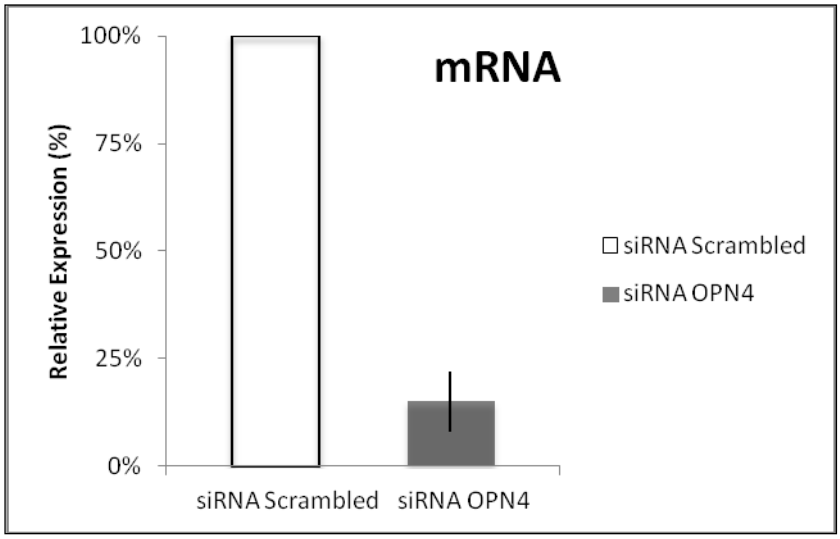

Fig 3.3. siRNA pan-Melanopsin in vitro expression data. Relative quantification of siRNA Opn4 expression plotted relative to the Scrambled siRNA (control). Expression levels of siRNA Opn4 were significantly decreased. Differences in expression were determined by *an unpaired two-tailed t-test, $p<0.01$, $n=4$. All data represent mean ± SEM* (part of experiment performed with Dr Aarti Jagannath).

3.2.2 siRNA Pan-Melanopsin (*Opn4*) *in vivo* – immunohistochemistry

Representative immunostaining photos of the whole retina showing the siRNA delivered to the retina 5 days after intravitreal injections with siRNA. The siRNA *Opn4* is labeled with Cy3 red. A pRGC is labeled in green.

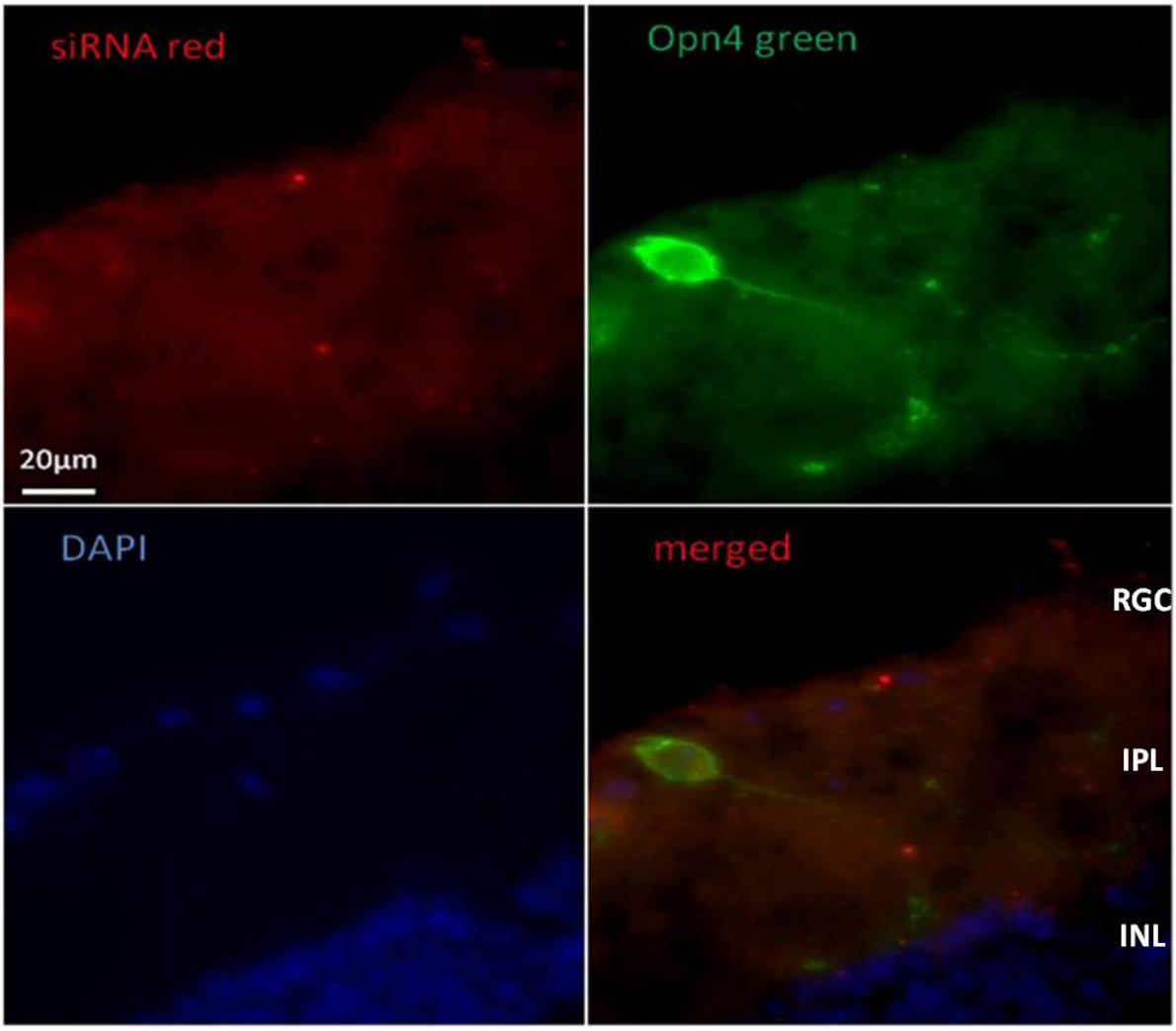

Fig 3.4. siRNA *Opn4* delivered to the retina. This figure illustrates siRNA *Opn4* (red) delivered to the retina and pRGC (green). In the merged image though slightly apparent a positive pRGC penetrated by siRNA at the nucleus of the cell.

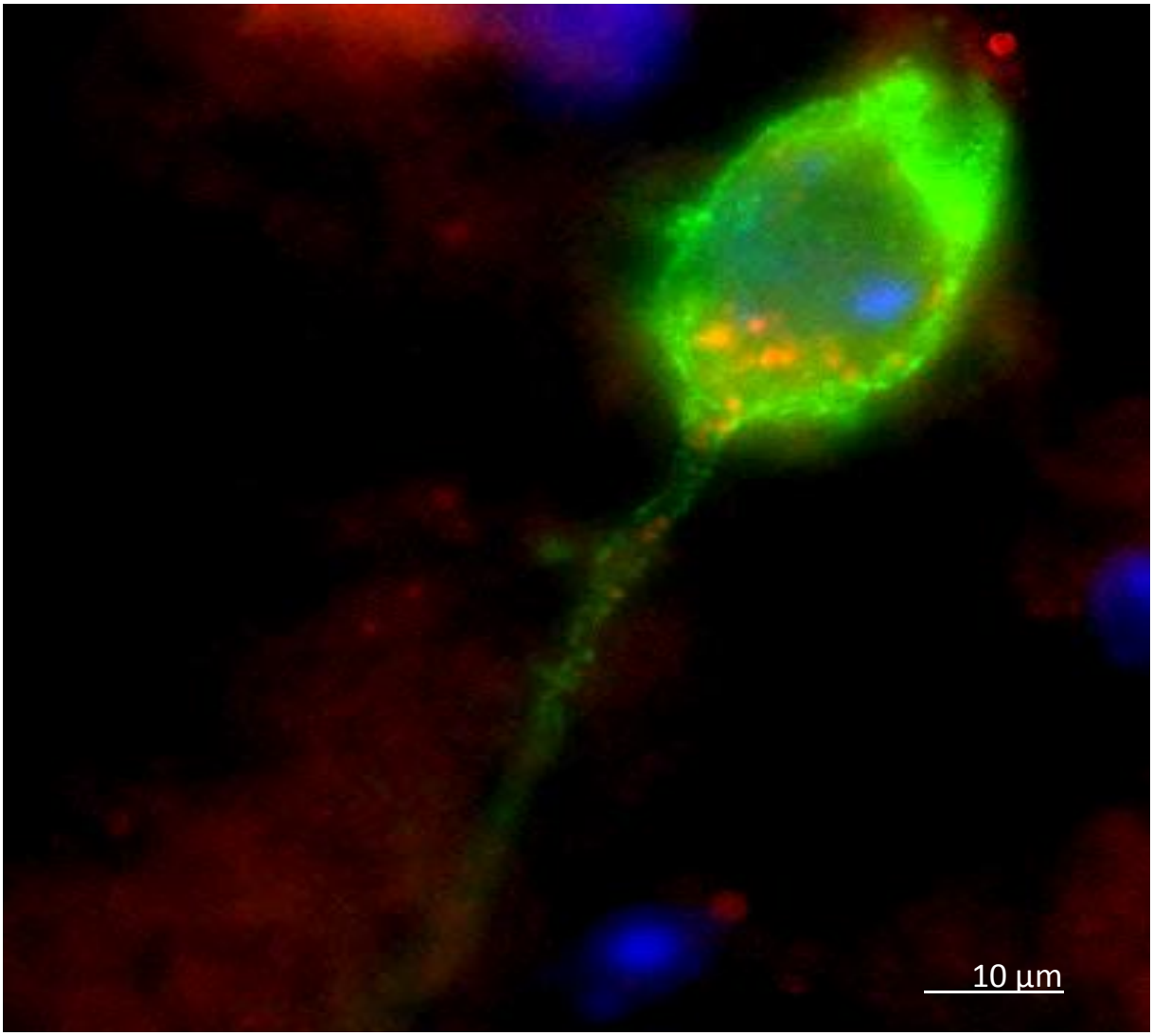

Fig 3.5. siRNA *Opn4* Cy3 molecules penetrated the pRGC. This figure illustrates the siRNA Cy3 red molecules penetrated the melanopsin RGC and are found localized to the translational machinery at the axon hillock, consistent with binding to RNA rich region of the cell (part of experiment jointly supervised by Dr Aarti Jagannath).

3.2.3 siRNA Pan-Melanopsin (*Opn4*) *in vivo* – Pupillometry

The pupil constriction was measured at 480nm which is the wavelength of OPN4 stimulation. We wanted to investigate if any residual cones contributed to the PLR. In a series of four experiments, we found that the pupil response to 480 nm light with light intensity at 14.8 log photons/cm2/s in the *rd* mice injected with siRNA OPN4 achieved 28% ± 5% pupil constriction, whereas the *rd* mice injected with the non-sequenced control siRNA achieved 90% ± 6%. Hence the RNA inhibition virtually completely ablated the pupil constriction response compared to sham treatment (*t= unpaired two-tailed t-test, p<0.01, n=4, data represent mean ± SEM*). (Fig 3.6)

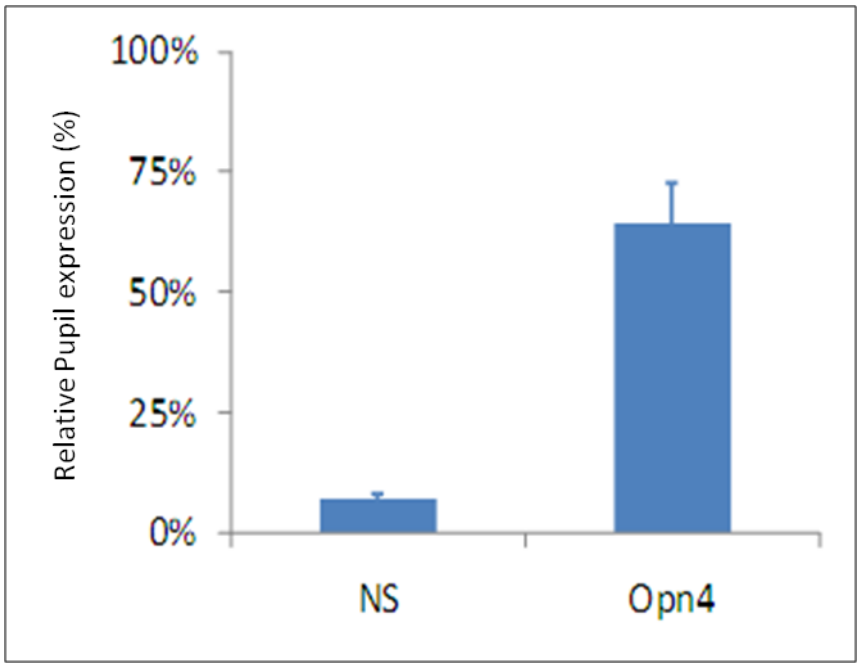

Fig 3.6. Melanopsin *in vivo* – Pupillometry data. The relative pupil area of the siRNA Opn4 injected eyes of *rd* mice compared with the injected with the non sequenced control. The pupil area is the represented as the ratio of the area measured in the light compared to the area measured in the dark. Hence any value below 100% represents a constriction response and comparing the area in the same eye before and after illumination corrects for the anatomical variations in eye size of individual animals (*t=unpaired two-tailed t-test, p=0.005, n=4. All data represent mean ± SEM).*

3.3 *Opn4* silencing time course *in vivo*

We were interested to know the time course of molecular silencing of *Opn4* transcripts *in vivo*. Mice on the *C3H/HeN* background harboring the *rd* mutation were aged to 80 days. At this point virtually all surviving cone cells are lost – similar to end-stage retinitis pigmentosa in humans. Since the pupillometry experiments above revealed virtually identical responses compared to the *rd* mice, we assumed that the most significant component of the PLR at this stage arises from the *Opn4* expressing ganglion cells rather than from any residual cone nuclei. siRNA probes against the transcript variant of murine *Opn4* mRNA were given by intravitreal injection into one eye in each of five animals, which was harvested at 1, 3 and 5 days for molecular analysis so that we could best determine the optimal time course of the siRNA elicited effects at the molecular level (Fig 3.7 - 3.9). This would allow us to then predict the optimal post-injection time to assess any effects on pupillometry. To confirm the level of knockdown we used molecular analysis to measure the time course of the Opn4 mRNA levels. With specific sequenced primers we also able to measure separately the time course of the Opn4 Short and Opn4 Long isoforms mRNA. All time course data are concentratedat at linear graph. (Fig 3.10).

3.3.1 *Opn4* silencing time course

The relative expression of all *Opn4* mRNA levels is maximum at 3rd day but is attenuated by the 5th day following intravitreal injection of 1.2 µg of siRNA *Opn4*. Here the sequence in the siRNA lies in a region of the mRNA common to both *Opn4 Short* and *Opn4 Long* isoforms (Fig 3.7).

A.

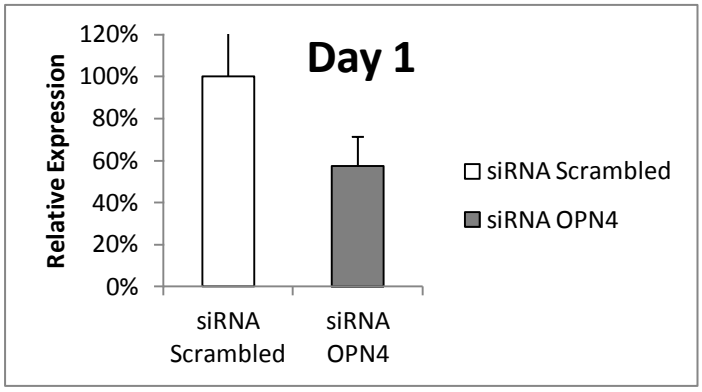

B.

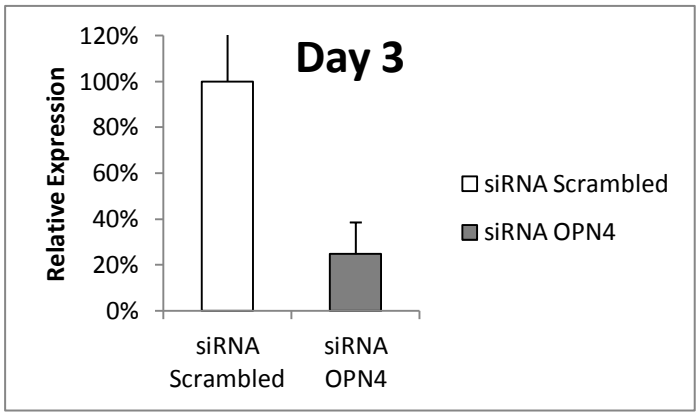

C.

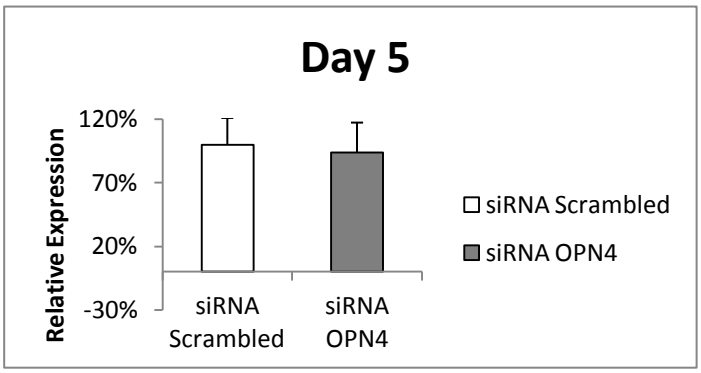

Fig 3.7. *Opn4* silencing time course. Relative quantification of siRNA Opn4 expression in *rd* mice (more than 80 days old) by real time quantitative PCR. Opn4 shows differences in sensitivity to *in vivo* silencing at days 1 and 3, but it is attenuated by day 5. A. Day 1: *t=unpaired Student's t-test, p< 0.05, n=5.* B. Day 3: *t=unpaired Student's t-test, p< 0.05, n=4,* C. Day 5: *t=unpaired Student's t-test, p = 0. 50, n=5. All data represent mean ± SEM* for all 3 timepoints.

3.3.2 Opn4 Short Isoform time course

The relative expression of the *Opn4 Short* mRNA levels show differences in sensitivity to *in vivo* silencing and it is attenuated by day 5 following intravitreal injection of 1.2ug of siRNA *Opn4*. Here the sequence in the siRNA targets a region of the mRNA to *Opn4 short* isoform (Fig. 3.8).

A.

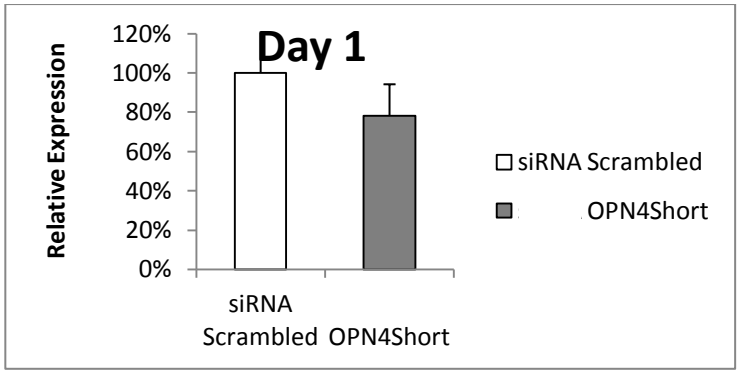

B.

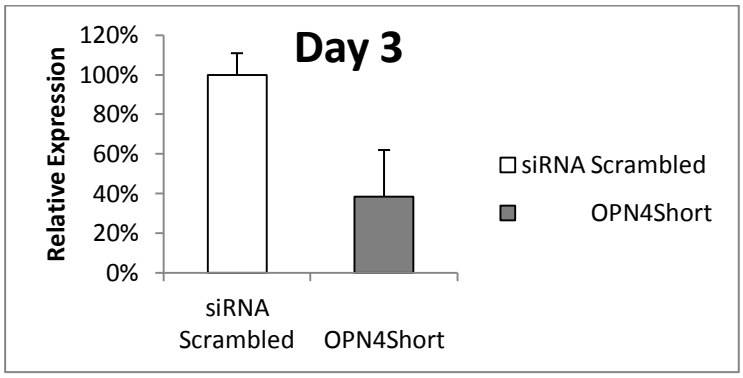

C.

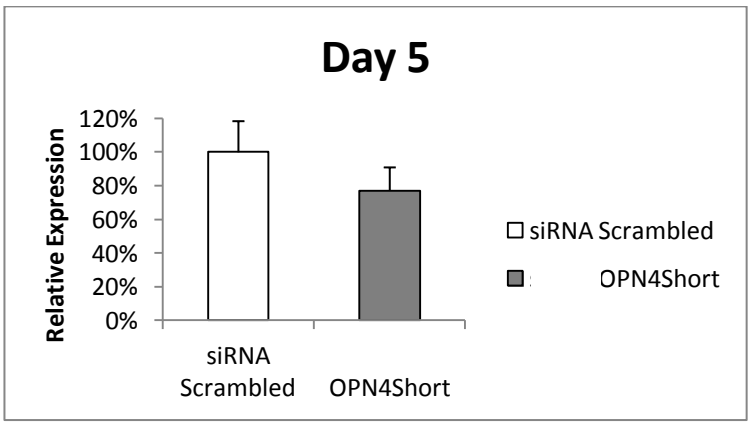

Fig 3.8. *Opn4 Short* Isoform timecourse. Relative quantification of siRNA *Opn4-Short* expression at *rd* mice (more than 80 days old) by real time quantitative PCR. *Opn4 Short* isoform shows differences in sensitivity to *in vivo* silencing but it is attenuated by day 5. Expression levels of siRNA *Opn4* were significantly decreased on day 3. A. Day 1: *t=unpaired Student's t-test, $p < 0.05$, n=5*. B. Day 3: *t=unpaired Student's t-test, $p < 0.05$, n=4*, C. Day 5: *t=unpaired Student's t-test, $p < 0.05$, n=5. All data represent mean ± SEM* for all 3 timepoints.

3.3.3 *Opn4 Long* Isoform time course

The relative expression of the *Opn4 Long* mRNA levels show differences in sensitivity to *in vivo* silencing following intravitreal injection of 1.2 ug of siRNA *Opn4*. Here the sequence in the siRNA targets a region of the mRNA of *Opn4 Long* isoform (Fig. 3.9). The relative expression of the *Opn4 Long* mRNA reaches the highest levels of knockdown in day 5. Hence the effects of the long isoform appear to be more manifest later, possibly due to a longer half-life of the translated protein.

A.

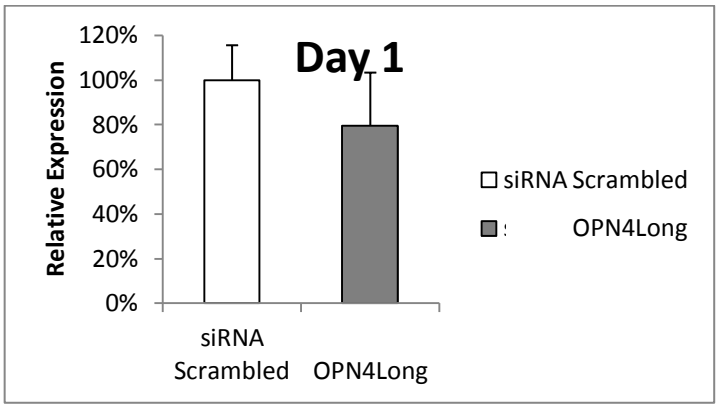

B.

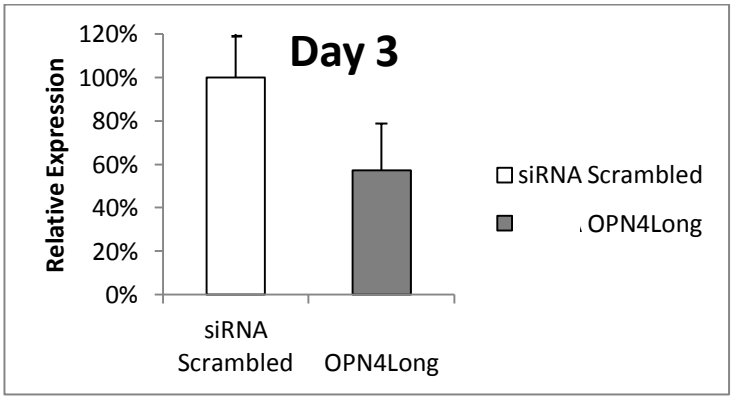

C.

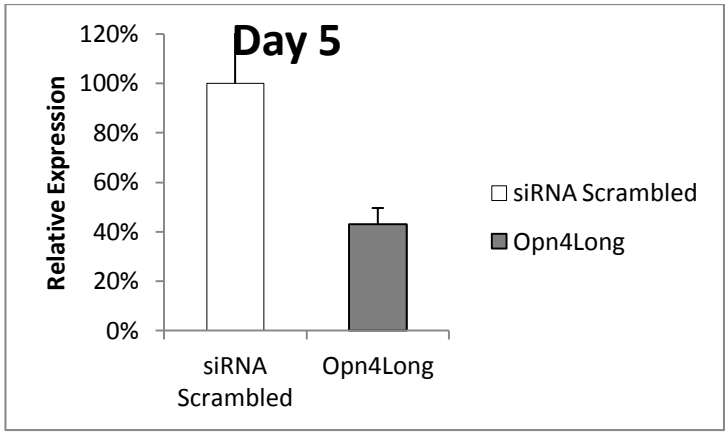

3.9. *Opn4 Long* Isoform time course. Relative quantification of siRNA *Opn4 Long* expression in *rd* mice (more than 80 days old) by real time quantitative PCR. *Opn4 Long* shows differences in sensitivity to *in vivo* silencing reaching highest levels by day 5. A. Day 1: *t=unpaired Student's t-test, p <0.05, n=5*. B. Day 3: *t=unpaired Student's t-test, p<0.05, n=4*, C. Day 5*: t=unpaired Student's t-test, p<0.05, n=5. All data represent mean ± SEM* for all 3 timepoints.

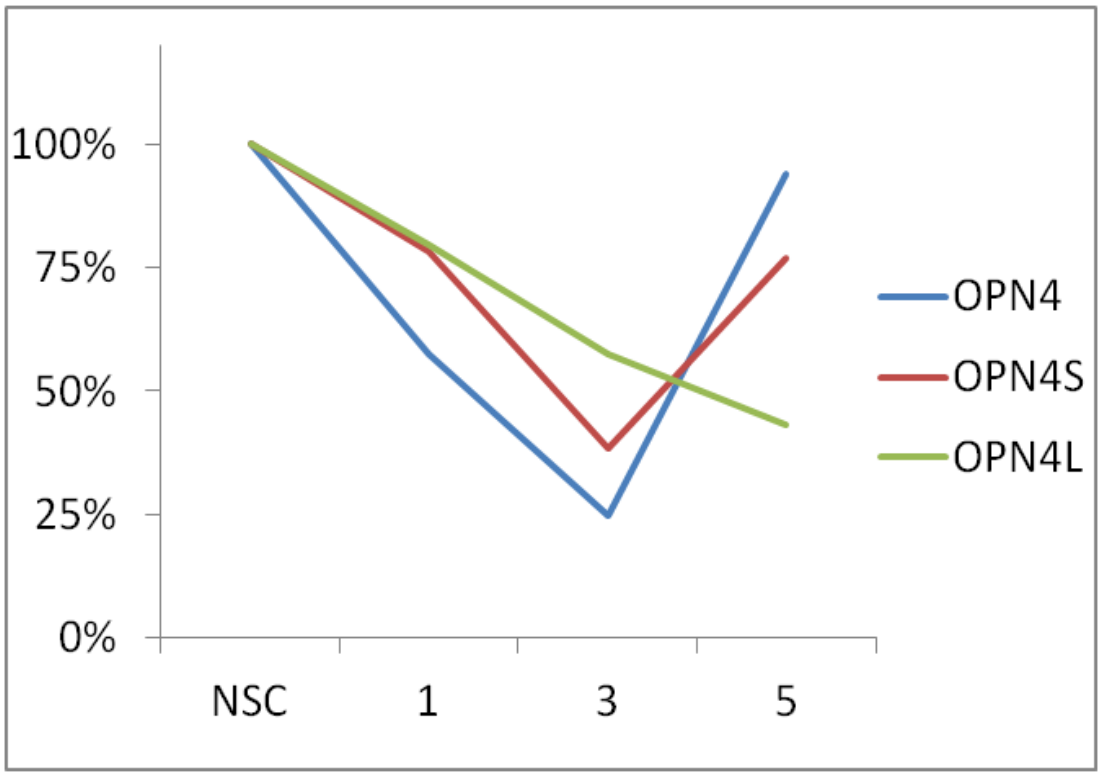

Fig 3.10. *Opn4* silencing time course *in vivo* linear graph summarizing the above knockdown data. The post-siRNA injection *Opn4* levels time course in all 3 time points are seen (Day 1, Day 3 and Day 5). *Opn4* and *Opn4 Short* shows differences in sensitivity to *in vivo* silencing but both are attenuated by day 5. *Opn4 Long* reaches highest levels of knockdown in day 5. Across the whole group, significant differences were determined by *a one way ANOVA, $p<0.05$. Data are plotted as ± mean expression* relative to the non sequence control (NSC). NSC = non-sequenced control siRNA; y axis = percentage from baseline; x axis = days.

3.3.4 *OPN4* timecourse – Immunopositive cells

Having identified the molecular basis of the Opn4 silencing we wished to see if this effect was also seen with regard to protein translation as detected by immuno-histochemistry. In order to avoid variability I sectioned eyes vertically through the optic nerve at 18 microns and selected five sections which had been cut sagittally through the optic nerve head. All melanopsin staining cells were counted from ora to ora and the total number of cells in five sections was calculated following sacrifice of 3 animals at each of the 3 time points of 1st, 3rd and 5th day to estimate a mean number.

By comparison to intravitreal injections of scrambled siRNA in the control eyes, I was able to calculate the number of *Opn4* positive cells as follows: day 1 (d1) – control = 209 ± 4, siRNA *Opn4* = 165 ± 5 (79,1% ± 2.4%); day 3 (d3) – control = 210 ± 7, siRNA *Opn4* = 134 ± 1 (63.8% ± 0.5%); day (d5) – control = 208 ± 13, siRNA *Opn4* = 167 ± 8 (80.0% ± 3.6%). It was difficult to quantify the intensity of straining between treated and control eyes as it looked similar. The reduction in cell counts observed therefore most likely represents a reduction in protein to below the threshold which was detectable with the naked eye using the antibody staining technique.

Alternatively it is possible that complete silencing is achieved in some ganglion cells but not in others, where *Opn4* protein production still occurs despite presumed reduction in mRNA transcripts. It is however apparent that the time course of the reduction in *Opn4* cell counts detected by immunostaining mirrors closely that observed with the mRNA assessed by RT-PCR and that *in vivo* silencing produces maximum *Opn4* silencing on the 3rd day. Hence there is good correlation across all three methods. A fluorescent microscope (Zeiss Axioskop) was used to image melanopsin positive cells with a 20x objective according to protocol.

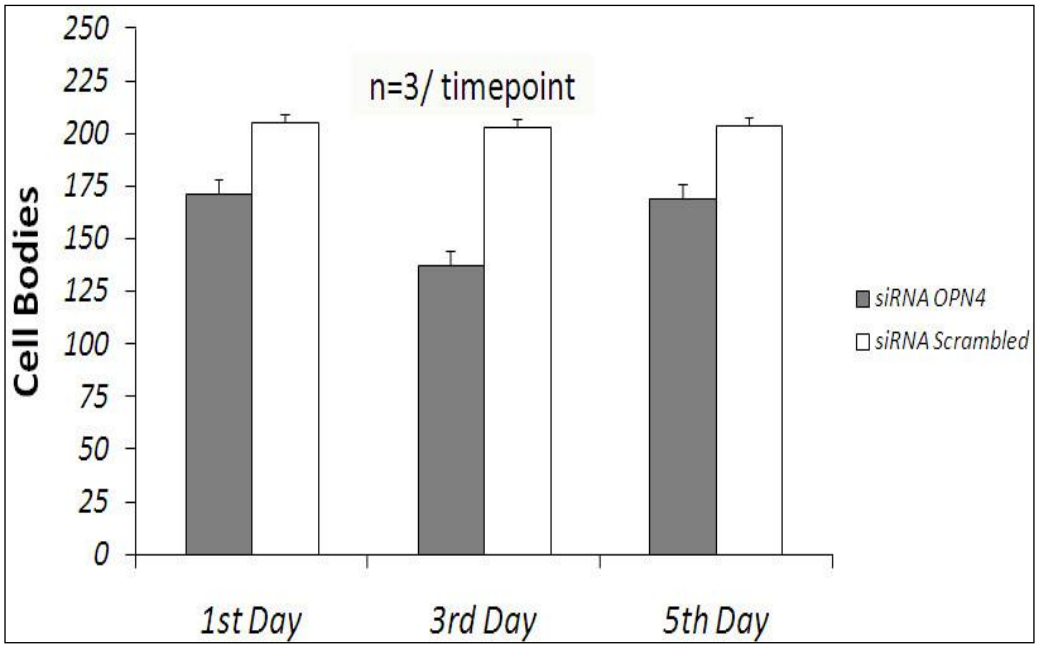

Fig 3.11. Opn4 time course – Immunopositive cells. Cell counts of immunopositive *Opn4* cells taken as a mean value per animal from five sagittal sections through the optic nerve head and stained for Opn4 using melanopsin anti-mouse polyclonal UF006 antibody (Advanced Targeting Systems, San Diego, CA). Counts were made successfully using fluorescent microscope according to the protocol. *In vivo* silencing results in a drop *in Opn4* cell counts by the 3rd day, but a partial recovery by 5, in keeping with a transient reversible rather than toxic effect. The data are plotted in comparison with the controls (Scrambled siRNA).

3.3.5 Immunohistochemistry - Confocal microscope images

Representative immunostaining confocal microscope image swere captured showing that the siRNA delivered to the retina reaches the pRGCs, as evidenced by red markers (Cy3 label) visible in the ganglion cell layer.

This figure illustrates siRNA Opn4 (Cy3, in red) delivered to the retina (DAPI, inner nuclear layer labeled in blue) and to the pRGC (Opn4 labelled in green).

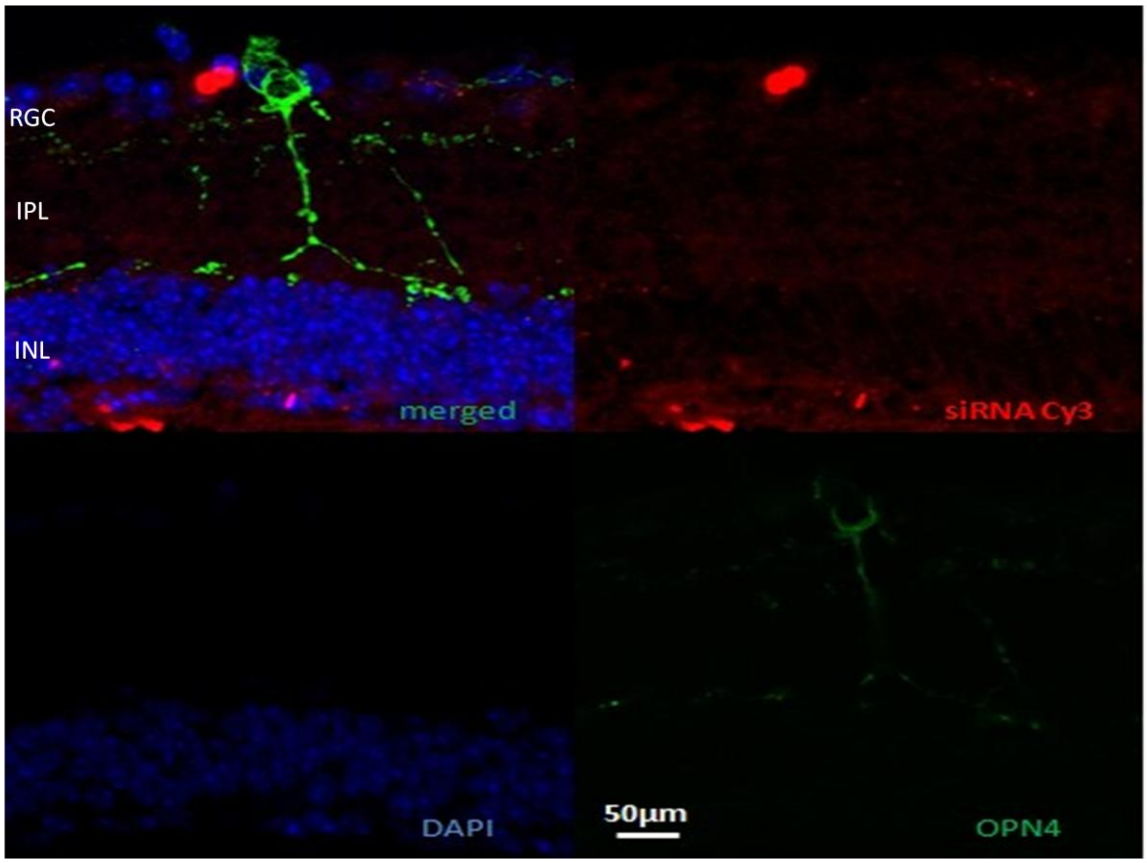

Fig 3.12 Confocal images of *Opn4* positive RGC**.** This figure illustrates siRNA Opn4 (Cy3 red) delivered to the retina (DAPI, inner nuclear layer labeled in blue) and to the pRGC (Opn4 labelled in green).

3.5 Investigating the role of Melanopsin isoforms using RNAi

Since we observed a statistically significant difference in the timecourse of the molecular silencing of the RNA *Opn4 Short* and *Opn4 Long* isoform transcripts *in vivo*, we were interested to know if this also translated into real functional differences in *Opn4* activity in terms of pupillometry. We generated siRNA probes against the transcript variant of murine *Opn4 Short* Isoform and *Opn4 Long* Isoform mRNA and tested them *in vitro* using cellular models expressing the respective isoform to confirm RNA knockdown prior to testing them *in vivo*. I performed bilateral intravitreal injections into >80 day mice with the *C3H/HeN* background harboring the *rd* mutation. At this point virtually all surviving cone cells are lost – similar to end-stage retinitis pigmentosa in humans. Of course to confirm the level of knockdown I also used molecular analysis with RT-qPCR and immunocytochemistry. I also performed pupillometry to quantify precisely the effect on the PLR.

3.5.1 *in vitro Opn4 Short* Silencing

We tested the probes that we generated against the Opn4 Short mRNA on the murine Neuro2A (N2a) cell line and RT-qPCR analysis confirmed Opn4 knockdown with siRNA Opn4 Short (Fig.3.13).

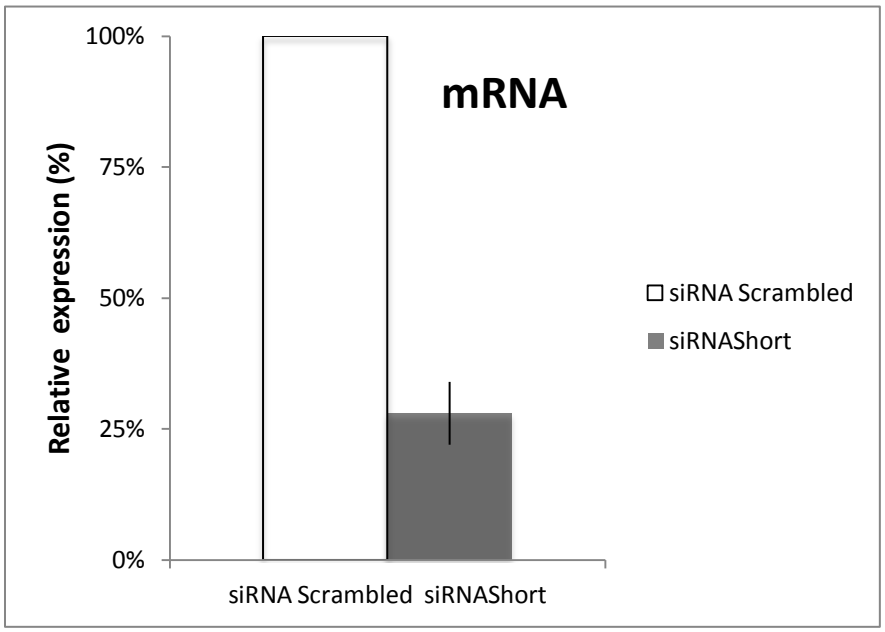

Fig 3.13 *In vitro Opn4 Short* silencing. Relative quantification of siRNA *Opn4 Short* expression plotted relative to the control (Scrambled siRNA). Expression levels of siRNA *Opn4 Short* were significantly decreased. Differences in expression were determined by an *unpaired two-tailed t-test, $p<0.05$, $n=4$. All data represent mean ± SEM.*

3.5.2 *In vivo Opn4 Short* silencing – pupillometry

The pupil constriction was measured at 480nm which is the wavelength of *Opn4* stimulation. We wanted to investigate if *in vivo* delivery of *Opn4 Short* isoform siRNA affected the pupillary responses to light in *rd* mice aged more than 80 days. We found that the pupil response in the injected with the siRNA *Opn4 Short* mice achieved 41% ± 6% pupil constriction, whereas the mice injected with the non targeting siRNA (control) achieved 20% ± 5%, which was significantly different (*t=unpaired two-tailed t-test, p<0.05, n=3*), although numbers are small. Hence we can conclude that *in vivo* delivery of siRNA *Opn4 Short* isoform in *rd* mice may reduce the pupillary responses to light. (Fig 3.15)

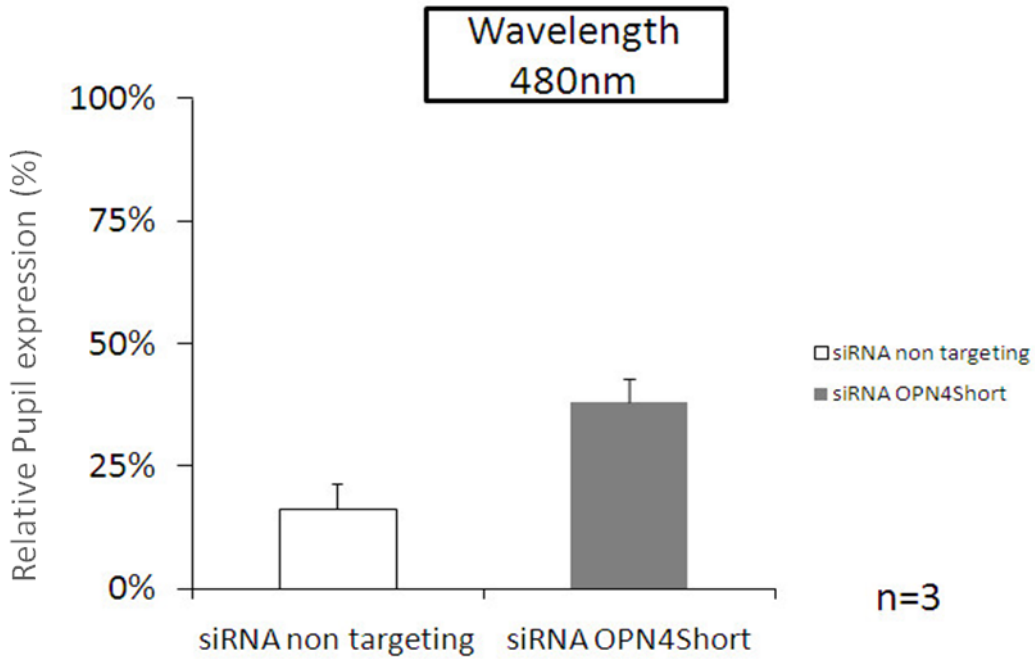

Fig 3.14. In vivo Opn4 silencing – pupillometry data. Comparison of the pupil constriction between injected eyes with siRNA Opn4 Short plotted relative to the control (non targeting siRNA). The pupil area is relative to dark. The pupil constriction was significantly decreased in mice injected with siRNA Opn4. Differences were determined by *unpaired two-tailed t-test, $p<0.05$. All data represent mean ± SEM.*

3.5.3 *In vivo Opn4 Short* silencing – qPCR results

In order to confirm observed attenuation of the PLR, I also analysed the retinas for molecular confirmation of knockdown after pupillometry. The relative expression of the *Opn4 Short* mRNA levels was consistent with the pupillometry in showing differences in sensitivity to *in vivo* silencing following intravitreal injection of 1.2 µg of siRNA *Opn4*. *In vivo* delivery of siRNA *Opn4 Short* does obtain mRNA silencing of *Opn4 Short* isoform. For this experiment we used the same *rd* mice that had undergone pupillometry exactly 72 hours (3 days) after siRNA injections (reported in section 3.5.2).

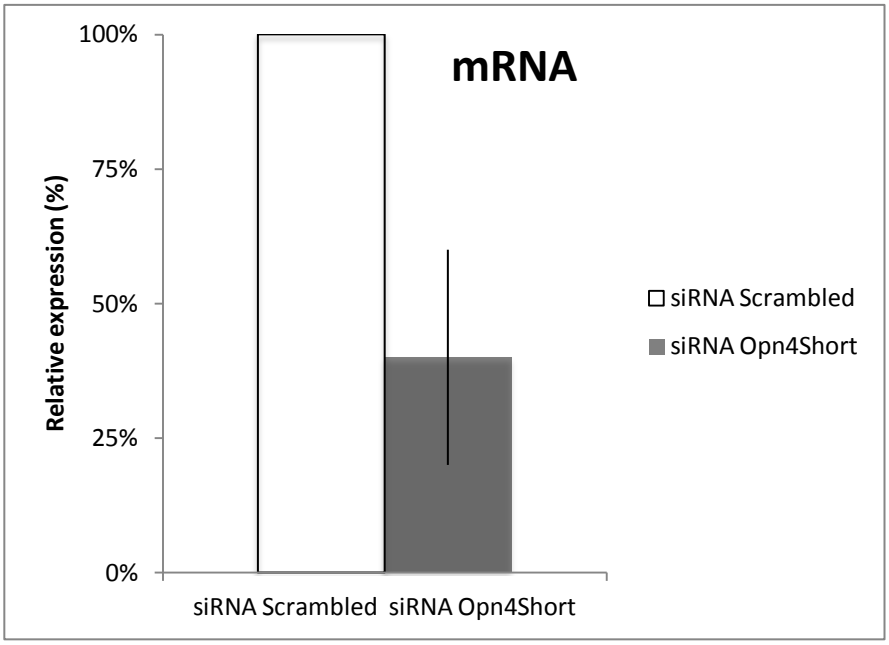

Fig 3.15. *In vivo Opn4 Short* silencing. Relative quantification of siRNA Opn4 Short expression by qPCR plotted relative to the control (Scrambled siRNA). Expression levels of siRNA Opn4 Short were significantly decreased. Differences in expression were determined by *an unpaired two-tailed t-test, $p<0.05$, $n=3$. All data represent mean ± SEM*

3.5.4 *In vitro* OPN4 Long silencing

Similar to with the previous *Opn4 Short* isoform experiment above, I first tested the probes that we generated against the *Opn4 Long* mRNA on the murine Neuro2A (N2a) cell line in vitro (Fig 3.17). The RT-qPCR analysis confirmed highly efficient Opn4 Long knockdown at > 95% silencing with siRNA *Opn4* (Fig.3.16).

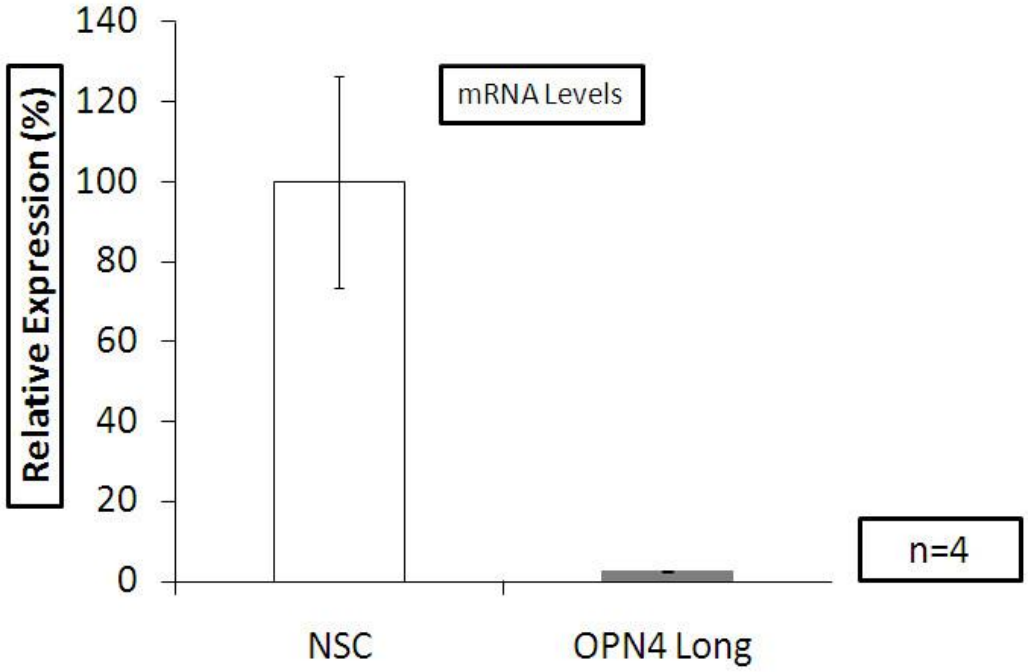

Fig 3.16. *In vitro Opn4 Long* silencing. Relative quantification of siRNA Opn4 Long expression plotted relative to the control (Scrambled siRNA). Expression levels of siRNA Opn4 Long were significantly decreased. Differences in expression were determined by an *unpaired two-tailed t-test,$p<0.05$,n=4. All data represent mean ± SEM*. *Opn4 Long* sequences provide >95% silencing *in vitro*

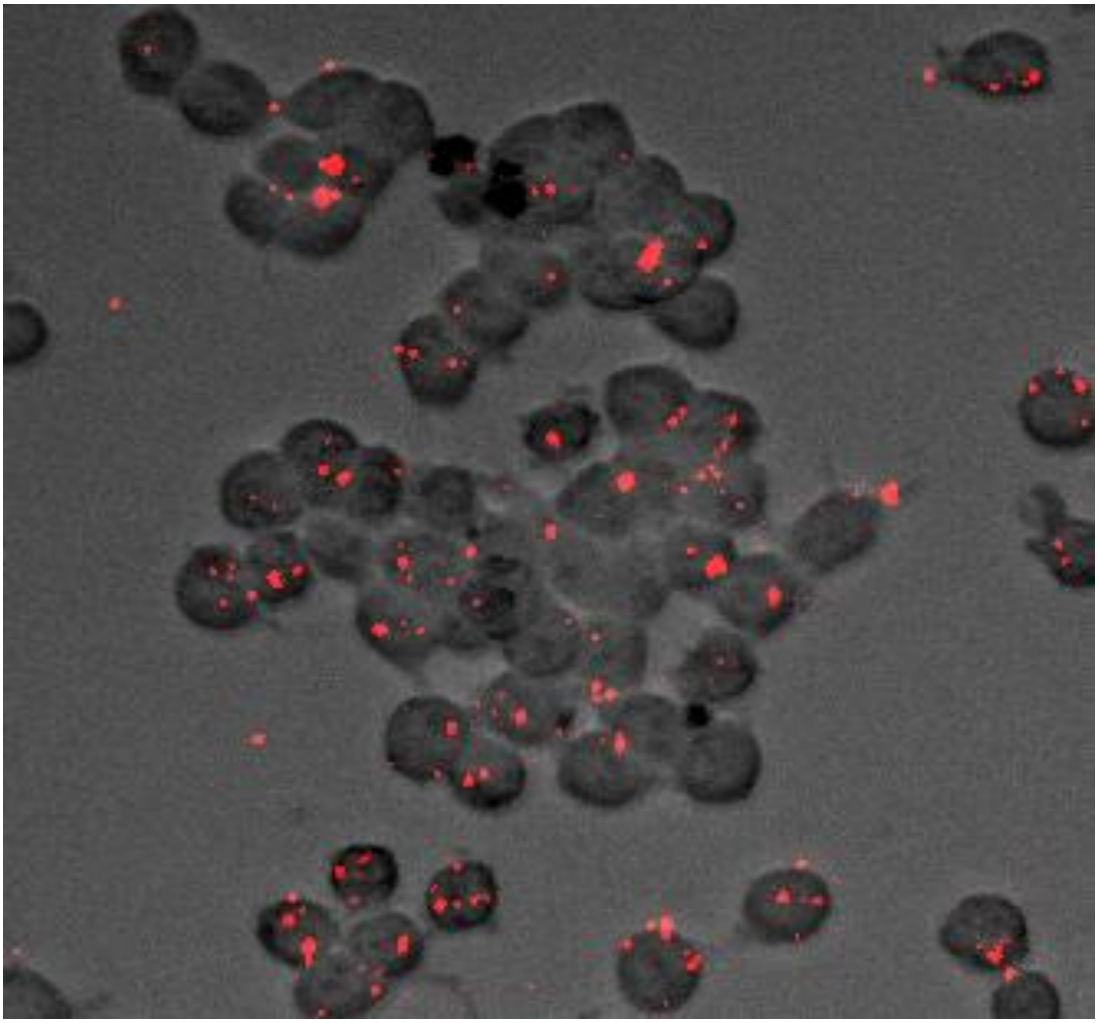

Fig 3.17. siRNA Opn4 Long penetrating pRGCs. This figure illustrates Cy3 red conjugated siRNA Opn4 molecules penetrating the cytoplasm of N2a cells (red dots). A Carl Zeiss fluorescent microscope to image *OpnLong* positive cells with at 20x objective and at excitation 405, 488, and 543 nm with emission wavelengths of 420–450, 505–530, and 550–754 nm for DAPI, green, and red.

3.5.5 *In vivo OPN4 Long* Silencing – Pupillometry

The pupil constriction was measured at 480nm, which is the wavelength of *Opn4* stimulation. We wanted to investigate if *in vivo* delivery of *Opn4 Long* isoform siRNA in *rd* mice affected the pupillary responses to light. Unexpectedly given the N2a data, I found that the pupil response in the injected with the siRNA *Opn4 Long* mice only achieved 23% ± 5% pupil constriction, whereas the mice injected with the non targeting siRNA (control) achieved 21% ± 6%, which was not significantly different (*t=unpaired two-tailed t-test, p=0.5, n=4. All data represent mean ± SEM*). Hence we can conclude that *in vivo* delivery of siRNA *Opn4 Long* isoform in *rd* mice did not affect the pupillary responses to light (Fig 3.18).

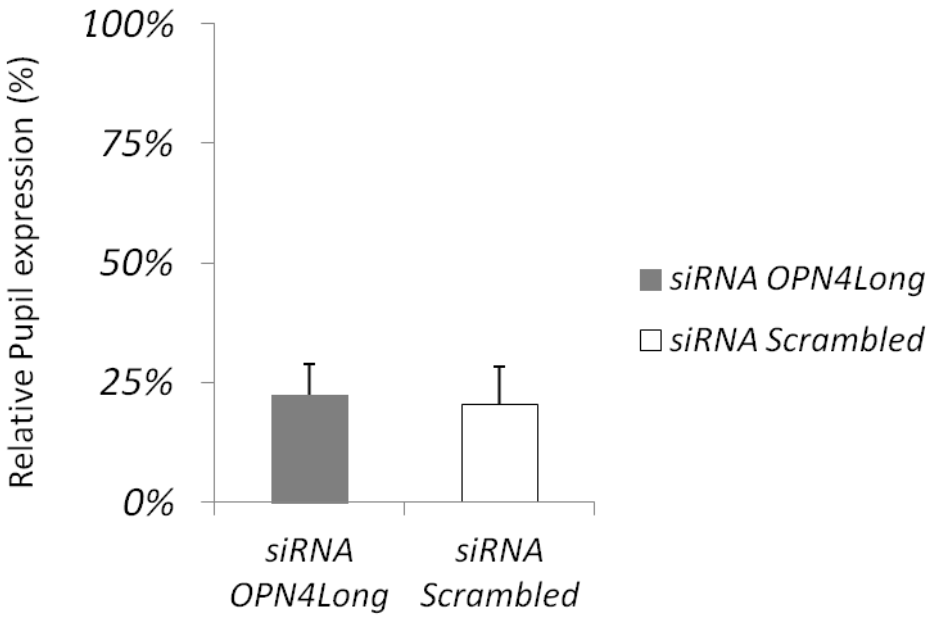

Fig 3.18 *In vivo Opn4 Long* Silencing. This figure illustrates a comparison of the pupil constriction between injected eyes with siRNA *Opn4 Long* plotted relative to the non sequence control (siRNA scrambled). There were no differences detected. The pupil area is relative to dark. (*t=unpaired two-tailed t-test, p=0.5, n=4). All data represent mean ± SEM.*

3.5.6 *in vivo OPN4 Long* Silencing - qPCR Results

In order to explore the finding that the siRNA did not affect the pupil response with the *Opn4 Long* isoform, I also performed qPCR of the retinas to see how much knockdown had been achieved by the intravitreal injection of siRNA *Opn4 Long* at the molecular level. Surprisingly this showed that the i*n vivo* delivery of siRNA *Opn4 Long* in the *rd* mice does not obtain mRNA silencing of *Opn4 Long* at the molecular level at 72 hours, the timepoint for the pupillometry (Fig 3.19).

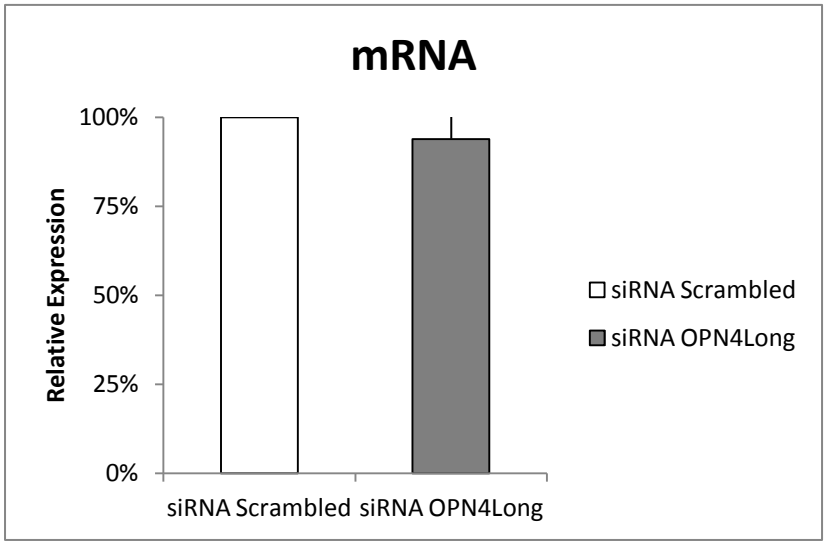

Fig 3.19. *In vivo Opn4* Silencing – qPCR results. Relative quantification of siRNA *Opn4 Long* expression plotted relative to the control (Scrambled siRNA). There were no differences detected. (*t= unpaired two-tailed t-test, p>0.5, n=7. All data represent mean ± SEM*).

3.6 *Trpc3* Silencing

Transient Receptor Potential-Canonical (*TRPC)* channels are mammalian homologs of Transient Receptor Potential (*TRP*), a Ca2+- permeable channel involved in the phospholipase C-regulated photoreceptor activation mechanism in Drosophila. The seven mammalian TRPCs constitute a family of channels which have been proposed to function as store operated as well as second messenger-operated channels in a variety of cell types. *TRPC* channels, together with other more distantly related channel families, make up the larger *TRP* channel superfamily (Vazquez et al., 2004).

Trpc channels have also been found to be expressed in the photoreceptor cells of several species. They were first identified in Drosophila rhabdomeric photoreceptors (Montell and Rubin , 1989; Montell et al., 1999; Vazquez et al., 2004), and *TRP* channel homologues have also been found in limulus (Bandyopadhyay and Payne., 2004) and squid (Monk et al., 1996) photoreceptor membranes. This suggests that these channels may constitute a common endpoint in phototransduction pathways. We wanted to investigate more candidates that may unravel the molecular interactions of the melanopsin signaling such as as *Trpc3*. As the first step in probing the function of this new molecule, I optimized the immunostaining of *Trpc3* in the mouse retina and confirmed localization to both the ganglion cell layer and the inner nuclear layer (Fig 3.20).

These last experiments went beyond the time of my MSc experimental work and have been continued by other members of the group who now routinely use the *in vivo* model of "pupil silencing" that I helped to develop. Similar to how I have probed the effects of the long and short isoforms of *Opn4*, *Trpc3* will be the next molecule in the pathway that will hopefully lead eventually to a complete unraveling of the light-induced melanopsin cascade.

3.6.1. Immunohistochemistry

Double immunostaining images showing the *Trpc3* red and the *Opn4 Short* antibodies at a retina section where captured with A Carl Zeiss fluorescent microscope to image *OpnLong* positive cells with at 20x objective and at excitation 405, 488, and 543 nm with emission wavelengths of 420–450, 505–530, and 550–754 nm for DAPI, green, and red. A *TRC3* (1:500, 1:700) (Alomone Labs, Jerusalem, Israel), and Opn4 Long and Short antibodies (Pires et al., 2009).

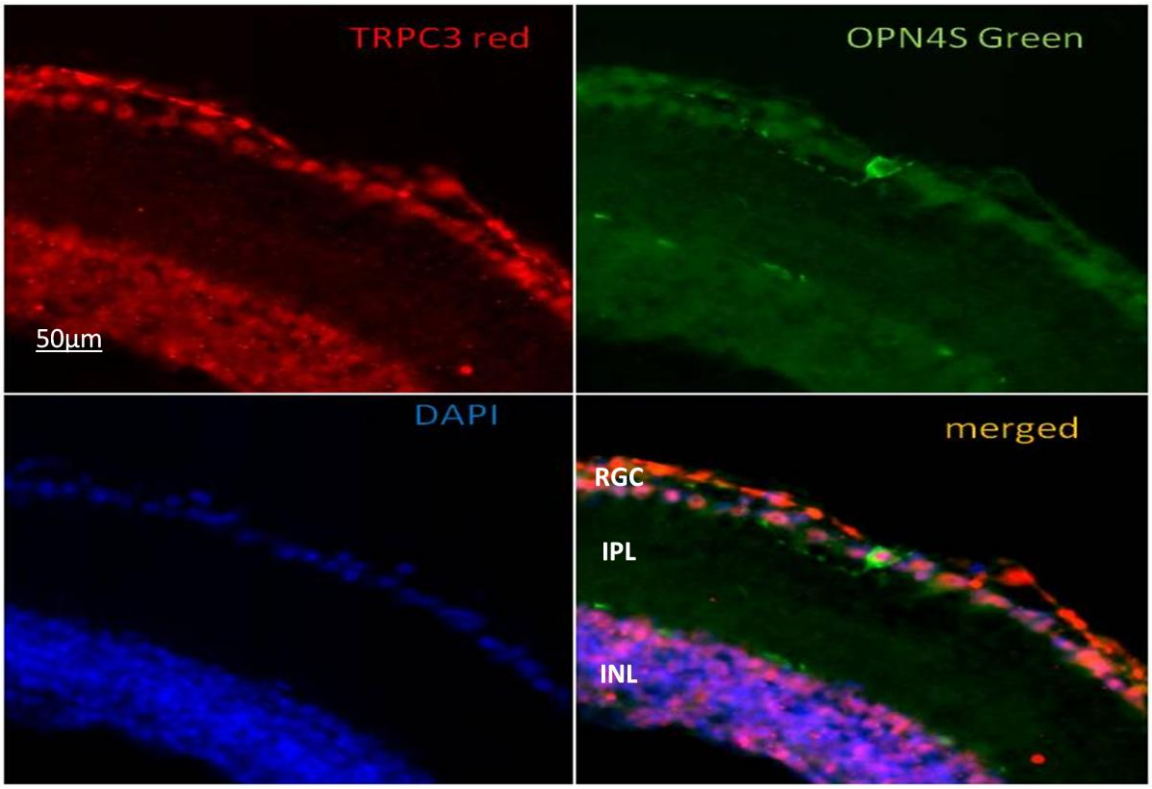

Fig 3.20. *Trpc3* Immunohistochemistry. This figure illustrates double immunofluorescent staining of *Trpc3* (red - 1:500, Alomone Labs, Jerusalem, Israel) and *Opn4 Short* (green - Pires et al., 2009).The *Trpc3* is weekly expressed in the retina.

Chapter 4: Discussion

The work presented in this thesis aimed to investigate the complexity of melanopsin signaling pathway and to explain the potential mechanism of the functional diversity observed between different subsets of pRGCs and the specific contributions of Opn4L and Opn4S isoforms to the different functional responses. This in turn would contribute towards a better understanding of the nature of melanopsin signalling pathway and its light induced sensitivity. In order to investigate the molecular basis of melanopsin we used siRNA based techniques. The data accumulated in this thesis suggest that intravitreal injection of siRNA provides an ideal tool for studying vision-related gene function, particularly in the RGC layer.

Melanopsin expressing retinal ganglion cells (pRGCs) represent a third class of ocular photoreceptors and are involved in irradiance detection and non-image-forming responses to light including pupil constriction, circadian entrainment, and regulation of sleep (Hughes et al., 2012a). During the last decade, there has been a rapid increase in understanding the regions of the brain which they innervate, and the behavioral responses of melanopsin-based light detection. From the non-ophthalmological perspective, the non-image forming responses to light drive sleep and circadian rhythm and are hence gaining significant interest with regard to potential influence in psychiatric disease, where sleep is typically disrupted (Pritchet et al., 2012). From the ophthalmological perspective, the non-image forming responses have gained interest with the development of blue light filtering intraocular lenses. Although to date these lenses have not blocked enough 480 nm light to affect circadian function significantly, there is increased awareness in the intraocular lens manufacturing industry that any filters should not block melanopsin responses (Cuthbertson et al., 2009).

Currently there is a lot still to unravel with regard to understanding the melanopsin pathway and transgenic mouse models are increasingly used to explore the effects of individual molecules (genes) on the cellular mechanisms.

Mice lacking rods and cones retain a variety of responses to environmental irradiance including pineal melatonin suppression, a PLR, inhibition of locomotor activity, and regulation of sleep propensity. In humans, there is evidence that this system regulates body temperature, mood and aspects of arousal and concentration. It seems, therefore, that melanopsin -expressing pRGCs represent a distinct sensory modality encoding environmental irradiance for a wide variety of physiological and behavioural systems (Foster et al., 2002; Hattar, 2003; Lucas et al., 2003).

Phototransduction in pRGCs begins with light absorption by melanopsin. These cells are capable of autonomous phototransduction and are thus true photoreceptors. Currently the molecules involved in this Opn4 light induced transduction cascade are less well characterized (Hughes et al., 2012b). Melanopsin-expressing pRGCs have several features that distinguish them from the classic photoreceptors. Whereas rods and cones hyperpolarize in response to light, melanopsin-containing pRGCs depolarize upon light stimulation. This reflects the differences between the signal transduction pathways triggered by activated melanopsin and those triggered by rhodopsin or cone opsins (Kawasaki et al., 2007). Nevertheless both use 11-cis vitamin-A (retinal) as a chromophore, as evidenced by reduced pRGC function in RPE65 knockout mice which cannot isomerise trans- to cis-retinal efficiently (Fu et al., 2005). This raises the obvious question about how much dark adaptation will affect the pupil response, as this will result in greater availability of the cis form of retinal. For this reason all the experiments I performed were after dark adaptation and at a

similar time of day. From a practical perspective, this limited using large groups of animals within cohorts.

The rods and cones convey visual information to the ganglion cells via the second order bipolar cells. At the outer plexiform layer (OPL), horizontal cells (H) facilitate lateral connectivity and feedback to the photoreceptors. At the inner plexiform layer (IPL) amacrine cells (A) allow lateral connections between bipolar and ganglion cells. The optic nerve is formed from the axons of all the ganglion cells. A subset of ganglion cells (pRGC) also detects light directly; for this, they require the photopigment melanopsin. Light, via melanopsin, activates a G-protein cascade in the cells that depolarizes the cell membrane. These cells also receive synaptic input in the IPL from bipolar cells and amacrine cells. Thus photodetection in the retina occurs both in the outer and inner retina. Since rods (and to a lesser extent cones) do convey non-image forming signals to the brain through the ganglion cells (Guler et al., 2008), this implies that there must be some dysfunction in patients with end-stage retinitis pigmentosa, albeit not as severe as following complete loss of ganglion cell inputs, such as might occur in glaucoma. For this reason the *rd* mouse serves as a useful model of the human situation and our imaging experiments have shown how there is also phenotype affecting the retinal pigment epithelium. What is not yet apparent, however, is how the retinal pigment epithelium changes also affect endogenous levels of retinal within the eye. Severe disruption of retinal pigment epithelial function might therefore influence non-image forming pRGCs indirectly, through reduced availability of the retinal chromophore.

Melanopsin is an opsin class of G-protein– coupled receptor that is expressed in pRGCs in mammals (Provencio et al., 1998. The light response properties of melanopsin are distinct from those of the rods or cones opsins (Hatori et al., 2010; Davies et al., 2010).

Melanopsin has a maximal peak spectral sensitivity at 480 nm, which lies in the blue range of the visible light. Like other opsins, melanopsin uses 11- cis retinaldehyde as a chromophore; light elicits photoisomerization of this chromophore resulting in conformational changes in the opsin receptor, which activates downstream signaling proteins (Kawasaki et al., 2007; Hatori et al., 2010). The signal transduction cascade triggered by activated melanopsin is different from that triggered by metarhodopsin in rods and cones (Hatori et al., 2010). In photoreceptors, light-activated metarhodopsin is coupled to the G protein transducin, which activates phosphodiesterase; this results in hydrolysis of 3'–5' cyclic guanosine monophosphate and closure of cyclic nucleotide-gated cation channels, leading to hyperpolarization (Kawasaki et al., 2007; Hankins et al., 2008; Davies et al., 2010). In contrast, melanopsin is coupled to Gq, which activates phospholipase C-β and a cascade that involves diacylglycerol as signal intermediate. This results in activation of transient receptor potential cation (TRPC) channels, eliciting influx of sodium and calcium and thus depolarization of pRGCs (Kawasaki et al., 2007; Hankins et al., 2008; Davies et al., 2010). Recent observations of isolated eyes in a culture dish have indicated that the pupil responses in mice may be maintained without an optic nerve, possibly directly through the iris via a melanopsin system (Xue et al., 2011). In the experiments I have described I did not observe *in vivo* knock-down of the pupil response to anywhere near to the same degree as observed *in vitro*. This may of course reflect phamacodynamics, but an alternative explanation would be that the iris-driven pupil constriction component is still intact and that either the intravitreal siRNA does not reach it, or possibly the *Opn4* isoform may be different.

Melanopsin-containing pRGCs also provide a contribution to the PLR (Tsujimura et al., 2010). A direct projection from these neurons is send to the OPN of the midbrain; this nucleus projects to the Edinger-Westphal nucleus, which sends efferents to the ciliary

ganglion. Melanopsin-containing pRGCs drive the PLR in the absence of input from photoreceptors (Mure et al., 2007). The discovery that melanopsin-containing ipRGCs mediate the PLR has provided new insights into the pupillary response to light (Kawasaki et al., 2007; Tsujimura et al., 2010). Under photopic conditions, a blue light stimulus produces a steady-state pupil constriction mediated primarily by direct intrinsic photoactivation of these cells. Preliminary studies in humans also indicate that cones primarily drive the transient phase of the PLR, whereas melanopsin-expressing ganglion cells directly activated by light mediate sustained pupil constriction (Kawasaki et al., 2007; Tsujimura et al., 2010). In my experiments I was unable to dissect out the specific components of the pupil response with regard to these early and late phases, mediated by each of the two isoforms, but I did notice a difference in the silencing ability. Although it is easy to speculate that this may relate to the half life of the protein or alternatively there may be other isoforms, the simple fact is that the molecular analysis did not confirm significant reduction of the mRNA for the long isoform. This indicates that either the targeting sequence is incorrect or that the transfection *in vivo* was inefficient in these experiments. Since we had a good knock down by day 5 in other mice, one possible explanation is that the metabolism of the retina is changed in the end-stage *rd* mice such that the siRNA might be turned over more rapidly.

As well as investigating the molecular aspects of melanopsin, we also wanted to compare the PLR of *C3H/HeN* and *rd/rd cl* transgenic mice. We can say that there is no difference between pupillary responses between the pupil phenotype of the two strains and it seems that the residual cones do not contribute to the PLR. This may seem an obvious fact, but recent work has highlighted the presence of residual cones even in very late end-stage outer retinal degeneration in *rd* mice and these cones remain connected to inner retinal circuits (Busskamp et al., 2010). Certainly for the purpose of my work described here any

residual non-imaging forming activity from these cells (if present) was not evident.

The work presented in this thesis demonstrated clearly that there is a robust *in vitro* silencing in all our experiments. We also achieved *in vivo* silencing on both mRNA and protein levels almost in all of our experiments. In our *Opn4* time course it was clear that melanopsin silencing was evident at all three time points and it was at its maximum at day 3 but attenuated by day 5. *Opn4 Short* and *Opn4 Long* isoforms were also silenced in all three time points. They both show differences in sensitivity to *in vivo* silencing and Opn4 Short is also attenuated by day 5. It appears that *Opn4 Long* reaches its maximum silencing by day 5. Differences may be due to variable distributions of *Opn4* isoforms in all the subtypes of pRGCs in the retina that may make one subtype an easier target to silence. Alternatively the inhibition may be variable due to alternative splicing or other undisclosed molecular mechanisms. When confirmed mRNA silencing of *Opn4* isoforms, *Opn4 Short* silencing produces an attenuated pupillary responses, whereas *Opn4 Long* isoform silencing produces no effect on pupillary responses but without the evidence of confirmed knockdown by molecular analysis. From the data accumulated in this thesis , taken together with previous literature, it could be hypothesized that that *Opn4 Long* does not appear to contribute to pRGC regulation of pupillary responses to light, whereas *Opn4 Short* does and that the qPCR used was not accurate enough to detect the change in *Opn4 Long* mRNA levels. *Opn4 Long* may be involved in circadian phase shifting, sleep or other non-image forming responses.

TRP channels have been found to be expressed in the photoreceptor cells of several species. This suggests that these channels may constitute a common endpoint in phototransduction pathways. Because melanopsin resembles an invertebrate-like opsin (Provencio et al.,1998) and melanopsin can couple to *TRPC* channels in expression systems (Panda et al., 2005; Qiu et al., 2005), it has been proposed that *TRPC* channels may be

involved in photosensitive RGC phototransduction (Sekaran et al., 2007). Data presented in this thesis was preliminary to investigate the role of *Trpc3* in the melanopsin phototransduction cascade, but the PLR-silencing model should be robust enough to explore this in future. Further thoughts will be to access the siRNA Opn4 timecourse with behavioural assays such as pupillomery. Opn4 Long and Opn4 Shorh isoforms need further probing investigating their role in the retinal connectivity.

The work presented on the molecular basis of melanospin induced light sensitivity is an ongoing project subject to further investigation. The data suggest that we could benefit in probing more molecules to unravel the *OPN4* pathway and to restore vision to the blind eye. In patients *OPN4* may have therapeutic potential if ectopically expressed in the degenerate retina in cases where photoreceptors are lost, in degenerative retinal diseases such as retinitis pigmentosa, but the molecules involved in this *Opn4* light induced transduction cascade are less well characterized and need further probing.

may be that maximal light sensitivity can be restored to the blind retina by gene therapy with a combination of *Opn4* and other essential second messengers of the non-image forming light transduction cascade. The recent work with the electronic retinal implant has highlighted the potential goal that might be achieved (Zrenner et al., 2011). As Foster (2005) would say, there are bright blue times ahead.

References

Arendt D. Evolution of eyes and photoreceptor cell types. Int J Dev Biol. 2003;47(7-8):563-71.

Arshavsky, V.Y. et al. G proteins and phototransduction. Annu.Rev. Physiol. 2002; 64, 153–187

Bailes HJ, Lucas RJ. Melanopsin and inner retinal photoreception. Cell Mol Life Sci. 2010 Jan;67(1):99-111.

Bandyopadhyay BC, Payne R. Variants of TRP ion channel mRNA present in horseshoe crab ventral eye and brain. J Neurochem. 2004 Nov;91(4):825-35.

Banin E, Cideciyan AV, Alemán TS, Petters RM, Wong F, Milam AH, Jacobson SG. Retinal rod photoreceptor-specific gene mutation perturbs cone pathway development. Neuron. 1999 Jul;23(3):549-57.

Baver SB, Pickard GE, Sollars PJ, Pickard GE. Two types of melanopsin retinal ganglion cell differentially innervate the hypothalamic suprachiasmatic nucleus and the olivary pretectal nucleus. Eur J Neurosci. 2008 Apr;27(7):1763-70.

Belenky MA, Smeraski CA, Provencio I, Sollars PJ, Pickard GE. Melanopsin retinal ganglion cells receive bipolar and amacrine cell synapses. J Comp Neurol 2003 Jun 2;460(3):380-93.

Bernstein E, Caudy AA, Hammond SM, Hannon GJ. Role for a bidentate ribonuclease in the initiation step of RNA interference. Nature. 2001 Jan 18;409(6818):363-6.

Berson DM, Dunn FA, Takao M. Phototransduction by retinal ganglion cells that set the circadian clock. Science 2002 Feb 8;295(5557):1070-3.

Berson DM. Strange vision: ganglion cells as circadian photoreceptors. Trends Neurosci. 2003 Jun;26(6):314-20.

Berson DM. Phototransduction in ganglion-cell photoreceptors. Pflugers Arch. 2007 Aug;454(5):849-55.

Berson DM, Castrucci AM, Provencio I. Morphology and mosaics of melanopsin-expressing retinal ganglion cell types in mice. JComp Neurol 2010 Jul 1;518(13):2405-22.

Billy E, Brondani V, Zhang H, Muller U, Filipowicz W. Specific interference with gene expression induced by long, double-stranded RNA in mouse embryonal teratocarcinoma cell lines. Proc Natl Acad Sci USA 2001;98:14428–14433

Bowes C, Li T, Danciger M, Baxter LC, Applebury ML, Farber DB. Retinal degeneration in the rd mouse is caused by a defect in the beta subunit of rod cGMP-phosphodiesterase. Nature. 1990 Oct 18;347(6294):677-80.

Brown TM, Gias C, Hatori M, Keding SR, Semo M, Coffey PJ, Gigg J, Piggins HD, Panda S, Lucas RJ. Melanopsin contributions to irradiance coding in the thalamo-cortical visual system. PLoS Biol. 2010 Dec 7;8(12):e1000558

Busskamp V, Duebel J, Balya D, Fradot M, Viney TJ, Siegert S, Groner AC, Cabuy E, Forster V, Seeliger M, Biel M, Humphries P, Paques M, Mohand-Said S, Trono D, Deisseroth K, Sahel JA, Picaud S, Roska B. Genetic reactivation of cone photoreceptors restores visual responses in retinitis pigmentosa. Science. 2010 Jul 23;329(5990):413-7.

Carter-Dawson LD, LaVail MM, Sidman RL. Differential effect of the *rd* mutation on rods and cones in the mouse retina. Invest Ophthalmol Vis Sci. 1978 Jun;17(6):489-98.

Chang GQ, Hao Y, Wong F. Apoptosis: final common pathway of photoreceptor death in rd, rds, and rhodopsin mutant mice. Neuron. 1993 Oct;11(4):595-605.

Chen SK, Badea TC, Hattar S. Photoentrainment and pupillary light reflex are mediated by distinct populations of ipRGCs. Nature. 2011 July 17; 476(7358): 92–95.

Cioca DP, Aoki Y, Kiyosawa K RNA interference is a functional pathway with therapeutic potential in human myeloid leukemia cell lines. Cancer Gene Ther. 2003 Feb;10(2):125-33.

Contin MA, Verra DM, Guido ME. An invertebrate-like phototransduction cascade mediates light detection in the chicken retinal ganglion cells. FASEB J. 2006 Dec;20(14):2648-50.

Contin MA, Verra DM, Salvador GA, Ilincheta MG, Giusto NM, Guido ME. Light activation of the phosphoinositide cycle in intrinsically photosensitive chicken retinal ganglion cells.Invest Ophthalmol Vis Sci. 2010 Nov;51(11):5491-8.

Cuthbertson FM, Peirson SN, Wulff K, Foster RG, Downes SM. Blue light-filtering intraocular lenses: review of potential benefits and side effects. J Cataract Refract Surg. 2009 Jul;35(7):1281-97.

Dacey DM, Liao HW, Peterson BB, Robinson FR, Smith VC, Pokorny J, Yau KW, Gamlin PD. Melanopsin-expressing ganglion cells in primate retina signal colour and irradiance and project to the LGN. Nature 433:749–754Davies WL, Foster RG, Hankins MW. Focus on molecules: melanopsin. (2005) Exp Eye Res Epub 2010 Aug 7.

Do MTH, Kang SH, Xue T, Zhong H, Liao HW, Bergles DE, Yau KW. Photon capture and signalling by melanopsin retinal ganglion cells. Nature. 2009 Jan 15;457(7227):281-7.

Drouyer E, Dkhissi-Benyahya O, Chiquet C, Wolde Mussie E, Ruiz G, Wheeler LA, Denis P, Cooper HM. Glaucoma alters the circadian timing system. PLoS One. 2008;3(12):e3931.

Dumitrescu ON, Pucci FG, Wong KY, Berson DM. Ectopic retinal ON bipolar cell synapses in the OFF inner plexiform layer: contacts with dopaminergic amacrine cells and melanopsin ganglion cells. J Comp Neurol. 2009 Nov 10;517(2):226-44.

Dykxhoorn DM, Novina CD, Sharp PA Killing the messenger: short RNAs that silence gene expression. Nat. Rev. Mol. Cell Biol. 2003 Jun; 4(6): 457-67.

Ecker JL, Dumitrescu ON, Wong KY, Alam NM, Chen SK, LeGates T, Renna JM, Prusky GT, Berson DM, Hattar S. Melanopsin-expressing retinal ganglion-cell photoreceptors: cellular diversity and role in pattern vision. Neuron 2010; 67:49-60.

Fedorov Y, King A, Anderson E, Karpilow J, Ilsley D, Marshall W, Khvorova A. Different delivery methods-different expression profiles. Nat Methods. 2005 Apr;2(4):241.

Fire A, Xu S, Montgomery MK, Kostas SA, Driver SE, Mello CC. Potent and specific genetic interference by double-stranded RNA in Caenorhabditis elegans. Nature. 1998 Feb 19;391(6669):806-11.

Foster RG, Provencio I, Hudson D, Fiske S, De Grip W, Menaker M. Circadian photoreception in the retinally degenerate mouse (rd/rd). J Comp Physiol A. 1991 Jul;169(1):39-50.Foster RG, Hankins MW: Non-rod, non-cone photoreception in the vertebrates. Prog Retin Eye Res. 2002 Nov;21(6):507-27.

Foster RG. Neurobiology: bright blue times. Nature. 2005 Feb 17;433(7027):698-9.

Freedman MS, Lucas RJ, Soni B, Schantz MV, Munoz M, David-Gray Z, Foster R. Regulation of Mammalian Circadian Behavior by Non-rod, Non-cone, Ocular Photoreceptor.Science1999 April; 284 (5413): 502–4.

Fu Y, Zhong H, Wang MH, Luo DG, Liao HW, Maeda H, Hattar S, Frishman LJ, Yau KW. Intrinsically photosensitive retinal ganglion cells detect light with a vitamin A-based photopigment, melanopsin. Proc Natl Acad Sci U S A. 2005 Jul 19;102(29):10339-44.

Fu Y, Yau KW. Phototransduction in mouse rods and cones. Pflugers Arch. 2007 Aug;454(5):805-19.

Fulci V and Macino G. Quelling: post-transcriptional gene silencing guided by small RNAs in Neurospora crassa. Current Opinion in Microbiology 2007, 10:199–203.

García-Fernández JM, Jimenez AJ, Foster RG. The persistence of cone photoreceptors within the dorsal retina of aged retinally degenerate mice (rd/rd): implications for circadian organization. Neurosci Lett. 1995 Feb 24;187(1):33-6.

Graham DM, Wong KY, Shapiro P, Frederick C, Pattabiraman K, Berson DM. Melanopsin ganglion cells use a membrane-associated rhabdomeric phototransduction cascade. J Neurophysiol. 2008 May;99(5):2522-32.

Green CB, Takahashi JS, Bass J. The meter of metabolism.Cell. 2008 Sep 5;134(5):728-42.

Güler AD, Ecker JL, Lall GS, Haq S, Altimus CM, Liao HW, Barnard AR, Cahill H, Badea TC, Zhao H, Hankins MW, Berson DM, Lucas RJ, Yau KW, Hattar S. Melanopsin cells are the principal conduits for rod-cone input to non-image-forming vision. Nature. 2008 May 1;453(7191):102-5.

Hankins MW, Peirson SN, Foster RG. Melanopsin: an exciting photopigment. Trends Neurosci. 2008 Jan;31(1):27-36.

Hardie RC, Minke B. The trp gene is essential for a light-activated Ca2+ channel in Drosophila photoreceptors. Neuron. 1992 Apr;8(4):643-51.

Hartwick AT, Bramley JR, Yu J, Stevens KT, Allen CN, Baldridge WH, Sollars PJ, Pickard GE. Light-evoked calcium responses of isolated melanopsin-expressing retinal ganglion cells. J Neurosci. 2007 Dec 5;27(49):13468-80.

Hatori M, Panda S. The emerging roles of melanopsin in behavioral adaptation to light. Trends Mol Med 2010;16:435–446.

Hattar S, Liao HW, Takao M, Berson DM, Yau KW. Melanopsin containing retinal ganglion cells: architecture, projections, and intrinsic photosensitivity. Science. 2002 Feb 8;295(5557):1065-70.

Hattar S, Kumar M, Park A, Tong P, Tung J, Yau KW, Berson DM. Central projections of melanopsin-expressing retinal ganglion cells in the mouse. J Comp Neurol. 2006 Jul 20;497(3):326-49.

Hattar S, Ecker JL, Dumitrescu ON, Chen SK, Wong KY, Alam NM, Prusky GT, Berson DM. Functions and target innervations of distinct subtypes of melanopsin cells. Invest OphthalmolVis Sci. 2009 May;50:ARVO E-Abstract 5027.

Hermans E. Biochemical and pharmacological control of the multiplicity of coupling at G-protein-coupled receptors. Pharmacol Ther.2003 Jul;99(1):25-44.

Hoshi H, Liu WL, Massey SC, Mills SL. ON inputs to the OFF layer: bipolar cells that break the stratification rules of the retina. J Neurosci. 2009 Jul 15;29(28):8875-83.

Hughes S, Hankins MW, Foster RG, Peirson SN. Melanopsin phototransduction: Slowly emerging from the dark. Prog Brain Res. 2012a;199:19-40.

Hughes S, Welsh L, Katti C, González-Menéndez I, Turton M, Halford S, Sekaran S, Peirson SN, Hankins MW, Foster RG. Differential expression of melanopsin isoforms Opn4L

and Opn4S during postnatal development of the mouse retina. PLoS One. 2012b;7(4):e34531.

Hutvagner G, McLachlan J, Pasquinelli AE, Balint E, Tuschl T, Zamore PD. A cellular function for the RNA-interference enzyme Dicer in the maturation of the let-7 small temporal. RNA. Science 2001;293:834–838

Hsi-Wen Liao and King-Wai Yau. *In vivo* gene delivery in the retina using polyethylenimine, Biotechniques.2007 Mar;42(3):285-6, 288.

Isoldi MC, Rollag MD, Castrucci AM, Provencio I. Rhabdomeric phototransduction initiated by the vertebrate photopigment melanopsin. Proc Natl Acad Sci U S A. 2005 Jan 25;102(4):1217-21

Izquierdo M. Short interfering RNAs as a tool for cancer gene therapy. Cancer Gene Ther. 2005 Mar;12(3):217-27. Review.

Jackson AL, Bartz SR, Schelter J, Kobayashi SV, Burchard J, Mao M, Li B, Cavet G, Linsley PS. Expression profiling reveals off-target gene regulation by RNAi. Nat Biotechnol. 2003 Jun;21(6):635-7.

Jackson AL, Linsley PS. Noise amidst the silence: off-target effects of siRNAs? Trends Genet. 2004: 521-24.

Jackson AL, Linsley PS. Recognizing and avoiding siRNA off-target effects for target identification and therapeutic application. Nat Rev Drug Discov. 2010 Jan;9(1):57-67.

Kaiser PK, Symons RC, Shah SM, Quinlan EJ, Tabandeh H, Do DV, Reisen G, Lockridge JA, Short B, Guerciolini R, Nguyen QD; Sirna-027 Study Investigators. RNAi-based treatment for neovascular age-related macular degeneration by Sirna-027. Am J Ophthalmol. 2010 Jul;150(1):33-39.e2.

Kawasaki A, Kardon RH. Intrinsically photosensitive retinal ganglion cells. J Neuroophthalmol 2007;27:195–204.

Khvorova, A., Reynolds A., Jayasena S. Functional siRNAs and miRNAs exhibit strand bias. Cell 115.1.2003: 209-16.

Koyanagi M, Kubokawa K, Tsukamoto H, Shichida Y, Terakita A. Cephalochordate melanopsin: evolutionary linkage between invertebrate visual cells and vertebrate photosensitive retinal ganglion cells. Curr Biol. 2005 Jun 7;15(11):1065-9.

Koyanagi M, Takano K, Tsukamoto H, Ohtsu K, Tokunaga F, Terakita A. Jellyfish vision starts with cAMP signaling mediated by opsin-G(s) cascade. Proc Natl Acad Sci U S A. 2008 Oct 7;105(40):15576-80.

Kumbalasiri T, Rollag MD, Isoldi MC, Castrucci AM, Provencio I. Melanopsin triggers the release of internal calcium stores in response to light. Photochem Photobiol. 2007 Mar-Apr;83(2):273-9.

Lang K. Atlas of Ophthalmology, 2000 Thieme Publishing, Stuttgart, Germany.

Laposky AD, Bass J, Kohsaka A, Turek FW. Sleep and circadian rhythms: key components in the regulation of energy metabolism. FEBS Lett. 2008 Jan 9;582(1):142-51.

Liao HW, Yau KW. *In vivo* gene delivery in the retina using polyethylenimine. Biotechniques. 2007 Mar;42(3):285-6, 288.

Li RS, Chen BY, Tay DK, Chan HH, Pu ML, So KF. Melanopsin expressing retinal ganglion cells are more injury-resistant in a chronic ocular hypertension model. Invest Ophthalmol Vis Sci. 2006 Jul;47(7):2951-8.

Lin B, Koizumi A, Tanaka N, Panda S, Masland RH. Restoration of visual function in retinal degeneration mice by ectopic expression of melanopsin. Proc Natl Acad Sci U S A. 2008 Oct 14;105(41):16009-14.

Lolley RN, Brown BM, Farber DB. Protein phosphorylation in rod outer segments from bovine retina: cyclic nucleotide-activated protein kinase and its endogenous substrate. Biochem Biophys Res Commun. 1977 Sep 23;78(2):572-8.

Lucas RJ, Foster RG. Photoentrainment in mammals: a role for cryptochrome? J Biol Rhythms. 1999 Feb;14(1):4-10. Review.

Lucas RJ, Freedman MS, Muñoz M, Garcia-Fernández JM, Foster RG. Regulation of the mammalian pineal by non-rod, non-cone, ocular photoreceptors. Science. 1999 Apr 16;284(5413):505-7.

Lucas RJ, Douglas RH, Foster RG. Characterization of an ocular photopigment capable of driving pupillary constriction in mice.Nat Neurosci. 2001 Jun;4(6):621-6.

Lucas RJ, Hattar S, Takao M, Berson DM, Foster RG, Yau KW. Diminished pupillary light reflex at high irradiances in melanopsin-knockout mice. Science. 2003 Jan 10;299(5604):245-7.

MacLaren RE, Pearson RA, MacNeil A, Douglas RH, Salt TE, Akimoto M, Swaroop A, Sowden JC, Ali RR. Retinal repair by transplantation of photoreceptor precursors. Nature. 2006 Nov 9;444(7116):203-7.

McCall MA, Gregg RG, Merriman K, Goto Y, Peachey NS, Stanford LR. Morphological and physiological consequences of the selective elimination of rod photoreceptors in transgenic mice. Exp Eye Res. 1996 Jul;63(1):35-50.

Melyan Z, Tarttelin EE, Bellingham J, Lucas RJ, Hankins MW. Addition of human melanopsin renders mammalian cells photoresponsive. Nature. 2005 Feb 17;433(7027):741-5.

Monk PD, Carne A, Liu SH, Ford JW, Keen JN, Findlay JB. Isolation, cloning, and characterisation of a trp homologue from squid (Loligo forbesi) photoreceptor membranes. J Neurochem. 1996 Dec;67(6):2227-35.

Montell C. and Rubin S. Chemical excitation and inactivation in photoreceptors of the fly mutants trp and nss. J Gen Physiol. 1989 September 1; 94(3): 465–491.

Montell C. Visual transduction in Drosophila, Annu. Rev. Cell Dev. Biol. 15. 1999;231– 268.

Mrosovsky N. Masking: history, definitions, and measurement. Chronobiol Int. 1999 Jul;16(4):415-29. Review.

Mrosovsky N, Hattar S. Impaired masking responses to light in melanopsin-knockout mice. Chronobiol Int. 2003 Nov;20(6):989-99.Mure LS, Rieux C, Hattar S, Cooper HM. Melanopsin dependent nonvisual responses: evidence for photopigment bistability *in vivo*. J Biol Rhythms 2007;22:411–424.

Newman LA, Walker MT, Brown RL, Cronin TW, Robinson PR. Melanopsin forms a functional short-wavelength photopigment. Biochemisty. 2003 Nov 11;42(44):12734-8.

Noseda R, Kainz V, Jakubowski M, Gooley JJ, Saper CB, Digre K, Burstein R. A neural mechanism for exacerbation of headache by light. Nat Neurosci. 2010 Feb;13(2):239-45. Epub 2010 Jan 10.

Ostergaard J, Hannibal J, Fahrenkrug J. Synaptic contact between melanopsin-containing retinal ganglion cells and rod bipolar cells. Invest Ophthalmol Vis Sci. 2007 Aug;48(8):3812-20.

Panda S, Sato TK, Castrucci AM, Rollag MD, DeGrip WJ, Hogenesch JB, Provencio I, Kay SA (2002) Melanopsin (Opn4) requirement for normal light-induced circadian phase shifting. Science. 2002 Dec 13;298(5601):2213-6.

Paddison PJ, Hannon GJ. RNA interference: the new somatic cell genetics? Cancer Cell. 2002 Jul;2(1):17-23. Review.

Panda S, Nayak SK, Campo B, Walker JR, Hogenesch JB, Jegla T. Illumination of the melanopsin signaling pathway. Science. 2005 Jan 28;307(5709):600-4.

Peirson SN, Butler JN, Foster RG. Experimental validation of novel and conventional approaches to quantitative real-time PCR data analysisNucleic Acids Res. 2003 Jul 15;31(14):e73.

Peirson SN, Bovee-Geurts PH, Lupi D, Jeffery G, DeGrip WJ, Foster RG. Expression of the

candidate circadian photopigment melanopsin (Opn4) in the mouse retinal pigment epithelium.Brain Res Mol Brain Res. 2004 Apr 7;123(1-2):132-5.

Peirson SN, Oster H, Jones SL, Leitges M, Hankins MW, Foster KG. Microarray analysis and functional genomics identify novel components of melanopsin signalling. Curr Biol 2007; 17: 1363–1372.

Pires SS, Hughes S, Turton M, Melyan Z, Peirson SN, Zheng L, Kosmaoglou M, Bellingham J, Cheetham ME, Lucas RJ, Foster RG, Hankins MW, Halford S.Differential Expression of Two Distinct Functional Isoforms of Melanopsin (Opn4) in the Mammalian Retina The Journal of Neuroscience, 2009 September;29(39):12332–12342.

Pittendrigh CS, Daan S.Circadian oscillations in rodents: a systematic increase of their frequency with age. Science. 1974 Nov 8;186(4163):548-50.

Pittler, S.J. & Baehr, W. Identification of a nonsense mutation in the rod photoreceptor cGMP-phosphodiesterase beta subunit gene of the rd mouse. Proc. Natl. Acad. Sci. USA 1991;88, 8322−8326

Pritchett D, Wulff K, Oliver PL, Bannerman DM, Davies KE, Harrison PJ, Peirson SN, Foster RG. Evaluating the links between schizophrenia and sleep and circadian rhythm disruption. J Neural Transm. 2012 Oct;119(10):1061-75.

Provencio I, Wong S, Lederman AB, Argamaso SM, Foster RG. Visual and circadian responses to light in aged retinally degenerate mice. Vision Res. 1994 Jul;34(14):1799-806.

Provencio I, Jiang G, De Grip WJ, Hayes WP, Rollag MD. Melanopsin: An opsin in melanophores, brain, and eye. Proc Natl Acad Sci U S A. 1998 Jan 6;95(1):340-5.

Provencio I, Rodriguez IR, Jiang G, Hayes WP, Moreira EF, Rollag MD.A novel human opsin in the inner retina.J Neurosci2000 Jan 15;20(2):600-5.

Provencio I, Rollag MD, Castrucci AM. Photoreceptive net in the mammalian retina. This mesh of cells may explain how some blind mice can still tell day from night. Nature. 2002 Jan 31;415(6871):493.

Qiu X, Kumbalasiri T, Carlson SM, Wong KY, Krishna V, Provencio I, Berson DM. Induction of photosensitivity by heterologous expression of melanopsin. Nature. 2005 Feb 17;433(7027):745-9.

Reid KJ, Zee PC. Circadian rhythm disorders.Semin Neurol. 2009 Sep;29(4):393-405.

Reynolds A, Leake D, Boese Q, Scaringe S, Marshall WS, Khvorova. A Rational siRNA design for RNA interference. Nat Biotechnol. 2004 Mar;22(3):326-30.

Ruby NF, Brennan TJ, Xie X, Cao V, Franken P, Heller HC, O'Hara BF.Role of melanopsin in circadian responses to light.Science. 2002 Dec 13;298(5601):2211-3.

Sahar S, Sassone-Corsi P. Metabolism and cancer: the circadian clock connection. Nat Rev Cancer. 2009 Dec;9(12):886-96.

Scacheri, P. C., et al. Short interfering RNAs can induce unexpected and divergent changes in the levels of untargeted proteins in mammalian cells. PNAS 101.7. 2004: 1892-97.

Schmidt TM, Taniguchi K, Kofuji P. Intrinsic and extrinsic light responses in melanopsin-expressing ganglion cells during mouse development. J Neurophysiol. 2008 Jul;100(1):371-84.

Schmidt TM, Kofuji P. Functional and morphological differences among intrinsically photosensitive retinal ganglion cells.J Neurosci. 2009 Jan 14;29(2):476-82.

Schmidt TM, Chen SK, Hattar S. Intrinsically photosensitive retinal ganglion cells: many subtypes, diverse functions. Trends Neurosci. 2011 Nov;34(11):572-80.

Schmidt TM, Kofuji P. Structure and function of bistratified intrinsically photosensitive retinal ganglion cells in the mouse. J Comp Neurol. 2011; 519:1492–1504

Sekaran S, Foster RG, Lucas RJ, Hankins MW . Calcium imaging reveals a network of intrinsically light-sensitive inner retinal neurons. Curr Biol. 2003 Aug 5;13(15):1290-8.

Sekaran S, Lupi D, Jones SL, Sheely CJ, Hattar S, Yau KW, Lucas RJ, Foster RG, Hankins MW. Melanopsin-dependent photoreception provides earliest light detection in the mammalian retina. Curr Biol. 2005 Jun 21;15(12):1099-107.

Sekaran S, Lall GS, Ralphs KL, Wolstenholme AJ, Lucas RJ, Foster RG, Hankins MW. 2-Aminoethoxydiphenylborane is an acute inhibitor of directly photosensitive retinal ganglion cell activity *in vitro* and *in vivo*.J Neurosci. 2007 Apr 11;27(15):3981-6.

Semizarov D, Frost L, Sarthy A, Kroeger P, Halbert DN, Fesik SW. Specificity of short interfering RNA determined through gene expression signatures. Proc Natl Acad Sci U S A. 2003 May 27;100(11):6347-52.

Semo M, Lupi D, Peirson SN, Butler JN, Foster RG. Light-induced c-fos in melanopsin retinal ganglion cells of young and aged rodless/coneless (rd/rd cl) mice. Eur J Neurosci. 2003 Dec;18(11):3007-17.

Sledz CA, Holko M, de Veer MJ, Silverman RH, Williams BR. Activation of the interferon system by short-interfering RNAs. Nat Cell Biol. 2003 Sep;5(9):834-9.

Snove, O., and T. Holen. Many commonly used siRNAs risk off-target activity. Biochem. Biophys. Res.Commun. 391.1. 2004: 256-63.

Soucy E, Wang Y, Nirenberg S, Nathans J, Meister M. A novel signaling pathway from rod photoreceptors to ganglion cells in mammalian retina. Neuron. 1998 Sep;21(3):481-93.

Takahashi JS, Hong HK, Ko CH, McDearmon EL. The genetics of mammalian circadian order and disorder: implications for physiology and disease. Nat Rev Genet. 2008 Oct;9(10):764-75.

Terakita A (2005) The opsins. Genome Biol. 2005;6(3):213.

Tsujimura S, Ukai K, Ohama D, Nuruki A, Yunokuchi K. Contribution of human melanopsin retinal ganglion cells to steady-state pupil responses. Proc Biol Sci 2010;277: 2485–2492.

Vazquez G, Wedel BJ, Aziz O, Trebak M, Putney JW Jr. The mammalian TRPC cation channels. Biochim Biophys Acta. 2004 Dec 6;1742(1-3):21-36.

Viney TJ, Balint K, Hillier D, Siegert S, Boldogkoi Z, Enquist LW, Meister M, Cepko CL, Roska B. Local retinal circuits of melanopsin-containing ganglion cells identified by trans-synaptic viral tracing. Curr Biol. 2007 Jun 5;17(11):981-8.

Vugler AA, Redgrave P, Semo M, Lawrence J, Greenwood J, Coffey PJ Dopamine neurones form a discrete plexus with melanopsin cells in normal and degenerating retina. Exp Neurol (2007); 205:26–35

Wang Y, Macke JP, Merbs SL, Zack DJ, Klaunberg B, Bennett J, Gearhart J, Nathans J. A locus control region adjacent to the human red and green visual pigment genes.Neuron. 1992 Sep;9(3):429-40.

Wang HZ, Lu QJ, Wang NL, Liu H, Zhang L, Zhan GL. Loss of melanopsin-containing retinal ganglion cells in a rat glaucoma model. Chin Med J 2008; 121: 1015–1019.

Warren EJ, Allen CN, Brown RL, Robinson DW. The light-activated signaling pathway in SCN-projecting rat retinal ganglion cells. Eur J Neurosci. 2006 May;23(9):2477-87.

Fu Y, Liao HW, Do MT, Yau KW. Non-image-forming ocular photoreception in vertebrates.Curr Opin Neurobiol. 2005 Aug;15(4):415-22.

Xue T, Do MT, Riccio A, Jiang Z, Hsieh J, Wang HC, Merbs SL, Welsbie DS, Yoshioka T, Weissgerber P, Stolz S, Flockerzi V, Freichel M, Simon MI, Clapham DE, Yau KW. Melanopsin signalling in mammalian iris and retina. Nature. 2011 Nov 2;479(7371):67-73.

Yu JY, DeRuiter SL, Turner DL. RNA interference by expression of short-interfering RNAs and hairpin RNAs in mammalian cells. Proc Natl Acad Sci U S A. 2002 Apr 30; 99(9): 6047-52.

Zhang DQ, Wong KY, Sollars PJ, Berson DM, Pickard GE, McMahon DG. Intraretinal signaling by ganglion cell photoreceptors to dopaminergic amacrine neurons. Proc Natl Acad Sci U S A. 2008 Sep 16;105(37):14181-6.

Zender L, Hutker S, Liedtke C, Tillmann HL, Zender S, Mundt B, Waltemathe M, Gosling T, Flemming P, Malek NP, Trautwein C, Manns MP, Kuhnel F, Kubicka S. Caspase 8 small interfering RNA prevents acute liver failure in mice. Proc Natl Acad Sci U S A. 2003 Jun 24;100(13):7797-802.

Zrenner E, Bartz-Schmidt KU, Benav H, Besch D, Bruckmann A, Gabel VP, Gekeler F, Greppmaier U, Harscher A, Kibbel S, Koch J, Kusnyerik A, Peters T, Stingl K, Sachs H, Stett A, Szurman P, Wilhelm B, Wilke R. Subretinal electronic chips allow blind patients to read letters and combine them to words. Proc Biol Sci. 2011 May 22;278(1711):1489-97.